

1989

Wave Height Changes and Mass Transport on Tague Reef, a Caribbean Reef, North Coast of St. Croix, U.S. Virgin Islands.

Alexis Lugo-fernandez
Louisiana State University and Agricultural & Mechanical College

Follow this and additional works at: https://digitalcommons.lsu.edu/gradschool_disstheses

Recommended Citation

Lugo-fernandez, Alexis, "Wave Height Changes and Mass Transport on Tague Reef, a Caribbean Reef, North Coast of St. Croix, U.S. Virgin Islands." (1989). *LSU Historical Dissertations and Theses*. 4858.
https://digitalcommons.lsu.edu/gradschool_disstheses/4858

This Dissertation is brought to you for free and open access by the Graduate School at LSU Digital Commons. It has been accepted for inclusion in LSU Historical Dissertations and Theses by an authorized administrator of LSU Digital Commons. For more information, please contact gradetd@lsu.edu.

INFORMATION TO USERS

The most advanced technology has been used to photograph and reproduce this manuscript from the microfilm master. UMI films the text directly from the original or copy submitted. Thus, some thesis and dissertation copies are in typewriter face, while others may be from any type of computer printer.

The quality of this reproduction is dependent upon the quality of the copy submitted. Broken or indistinct print, colored or poor quality illustrations and photographs, print bleedthrough, substandard margins, and improper alignment can adversely affect reproduction.

In the unlikely event that the author did not send UMI a complete manuscript and there are missing pages, these will be noted. Also, if unauthorized copyright material had to be removed, a note will indicate the deletion.

Oversize materials (e.g., maps, drawings, charts) are reproduced by sectioning the original, beginning at the upper left-hand corner and continuing from left to right in equal sections with small overlaps. Each original is also photographed in one exposure and is included in reduced form at the back of the book.

Photographs included in the original manuscript have been reproduced xerographically in this copy. Higher quality 6" x 9" black and white photographic prints are available for any photographs or illustrations appearing in this copy for an additional charge. Contact UMI directly to order.

U·M·I

University Microfilms International
A Bell & Howell Information Company
300 North Zeeb Road, Ann Arbor, MI 48106-1346 USA
313 761-4700 800 521-0600

Order Number 9025319

**Wave height changes and mass transport on Tague Reef, a
Caribbean reef, north coast of St. Croix, U.S. Virgin Islands**

Lugo-Fernandez, Alexis, Ph.D.

The Louisiana State University and Agricultural and Mechanical Col., 1989

U·M·I
300 N. Zeeb Rd.
Ann Arbor, MI 48106

**Wave Height Changes and Mass Transport on Tague Reef, a Caribbean Reef,
North Coast of St. Croix, U.S. Virgin Islands**

A Dissertation

**Submitted to the Graduate Faculty of the
Louisiana State University and
Agricultural and Mechanical College
in partial fulfillment of the
requirements for the degree of
Doctor of Philosophy**

in

The Department of Marine Sciences

by

Alexis Lugo-Fernandez

B.S., University of Puerto Rico, 1977

M.S., University of Puerto Rico, 1983

December, 1989

Acknowledgments

The author is indebted to Dr. Harry H. Roberts, whose guidance and supervision made this research possible. Without his generous support and dedication this research could not have been done. Thanks are due to Drs. William J. Wiseman, Jr., Joseph N. Suhayda, S.A. Hsu, and John Day, Jr., members of the graduate committee whose comments and suggestions have improved this research considerably. Thanks also to my beloved wife, Mercedes, and my sons, Alexis, Alexander, Andres, and Alejandro, whose patient and continual inspiration kept me going through this endeavor.

The field work was conducted with the skillful assistance of Messrs. Walker D. Winnans, Floyd DeMers of the Coastal Studies Institute Support Group, and Messrs Brian L. Carter and Mike Sims of Dept. of Geology and Geophysics at LSU. Mrs. Celia Harrod drew the scientific illustrations. Mr. George Watson provided the computer facilities.

Support for this research was provided by Sigma Xi, the Puerto Rico Sea Grant College, the American Geological Institute, and Chevron Oil Company. The author wishes to thank the Department of Marine Sciences of LSU, Dr. Ralph J. Portier of the Institute of Environmental Studies, and Dr. Stephen P. Murray of the Coastal Studies Institute for support through research assistantships during his studies. Thanks also to Dr. Eugene Turner for providing computer facilities for printing the final drafts of this manuscript.

Dedication

To Ernesto and Maria, loving parents, Mrs. Miriam Fernandez de Machado, and Mr. Severiano Fernandez, sources of inspiration and dedication.

Table of Contents

List of Tables.....	vi
List of Figures	vii
List of Symbols.....	xv
Abstract.....	xviii
1.0 Introduction.....	1
2.0 Study Area.....	8
3.0 Methodology	13
Experiment 1.....	16
Experiment 2.....	16
Experiment 3.....	19
Experiment 4.....	19
Data reduction	19
4.0 Meteorological Conditions	22
5.0 Infragravity and Long-Period Physical Processes.....	32
Water level measurements	32
Water Temperatures.....	41
In-situ Winds	44
Water Level Differences	49
Long-term Current Measurements	53
6.0 Wave Processes.....	59
Data Analysis.....	59
Experiment 3.....	63
Experiment 4.....	80
Numerical Prediction of Wave Height.....	85

7.0 Currents and Mass Transport	100
Vertical Current Profile.....	100
Currents Across the Reef Profile.....	107
Experiment 4.....	110
Mass Transport.....	118
Instantaneous Currents and Sediment Transport	122
8.0 Discussion of Results	128
Water Levels	128
Water temperature.....	130
In-situ Winds	130
Long-term Currents	131
Water Level Differences	131
Wave Results.....	132
Currents, Mass, and Sediment Transport	137
Integrated Circulation Model.....	140
9.0 Conclusions	145
10.0 References.....	149
Appendix A.....	159
Appendix B.....	167
Appendix C	184
Vita.....	185

List of Tables

Table		Page
6.1	Average friction coefficients for each experiment and reef interval.	96
7.1	Average volume flux at the reef crest and backreef in m^3s^{-1} during the study using linear and solitary wave theories	122

List of Figures

Figure		Page
	Fig. 2.1. Map of St. Croix showing study area, Tague Reef and location of anemometer.	9
	Fig. 3.1. Instrument arrangement across the reef profile employed during Experiment 1.	17
	Fig. 3.2. Instrument arrangement across the reef profile employed during Experiment 2.	18
	Fig. 3.3. Instrument arrangement across the reef profile employed during Experiments 3 and 4.	20
	Fig. 4.1. Synoptic weather maps of the tropical Atlantic region during March 23 (A) and 26 (B) of 1987. Notice the southerly flow in A and the cyclonic (C) circulation present in B.	23
	Fig. 4.2. Synoptic weather maps of the tropical Atlantic region during March 31 (A) and April 5 (B) of 1987. The cyclonic (C) circulation is still present in A; in B a large anticyclonic (A) circulation appears with the cyclonic pattern displaced eastward, representing easterly atmospheric waves.	25
	Fig. 4.3. Synoptic weather maps of the tropical Atlantic region during April 8 (A) and 11 (B) of 1987. The anticyclonic (A) circulation is still present in A; in B the lower part of both cyclonic and anticyclonic patterns of easterly atmospheric waves is present.	28

List of Figures

Figure	Page
Fig. 4.4. Barometric pressure observed at the Puerto Rico airport showing the passage of atmospheric waves.	31
Fig. 5.1. Water level curves showing diurnal tidal variations at the forereef and reef lagoon during the study period.	33
Fig. 5.2. High pass (cut-off 1 min) of the lagoon water level showing infragravity oscillations of 30 min period.	35
Fig. 5.3. Autospectra of the lagoon water level showing three distinct peaks at diurnal and semidiurnal, and the 27.7 min periods. The latter represents the infragravity oscillations present in Fig. 5.2.	37
Fig. 5.4. Coherence squared and phase between the water levels at the forereef and lagoon. Notice the high coherence for periods greater than 20 min. The horizontal line represents the 95% significance level.	39
Fig. 5.5. Water temperatures from the tide gages at the forereef and lagoon showing diurnal oscillations. Notice that the lagoon waters are always warmer than forereef waters.	42
Fig. 5.6. Wind speed and direction measured at the reef crest during the study period.	45
Fig. 5.7. Alongshore (U) and cross-shelf (V) components of the wind vectors using the coordinate system shown in Fig. 2.1.	47

List of Figures

Figure	Page
Fig. 5.8. Autospectra of the wind components with 6 degrees of freedom. The frequency step is 0.000172 cpm.	48
Fig. 5.9. Relative water level differences across the reef crest during the study period.	50
Fig. 5.10. Autospectra of the water level differences with 20 degrees of freedom. The frequency step is 0.00071473 cpm.	51
Fig. 5.11. Speed and direction of the Buck Island channel currents measured during the study period.	54
Fig. 5.12. Alongshore (U) and cross-shelf (V) components of the current vectors using the coordinate system shown in Fig. 2.1.	55
Fig. 5.13. Autospectra of the current components with 10 degrees of freedom. The frequency step is 0.0004396 cpm.	56
Fig. 6.1. Tidal curves with inset showing the tide stage of wave data sets selected for discussion during Experiments 3 and 4.	65
Fig. 6.2. Wave autospectra during high and flood tide during Experiment 3 across the reef profile with 16 degrees of freedom.	67
Fig. 6.3. Wave autospectra during low and ebb tide during Experiment 3 across the reef profile with 16 degrees of freedom.	68

List of Figures

Figure	Page
Fig. 6.4. Wave height time series at the forereef(F), crest(C), and backreef(B) during Experiment 3. (HT= high tide, LT= low tide).	71
Fig. 6.5. Wave transmission coefficients during Experiment 3. (HT= high tide, LT= low tide).	71
Fig. 6.6. Relative wave energy change from forereef to crest (F-C) and forereef to backreef (F-B) during Experiment 3. (HT= high tide, LT= low tide).	73
Fig. 6.7. Coherence squared from forereef and crest waves for April 7, 1800; April 8, 0500, 1100, and 1900; April 9, 0100 and 0600 hours.	75
Fig. 6.8. Wave attenuation from forereef to crest as a function of frequency during April 7, 1800; April 8, 0500, 1100, and 1900; April 9, 0100 and 0600 hours.	78
Fig. 6.9. Wave attenuation from forereef to backreef as a function of frequency during April 7, 1800; April 8, 0500, 1100, and 1900; April 9, 0100 and 0600 hours.	79
Fig. 6.10. Wave autospectra across the reef profile during Experiment 4 with 20 degrees of freedom.	81
Fig. 6.11. Coherence squared between the forereef and crest (A), forereef and backreef (B), and crest and backreef (C) during Experiment 4. The horizontal line represents the 95% significance level.	83

List of Figures

Figure		Page
Fig. 6.12.	Water level, low passed (cut-off 1 min) at the forereef, crest and backreef during Experiment 4 illustrating the 30-min oscillation.	86
Fig. 6.13.	Grid across the reef profile used during the numerical calculations of energy dissipation.	90
Fig. 6.14.	Predicted wave height across the reef profile. High tide A,B; low tide C,D; flood E; and ebb F during Experiment 3.	92
Fig. 6.15.	Energy dissipation by bottom friction (TF) and turbulence dissipation (TD) across the reef. High tide A,B; flood C during Experiment 3.	94
Fig. 6.16.	Energy dissipation by bottom friction (TF) and turbulence dissipation (TD) across the reef. Low tide A,B; ebb C during Experiment 3.	95
Fig. 6.17.	Comparison of predicted and observed wave heights at the reef crest with no refraction.	98
Fig. 6.18.	Comparison of predicted and observed wave heights at the reef crest with 30° refraction.	98

List of Figures

Figure	Page
Fig. 7.1. Current autospectra with 16 degrees of freedom, from measurements at the reef crest by two ducted current meters oriented in an onreef-offreef direction and stacked vertically (at 0.95 and 0.65 m above the reef floor). During Experiment 1, data on which the above autospectra were generated were collected at high and flood tide.	101
Fig. 7.2. Current autospectra with 16 degrees of freedom, from measurements at the reef crest by two ducted current meters oriented in an onreef-offreef direction and stacked vertically (at 0.95 and 0.65 m above the reef floor). During Experiment 1, data on which the above autospectra were generated were collected at low and ebb tide.	103
Fig. 7.3. Coherence squared between waves and currents of April 4, 1900(A) and 2200(B); April 5, 0100(C), 1000(D), and 1400(E) at the reef crest during Experiment 1.	105
Fig. 7.4. Current autospectra with 16 degrees of freedom, from measurements at the forereef and backreef during Experiment at high and flood tide.	108
Fig. 7.5. Current autospectra with 16 degrees of freedom, from measurements at the forereef and backreef during Experiment 3 at low and ebb tide with 16 degrees of freedom.	109

List of Figures

Figure		Page
Fig. 7.6.	Coherence squared between waves and currents of April 7, 1800(A), April 8, 0500(B), 1100(C), and 1900(D), April 9, 0100(E) and 0600(F) at the forereef during Experiment 3.	111
Fig. 7.7.	Current autospectra with 20 degrees of freedom, from measurements at the forereef and backreef during Experiment 4.	113
Fig. 7.8.	Coherence and phase angles between waves and currents at the forereef and backreef during Experiment 4. The horizontal line represents the 95% significance level.	115
Fig. 7.9.	Low passed (1 min cut-off) current records at the forereef and backreef during Experiment 4 showing 30-min oscillations.	117
Fig. 7.10.	Mean (M), largest onshore (I) and offshore (O) current speeds for each record collected at the reef crest during Experiment 1. Upper level (A) and lower level (B).	120
Fig. 7.11.	Mean (M), largest onshore (I) and offshore (O) current speed for each record collected at the forereef (A) and backreef (B) during Experiment 3.	121
Fig. 7.12.	A 300-s section of the forereef wave and lower current records collected at 0100 April 5, during Experiment 1.	124

List of Figures

Figure	Page
Fig. 7.13. A 300-s section of the forereef wave and lower and upper current records collected at 1400 April 5, during Experiment 1.	125
Fig. 7.14. A 300-s section of the forereef waves and currents, and backreef records collected at 0600 April 9, during Experiment 3.	126
Fig. 8.1. Summary diagram showing the time scales of the currents across the reef and potential particle movement.	139
Fig. 8.2. Mean currents at the forereef and backreef showing the tidal modulation.	143

List of Symbols

t	time
τ	time lag
h	water depth
g	gravitational acceleration equal to 9.8 ms^{-2}
θ_{xy}	phase lag
γ^2_{xy}	coherence squared
T	temperature
R	solar radiation
ρ	density
C_P	seawater specific heat at constant pressure
η	sea level (water surface elevation)
G_{xy}	one-sided cross spectral density
G_{xx}	one-sided autospectral density
G_{yy}	one-sided autospectral density
d	reef crest width
u	alongshore current component
v	cross-shelf current component
H	significant wave height
K_T	transmission coefficient
K_R	reflection coefficient
ν	spectral bandwidth
E	wave energy density
c	wave celerity
α	attenuation coefficient
ϵ_f	bottom friction dissipation function

List of Symbols

ϵ_b	turbulent dissipation function
f	frequency
C_f	bottom friction coefficient in quadratic law
k	wave number
λ	wavelength
L	reef length or arc length
M	wave mass transport
U	mean speed
ω	frequency in rads^{-1}
D	wave energy dissipation
τ_b	bottom friction stress
κ	friction coefficient in linear frictional law
‰	Parts per Thousand
\tilde{X}	Nondimensional fetch
f_m	autospectrum peak frequency
ΔT	temperature range
$G_{\Delta\eta}$	one-sided water level differences autospectral density
G_F	one-sided forereef water level autospectral density
V	water speed across the reef
K	friction coefficient in quadratic law
$\Delta\eta$	water level difference
z_s	sensor depth
B	breaker coefficient
kn	roughness of sea floor
V_L	lagrangian mass speed

List of Symbols

V_E	record mean speed
k	wave number
$\frac{dV}{dt}$	across reef water acceleration
$\frac{d\eta}{dy}$	water slope across the reef
κ	bottom friction in linear law

Abstract

This study of wave and current transformations across a modern coral reef was conducted on Tague Reef, St. Croix (U.S.V.I.), during late March and early April 1987. The project objective was to improve our understanding of the magnitudes and frequencies as well as the spatial and temporal variations of waves and currents as they interact with a modern reef. Data were collected in 4 experiments over a 2-week period. During the observation period atmospheric and sea state conditions were typical of Caribbean-Atlantic trade wind dominated areas. Results verify that infragravity waves of 27.7 min period and diurnal tides modulated high frequency wave and current processes. Phase lags associated with these long-term motions cause sea level differences across the reef crest that influence mass transport of water and suspended sediment.

Spectral analyses of wave data indicate that spectra shape was conserved between the forereef and reef crest, and spectral broadening at the crest was induced by redistribution and dissipation (average of 65%). Wave propagation into the backreef caused further spectral broadening and increased energy dissipation (average of 78%). Water depth reduction during falling tides increased wave energy dissipation by 15% and 20% from forereef to crest and from forereef to backreef, respectively. A steady wave energy model, including frictional and turbulent dissipation, gives reasonable estimates of wave heights across the reef. This model reveals that, in contrast to sandy beaches, bottom friction on coral reefs is comparable to turbulent energy dissipation. Currents at the reef crest occur on three important time scales: (a) short period (seconds), associated with wave activity, (b) infragravity fluctuations, and (c) diurnal variations of uncertain, but probably tidal origin.

Vertical shear of these currents was found to be negligible. The reef crest mean and instantaneous flow fields suggest that seawater, and perhaps sediments and nutrients, are continuously transported lagoonwards. In contrast, wave related instantaneous currents over the forereef indicate off-reef transport.

A time-dependent, vertically integrated circulation model with surface slope and bottom friction explains the observed current patterns. Under low trade wind wave conditions the volume flux at the reef crest is $0.024 \text{ m}^3\text{s}^{-1}$, which can flush the lagoon in 37 hours.

1.0 Introduction

Modern coral reefs consist of a framework built by hermatypic corals, infilling material provided by organisms living within the framework, and rubble from broken reef builders. Benthic plants, e.g. coralline algae, secrete carbonate, which provides an important cement for the framework (Kennett, 1982) in addition to cements precipitated by physical or chemical processes from pore waters (MacIntyre, 1977). The cementation process creates a structure that can resist wave action and modify the oceanic currents impinging on it. Ecologically, the coral reef is a place of high organic productivity, intense calcium metabolism, and complex food chains (Stoddart, 1969). These biological processes have been identified by numerous investigations of coral reefs, which have, also, recognized the importance of physical processes to the well-being of the reef (Glynn, 1977). However, our knowledge of the physical processes in coral reefs is limited, and most of it is qualitative. Quantitative studies of the physical processes and their role have been very few. Our understanding of the physical processes in the reef environment lags behind other disciplines such as biology and geology. The study presented in this manuscript focuses on the details of wave and current interactions with a shallow reef and was designed to improve our understanding of the magnitudes, frequencies, and spatial scales of physical processes operating in modern reef systems.

Coral reefs develop many forms ranging from linear barriers and fringing reefs to subcircular atolls enclosing deep lagoons (Kennett, 1982; Stoddart, 1969). Each reef type modifies the marine environment and, in turn, marine processes modify reef geometry and associated sediment distribution. The

degree of modification of marine energy incident on the reef depends on reef geometry, morphology, and surface roughness. Wave modifications include redistribution of wave energy by shoaling and refraction, and energy dissipation by bottom friction and turbulence during wave breaking at the reef crest (Roberts et al., 1977; Suhayda and Roberts, 1977). These energy changes give rise to currents and sea level gradients that represent an energy subsidy to the ecosystem. Oceanic currents are important for renewal the of water, oxygen, food supply and for coral larval dispersion in the reefs, and their modification by the reef are just beginning to be understood. Tidal modifications induced by the reef give rise to sea level differences that drive currents and mass transport across the reef crest (Ludington, 1979; Frith, 1981).

A quantitative understanding of physical forces acting in coral reefs is needed if predictions of these physical forces and their effects are desired. Their direct and indirect influence on both biological and geological reef functions makes the understanding of these changes necessary. Distribution of wave energy, currents, and resultant mass transport have direct application to the quantification of both biological and geological-geochemical processes. Biologically, water motion is important for removing metabolic wastes, renewing food and oxygen (Stoddart, 1969), dispersion of planktonic coral larvae (Oliver and Willis, 1987), trophic energy fluxes (MacIntyre et al., 1974), understanding reef zonation (Dollar, 1982; Bradbury and Young, 1981), and removal of damaging pollutants and suspended sediments. Geologically, water motion is important to the distribution of sediments and diagenesis (Suhayda and Roberts, 1977; Roberts, 1980), and morphological changes of reefs (Stoddart, 1962; Glynn et al., 1964; Hernandez-Avila et al., 1977; Baines et al., 1974). Other areas that can benefit from this knowledge are coastal engineering, physical oceanography, management, and environmental studies.

Up to the late 1970's (Milliman,1977), studies of coral reefs in the Indo-Pacific region concentrated mainly on their biology and geologic structure, while studies in the Atlantic focused on sedimentology. This difference in emphasis has provided guidelines for programs of research on physical processes on coral reefs. As a consequence, two different schools of research have emerged. Pacific studies have concentrated primarily on the large-scale circulation that impacts the reef biology of barriers and atolls, while Caribbean-Atlantic studies have focused on more local and detailed wave-current interactions with reefs, which processes drive sediment movement and affect local reef morphology.

Currents

Currents have been studied both around and in the lagoons of reefs. One of the pioneering works was the circulation study of Bikini and Rongelap atoll lagoons by von Arx (1948). He found that flow at the reef crest was lagoonward and driven by a higher sea level behind the breaking zone. During periods of low winds and waves, the sea level difference decreased, and the flow diminished or was reversed. Atkinson et al. (1981) studied the circulation of Eniwetok atoll and found that flow across the windward crest was always lagoonward under the action of wave set-up, which depended on wave height and the tidal stage. No reversal of the flow with the tidal stage was observed. Currents at the leeward crest were weaker and experienced tidal reversals. Other large-scale currents studies have indicated that isolated reef systems like atolls can modify oceanic flows to create down-drift eddies that are important for concentrating plankton and nutrients (Hamner and Hauri, 1981).

Ludington (1979) and Frith (nee Ludington) (1981) studied tidal current modifications induced by a small atoll. She found that ponding of water inside the lagoon drove water outside the reef at low points and through the reef's

porous walls during periods of falling to low tides. At flood stage, wave set-up reinforces the tidally dominated lagoonward flow. A study of lagoon flushing by Wolanski and Pickard (1983) showed that a lagoonward flow of $6 \text{ cm}\cdot\text{s}^{-1}$ at the reef crest was necessary to satisfy the water mass balance. Current measurements by Davies and Hughes (1983) in a lagoon during a tropical depression documented the change of tidally-driven currents to a wind-driven regime. This study is important because it shows that during storm conditions the force balance can be totally different from the one that exists under normal conditions. Pickard (1986) studied the currents at Davies Reef. Measurements at the reef flat showed that during strong winds the currents were unidirectional and lagoonward, but during low winds and large tidal ranges, reversal of the currents occurred. Wave overtopping effects on the net flow were estimated at 40%.

Current studies in small reef-lagoon systems around islands or continents are few. Marsh et al. (1981) illustrated that currents near the reef crest forming the seaward boundary of the lagoon were reef-normal, wave-driven, and directed lagoonwards. In the backreef lagoon the flow field changed direction and became nearly parallel to the backreef shoreline. A similar pattern was observed in a Caribbean reef-lagoon system along the south coast of St. Croix (Roberts et al., 1981a). Major breaks in the linear reef that fronts these lagoons function as points of tidal exchange, while currents in the shallow backreef lagoon may be wind-driven (Greer and Kjerfve, 1982; Kjerfve, 1982).

Waves

Several wave-reef interaction studies have been conducted. However, the complexity of the problem, coupled with the reef geometry, makes each study site-specific. Recognition of the importance of wave action to coral

growth, sediment, and water transport dates back to Darwin (1842), Dana (1853), and Davis (1928). These works were based mainly on visual observations and correlations of coral growth and sediment deposition. Munk and Sargent (1948) appear to have conducted the first quantitative study of wave transformation on reefs. They discovered important sea level differences caused by wave set-up and capable of driving strong lagoonwards currents. An explanation of the phenomena was given by Longuet-Higgins and Stewart (1962). Tait (1972) applied the analytical wave set-up theory to a coral reef; Gerritsen (1981) extended Tait's theory and verified it in a field study in Hawaii. Another finding of Munk and Sargent (1948) was that grooves and surge channels in the reef were oriented parallel to the direction of wave incidence and had an active role in wave attenuation. Similar results were obtained by Roberts (1974) in the Atlantic region. Wave modifications and currents induced at the reef crest were studied at several locations in the Caribbean by Roberts et al., (1975, 1977), Suhayda and Roberts (1977), Roberts and Suhayda (1983), and Roberts (1980). By means of instrument arrays deployed on a transect from the forereef to backreef, they were able to quantify wave attenuation, changes in wave frequencies, energy transmitted to the backreef lagoon, and wave-related currents.

By means of refraction diagrams Lugo-Fernandez (1982) studied wave energy distribution around a coral reef. His conclusions point out that shoaling and refraction in general explained more than 80% of the wave heights measured, and that wave energy dissipated by wave breaking at the reef crest was approximately 80%. Working in north Australia, Davies (1977) found that, under the present high-wave energy regime, reefs tend to grow towards the leeward side. Gerritsen (1981) found that bottom friction and wave breaking were the main agents of wave energy dissipation.

Storm effects on coral reefs have been described by Stoddart (1962, 1969b), Blumenstock (1958), Glynn et al. (1964), and Harmelin-Vivien and Laboute (1986). Modifications caused by the storm waves consist mainly of scouring, erosion of localized areas of the reefs, and creation of boulder ramparts in areas of sediment accumulation (Hernandez-Avila et al., 1977; Baines et al., 1974).

Development and shape of coral reefs have also been interpreted as a result of the existing wave fields and current patterns by Umbgrove (1929) in the Indian Ocean and recently by Roberts and Murray (1984) in the Gulf of Suez, Red Sea.

To summarize existing physical process studies in modern reef systems, it is generally true that most studies of currents have focused on describing the circulation of lagoons, thus concentrating on currents, tides, and wind measurements. Even though the importance of the wave-driven flow at the reef crest has been recognized, few attempts have been made to monitor it. Wave studies, on the contrary, have, in general, lacked current measurements. Recognizing these shortcomings, Gerritsen (1981) recommended that future wave studies include current measurements. The experimental design of the study reported in this manuscript allowed for wave and current measurements at the same location over several tidal cycles on a profile across the reef. Water levels were monitored both at the forereef and lagoon to calculate sea level differences. A current meter mooring in front of the reef was designed to provide continuous monitoring of the current field impinging on the reef. In the carrying out of this design, lagoon currents were not measured, and only inferences concerning lagoon circulation can be made.

Specific objectives of the study were the following:

1. Determination of wave energy changes across the reef profile caused by shoaling, reflection, bottom friction, and wave breaking.
2. Determination of types of waves and their specific interactions with the reef (long waves vs. short waves)
3. Determination of the mass flux of water across the reef crest and variations with changing physical process conditions.
4. Estimation of sea level temporal variations on scales of days to seconds.
5. Estimation of the tide effect on wave energy changes and water transport across the reef crest.
6. Determination of the transmission of wave energy across the reef as a function of frequency.

2.0 Study Area

This project was conducted on Tague Reef, located off the north coast of the Caribbean island of St. Croix (17°40' N, 64°36' W), U.S. Virgin Islands (Figure 2.1). The island is approximately 174 km southeast of San Juan, Puerto Rico. St. Croix's eastern and western highlands are of Cretaceous age and composed primarily of sedimentary and reworked volcanoclastic sediments deposited in deep water. In these regions, several late Cretaceous dioritic and gabbroic intrusives cut the sedimentary rocks (Whetten, 1974). The central part of the island is underlain by Tertiary pelagic and hemipelagic carbonates. These are overlain on the southern and western coasts by reefs and bank deposits of Miocene-Pliocene age (Gill and Hubbard, 1987). The geological formation of St. Croix has two important consequences. First, the island is not part of the large platform that contains the islands of Puerto Rico, St. Thomas, and St. John, but is separated from them by the Anegada Passage and Virgin Islands Trough (4.5 km maximum depth). Secondly, the island is part of its own platform with a narrow (less than 1 km) shelf on the northwestern and western parts. This shelf widens to 6 km on the northeastern and southern flanks of the island. The shelf is narrow, and the edge is at a depth of approximately 20 m around the island; the oceanographical consequences of this configuration will be discussed in later sections.

St. Croix is the largest of the U.S. Virgin Islands with an area of 217.6 km². Its length in an east-west direction is about 30.4 km, its widths on the western and eastern ends about 9.0 km and 1.5 km, respectively. There are three main topographical regions on the island. The first is a range of hills that runs along the northern coast. The second is a hill group in the east. The third topographical

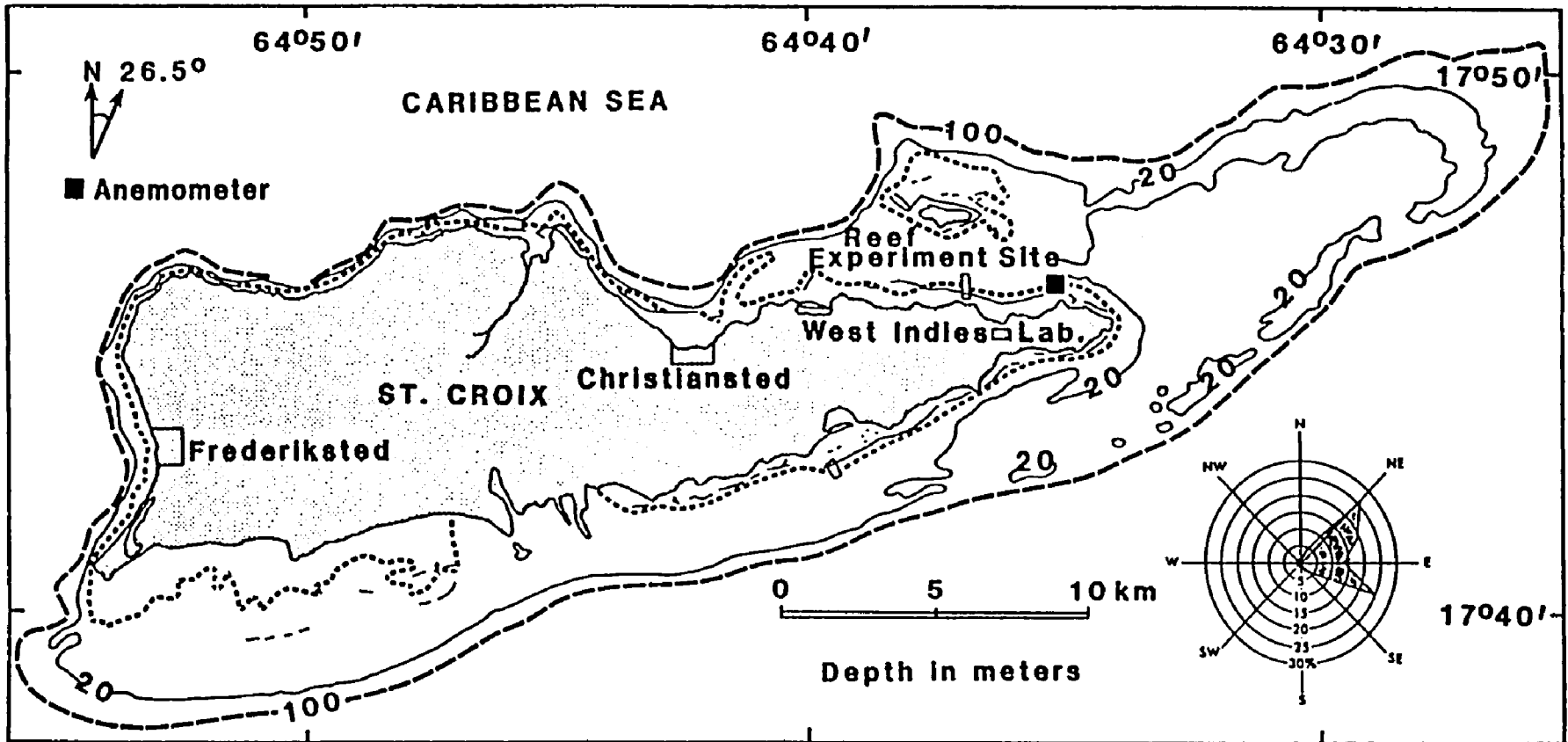


Fig. 2.1. Map of St. Croix showing study area, Tague Reef and location of anemometer.

feature is a broad plain in the central and southern two-thirds of the island (Ruffner and Bair, 1978).

Running streams have virtually disappeared during the last forty years due to a reduction of ground water recharge by high evapotranspiration, as well as the lowering of the water table by pumping (Adams, 1974).

The geographical position of St. Croix within the tropical region of the North Atlantic Ocean determines its climatological and oceanographical conditions. Synoptic distribution of temperature for this area varies yearly from 21°-32°C, with an annual range of 3°-6°C (Goode's World Atlas, 1982). Rainfall on the island is produced mainly by orographic lifting, easterly waves, and tropical hurricanes, and well-defined wet-dry seasons are absent. A spatial gradient of rainfall exists over the island; 127 cm·yr⁻¹ of rain in the northwestern corner decreases to 114.3 cm·yr⁻¹ in the central region and to 76.2 cm·yr⁻¹ on the eastern corner. Even though rainfall variations are small, they can be greatly affected by occasional tropical hurricanes between June and November. Evaporation is high throughout the year with an average of 184.6 cm·yr⁻¹, which increases in the coastal areas. This value compares well with the annual evaporation rate of 161 cm·yr⁻¹ estimated by Colon (in Wüst, 1964).

The following discussion of the wind field is based on data presented by Ruffner and Bair (1978), who reported winds at Alexander Hamilton airport (Figure 2.1) on the south coast of St. Croix, and on data over water (20°N,65°W) from the Marine Climatic Atlas of the World (US Navy,1955). The wind direction mean annual frequency on the south of the island shows that ENE winds are the most frequent (31%), followed by the ESE (19%), the NE (14%) and the E (11%) (Figure 2.1). The monthly distribution shows that ESE is the prevailing direction during summer, and the ENE prevails during winter.

Speed data show that over 95% of all observations are less than $8.0 \text{ m}\cdot\text{s}^{-1}$ under normal conditions. Wind data over the ocean indicate a seasonal directional pattern; the NE is more frequent during the four months of winter, and the E is more frequent during the remaining 8 months, peaking during the months of June and July. This trend reflects the seasonal changes of high pressure centers that develop over the North Atlantic.

The surface temperature of waters around the island varies from near 25.6°C during winter to around 28°C in summer (Wüst,1964). These figures agree with the range ($23^\circ\text{-}26^\circ\text{C}$ during winter, to 28°C during summer) reported by Ogden (1974). Mean surface salinity values obtained from charts of Wüst (1964) indicate 35.9 ‰ during winter and 34.9 ‰ in summer. It is important to note that these values do not include salinities from waters shallower than 200 m; a greater range of values in the shelf waters is to be expected. Tides around the island are mainly diurnal (Ogden,1974; Kjerfve,1981). Tidal range is 30 cm according to Ogden (1974), 10-20 cm according to Kjerfve (1981), and 24 cm according to the tide tables. Despite the small tidal range, currents around the island display a strong semidiurnal tidal signature (Roberts et al.,1981b). The predominantly west-flowing surface currents are derived from the combination of North Equatorial and South Equatorial currents (Pickard and Emery,1982; Wüst,1964). Composite synoptic charts derived from ship logs (Wüst,1964) show a WNW drift of $20.6\text{-}41.2 \text{ cm}\cdot\text{s}^{-1}$ in January, a NW drift with the same speed in April, a NNW drift with the same speed in July, and a N drift of $41.2\text{-}61.7 \text{ cm}\cdot\text{s}^{-1}$ in October. Again, the influence of shallow waters and topographical effects may change these values, so they should be viewed as first-order estimates.

In summary, the St. Croix setting is characterized by a small range of temperature and sea level variations, relatively steady easterly winds at about

8 m·s⁻¹. Oscillatory currents with a net westward surface drift, occasionally disturbed by tropical hurricanes, constitute the physical environment around Tague Reef along the northeast coast. The reef, which is a bank barrier type (Ogden, 1974), is about 6 km long, encloses a lagoon 600-m wide with an average depth of 5 m. The forereef slopes gently (5°) to a 5-m depth and ends in a steep slope (30°-40°) to a depth of 11 m, where a flat shelf is encountered. The backreef is dominated by the corals *Montastrea annularis*, *Porites porites* and *Acropora palmata*, while the crest is composed primarily of *Montastrea complanata*, mixed with *A palmata* (Ogden, 1974). The forereef is dominated by *A palmata* from 1 to 5-m depths (Rogers et al., 1982) and by *P. porites*, *A cervicornis*, *M. annularis*, and *Diploria spp.* in the deeper parts. The reef crest at the study site was 1.2 m deep, and a narrow channel-like feature was present from the backreef area through the reef crest and into the forereef. The width of this feature was about 9 m in the backreef and approximately 2 m through the reef crest. Drilling data suggest that the reef is made of Holocene carbonates approximately 9 m thick resting over Pleistocene(?) rocks (Brian Carter personal communication).

3.0 Methodology

Data for this investigation were collected over a period of 15 days between March 29 and April 11, 1987. During this time, continuous in-situ measurements of wind speed and direction, sea level variations, water temperature, and currents were made at or near the experiment site (Figure 2.1). Concurrent with these observations, four experiments designed to measure wave energy decay and wave induced currents were carried out. To complement these measurements, information on reef geometry, coral zonation, angle of wave approach, and position of the breaking point were collected.

Wind observations were made from a fixed platform located over the reef crest, about 1.7 km east of the experiment site (Figure 2.1). Measurements started on March 29 at 1700 hours and lasted until April 10 at 1600 hours local time. The anemometer consisted of an Aerovane sensor mounted 3.6 m above the water surface and an analog recorder driven by a 12-V power supply. Recorder accuracy was 2% of full scale, which translates into an error of $\pm 0.51 \text{ m}\cdot\text{s}^{-1}$ in speed and $\pm 3.6^\circ$ in direction. An additional error in direction was introduced during the Aerovane alignment, which is estimated as $\pm 1^\circ$. The total error in the direction data is estimated at $\pm 5^\circ$, after rounding. The wind record was sampled at increments of 0.33 hour for subsequent analysis.

Water level variations across the reef profile were measured with two tide gages, Sea Data Corporation Model 636-6, which recorded total pressure (atmospheric plus water) and internal temperature. Both internal temperature and pressure measurements were recorded in digital format on magnetic tape at a rate of 32 points per hour. Observations started on March 29. On April 1, one instrument was moved to a new position on the forereef (1.5 m deep),

where it remained throughout the study. The other sensor was located in the lagoon throughout the investigation, where the water depth was 4.0 m (Figure 3.1). These instruments were designed to withstand maximum pressures of 3.1026 bars (45 psi) with an accuracy of $\pm 0.15\%$ of the applied pressure, which means that, at the operational limit, the error is 3.2 mb or 3.2 cm in a water depth of ~ 20 m. Precision of the instruments is rated as $\pm 0.015\%$ of a given pressure range. Sea level changes of 3.2 mm can be detected over the operating pressure range. Pressure measurements were converted to equivalent water depths by means of the hydrostatic relationship as described in Appendix A. To calculate sea level differences that may exist between the forereef and lagoon, both instruments were surveyed with a theodolite. The survey error was estimated at 1.52 cm, calculated as half of the smallest division of the survey rod. The calculations of the absolute sea level differences, however, suggest that the error is close to 10 cm. A possible explanation for this large error is a misalignment of the theodolite from the horizontal coupled with non-vertical placement of the rod during the survey. Besides allowing computations of sea surface slopes, the high-resolution tide gauges allowed the evaluation of reef effects on tidal and other long-period waves present at the study site.

Temperature was measured and recorded by sensors inside the tide gauges. Assuming the time required to reach thermal equilibrium between water and tide gauge is short, this internal temperature can be equated to water temperature. Arguments in favor of this hypothesis are presented in Appendix A. The results provide support to the thermal equilibrium hypothesis.

In-situ current measurements were made with an Endeco Model 174 impeller current meter. The mooring, located over the shelf, was deployed in 10.7-m water depth on April 2 at 1411 hours and remained in operation until

April 10 at 1425 hours local time. The meter was attached 7.0 m below the surface, to a steel cable kept under tension by a submerged buoy (Figure 3.1). Instrument specifications claim an error of $\pm 3\%$ of full scale on the speed sensor and $\pm 7.2^\circ$ in direction observations at the threshold speed of $2.54 \text{ cm}\cdot\text{s}^{-1}$. Directional calibrations made at the CSI Field Support Facility indicate that this error varies systematically from $\pm 4^\circ$ along the north-south axis to $\sim \pm 2^\circ$ along the east-west axis. Speed and direction observations were recorded in digital form on magnetic tape at a rate of 30 samples per hour. The purpose of this mooring was to monitor ambient currents impinging on the reef and to help provide information for understanding mass transport across the reef.

High frequency variations of pressure induced by surface gravity waves were monitored using Omega Corporation absolute pressure transducers. These sensors have a pressure range of 0-2 bars (0-30 psi) with an error of $\pm 1\%$ of the pressure range. The response of each sensor was highly linear. Wave-induced currents were measured with three bidirectional ducted current meters constructed by the CSI Technical Support Group. These meters had a linear response (1 Hz) and could follow the high frequency reversing flows existing in the surf zone (Murray, 1969). Statistical analysis of the calibration data indicated thresholds between 0.8 and $0.9 \text{ cm}\cdot\text{s}^{-1}$.

During actual field data collection, a burst of 20 minutes was taken every hour and sampled at a rate of one point per second. Outputs from all six sensors were processed by an electronic digitizer. These signals were fed into a computer, which recorded the "instantaneous" values from each sensor. No averaging was performed before recording the measurements. Digital records were stored on floppy diskettes and duplicated every day. This system eliminated errors introduced by digitizing analog recorders, minimized potential

loss of information, and speeded data analysis. Later the data were transferred to an IBM 360 computer for subsequent data reduction and analysis.

Experiment 1

A total of 4 individual experiments were performed to study wave energy decay and wave-generated currents (Fig. 3.1). The first experiment commenced on April 4 1300 hours and lasted until 1400 hours the next day, for a duration of 25 hours. Observations of wave characteristics at the forereef (3.8 m), crest (1.2 m), and backreef lagoon (4.0 m) were made to detect modifications as they traversed the reef profile. Current measurements under these waves were made at the reef crest and backreef lagoon. The current measurements made (0.92 m and 0.60 m above the floor) at the crest were used to estimate the mass transports across the reef crest.

Experiment 2

Experiment 2 started on April 5 at 1800 hours, an hour past low tide, and continued until April 7, 1120 hours. The instrument deployment scheme illustrated in Figure 3.2 was used over a period of two tidal cycles. In this experiment, the lagoon station was eliminated. Changes in wave characteristics as they traveled from forereef to the crest only were studied. Monitoring of wave currents at the reef crest using the configuration of the previous experiment was continued. A third current meter was installed in the backreef area (total water depth of 1.15 m) at a depth of 0.5 m which represented midwater at low tide. This change was motivated by the fact that current speeds in the lagoon was below the detection limit of the instrument.

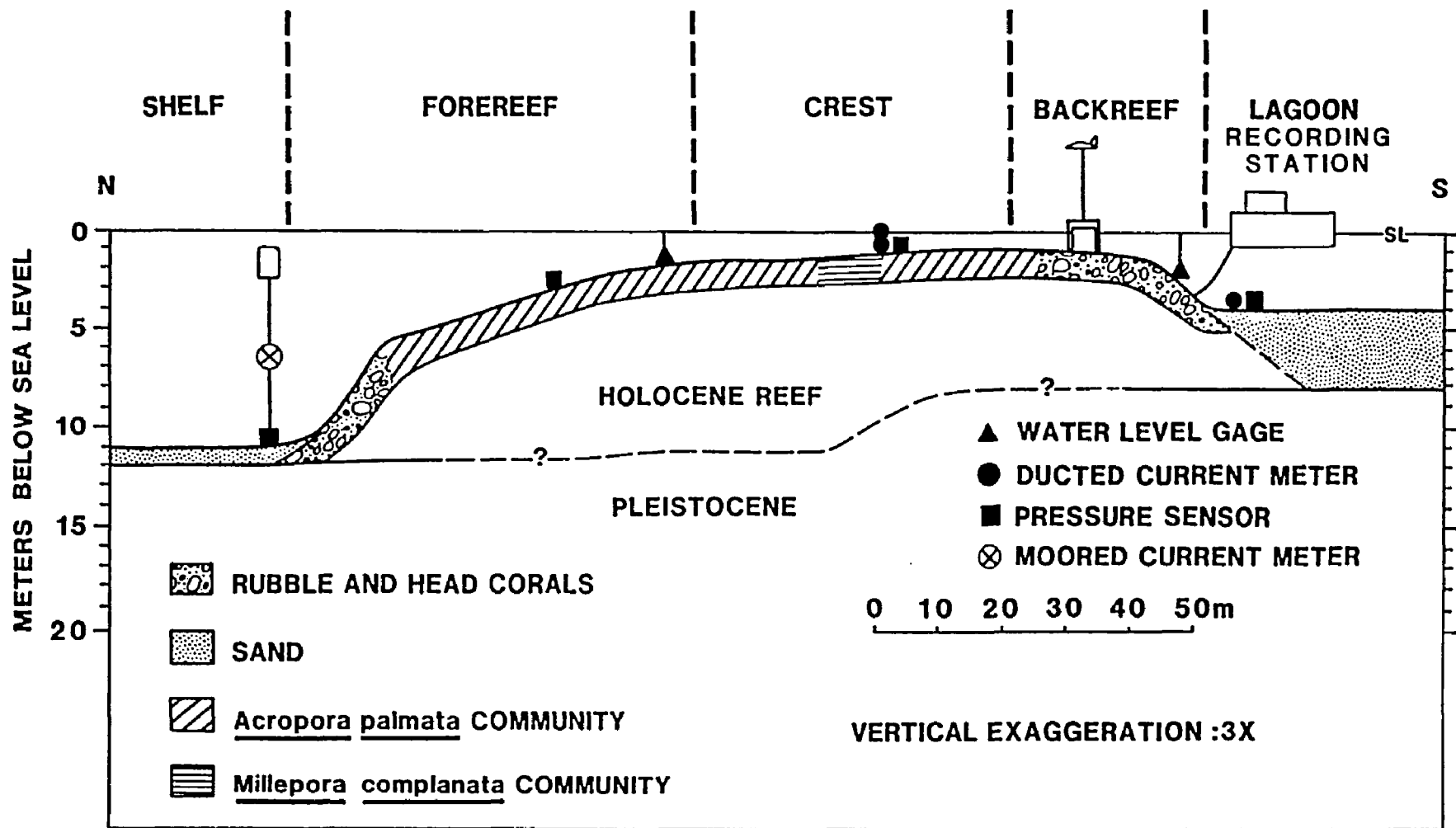


Fig. 3.1. Instrument arrangement across the reef profile employed during Experiment 1.

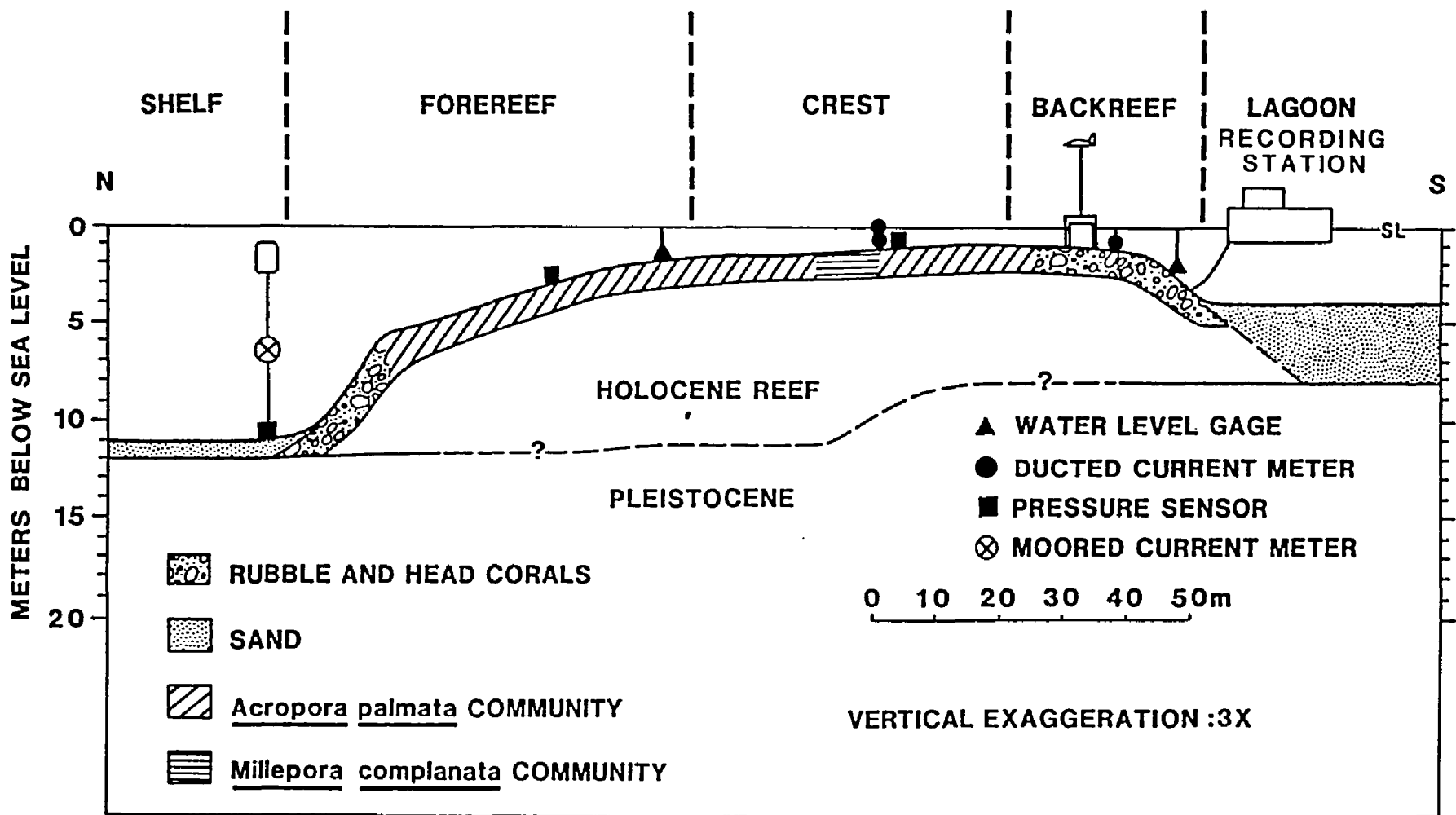


Fig. 3.2. Instrument arrangement across the reef profile employed during Experiment 2.

Experiment 3

Experiment 3 started on April 7, 1400 hours, and ran until April 9, 1400 hours --two tidal cycles. The experimental design for instrument deployment is illustrated in Figure 3.3. In this experiment, waves and their currents were measured at the forereef, crest, and backreef stations. A third wave sensor was installed at the backreef station, 0.15 m above the floor. A current meter fixed 1.0 m above the sea floor was also installed over the forereef for this experiment. This configuration was designed to study wave energy decay across the reef transect, and the forereef to backreef flow field.

Experiment 4

Finally, Experiment 4 was conducted on April 9, beginning 1300 hours, and lasted for 1 hour and 55 minutes. Instrument arrangement was identical to the one used for Experiment 3. The objective of this experiment was to collect data that might contain information about infragravity oscillations that may exist at the experiment site.

Most data collected during the study consisted of digital time series records. Data reduction was accomplished using standard methods of time series analysis. Differences in record duration and sampling rates of the instruments allowed estimation of parameters in three spectral bands: surface gravity, infragravity, and tidal bands. Tidal and infragravity information was determined using tidal records from the Sea Data pressure gages and Endeco records whose Nyquist frequencies were 0.267 and 0.25 cpm, respectively. Surface gravity wave characteristics were estimated using the records obtained with the pressure sensors across the reef profile. Spectral components were calculated using a Winograd Fourier Transfer algorithm of the CSI computer library. Quantities such as coherence squared and phase angles, transfer functions, and attenuation coefficients were estimated following procedures

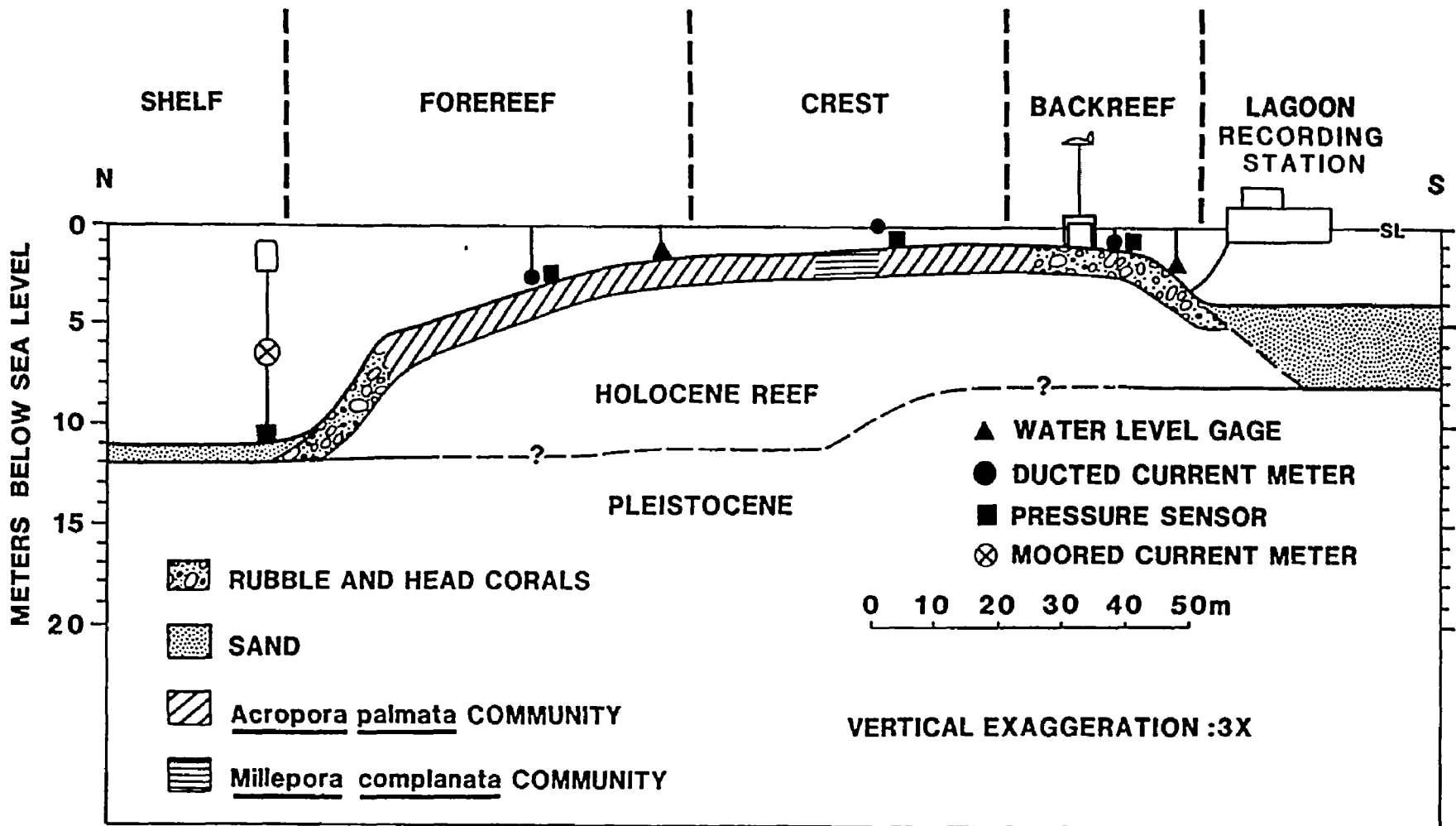


Fig. 3.3. Instrument arrangement across the reef profile employed during Experiments 3 and 4.

outlined in Bendat and Piersol (1986). Numerical filtering techniques were applied in some instances to isolate frequency components of interest in the records. This procedure consisted of suppressing the Fourier components of the undesired frequencies. When the amount of data was not sufficient to satisfactorily resolve the parameters of interest using spectral calculations, other methods were employed. These methods are discussed in the appropriate chapters.

4.0 Meteorological Conditions

Meteorological factors can influence and control oceanographic processes such as waves, surface slopes, and water circulation. Knowledge of these meteorological conditions prevalent during an oceanographic experiment is necessary to fully understand the oceanographic observations. The objective of this chapter is to present the regional meteorological framework within which the specific data sets regarding reef dynamics at Tague Bay (St. Croix) were taken. Winds and barometric pressure in the area are described. Since many physical processes in the ocean are not related to concurrent meteorological observations but with previous conditions, due to thermal and dynamical inertia, the selection of data for this chapter start on March 23, 1987, one week prior to our field data collection period.

Prior to the experiment on Tague Reef, a high pressure center over the eastern Atlantic caused the winds to flow from the southern quadrant at speeds of 1 to 10 $\text{m}\cdot\text{s}^{-1}$ for 3 days (Figure 4.1a). During this period there were two fetches, wave generation regions, that may have influenced the wave field around the island; one lay to the east and was driven by easterly winds with speeds of 7.5 $\text{m}\cdot\text{s}^{-1}$. The second was to the northwest of the island with winds of 15 $\text{m}\cdot\text{s}^{-1}$. On the 26th (Figure 4.1b) a high pressure center moving from the west displaced all weather systems to the east and dominated the wind circulation. Winds shifted to the NE and continued to blow until the 29th at speeds ranging from 1 to 8 $\text{m}\cdot\text{s}^{-1}$. A fetch directly north of St. Croix, with winds having maximum speeds of 18 $\text{m}\cdot\text{s}^{-1}$, was the most significant wave generation area during this period. On the 31st (Figure 4.2a) winds started shifting to the ENE under the clockwise circulation of a high centered at latitude 35° N and longitude 70° W and continued rotating until blowing from the SSE

Fig. 4.1. Synoptic weather maps of the tropical Atlantic region during March 23 (A) and 26 (B) of 1987. Notice the southerly flow in A and the cyclonic (C) circulation present in B.

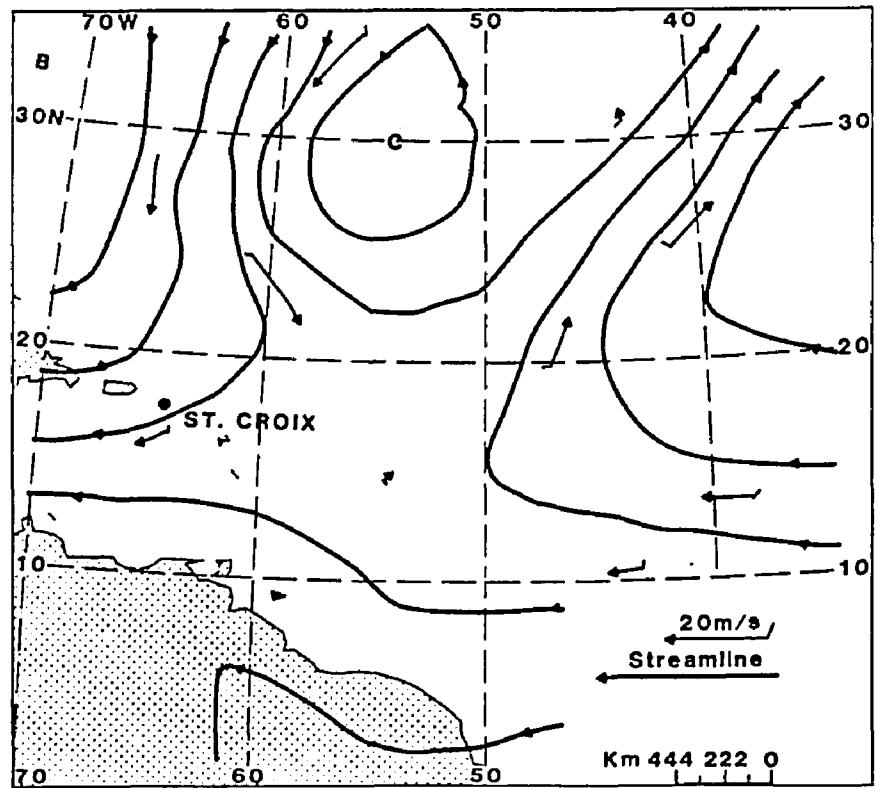
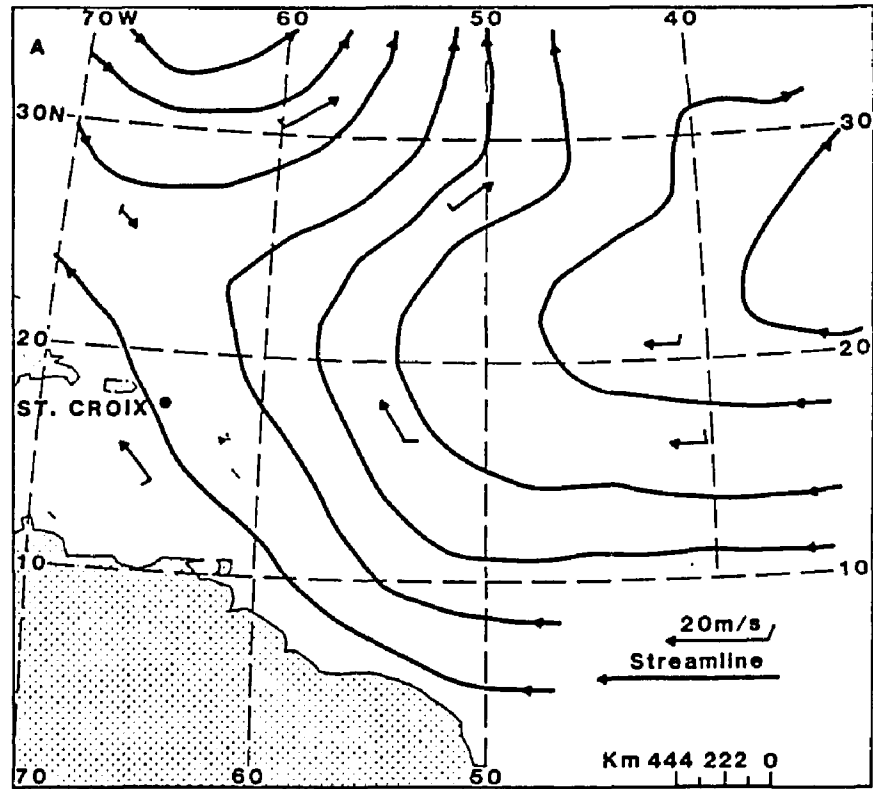
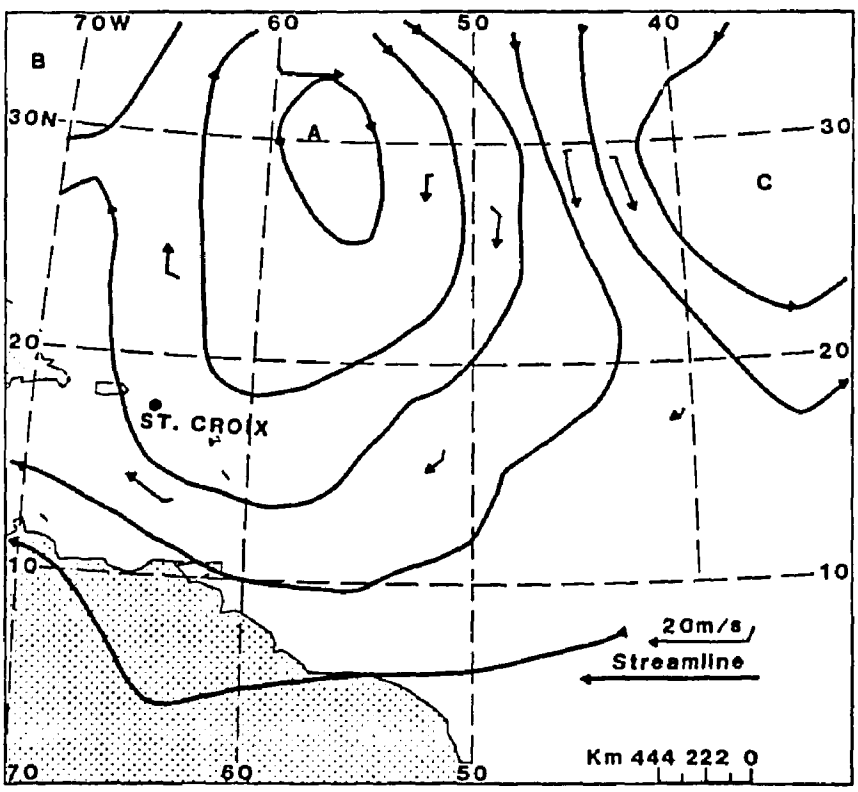
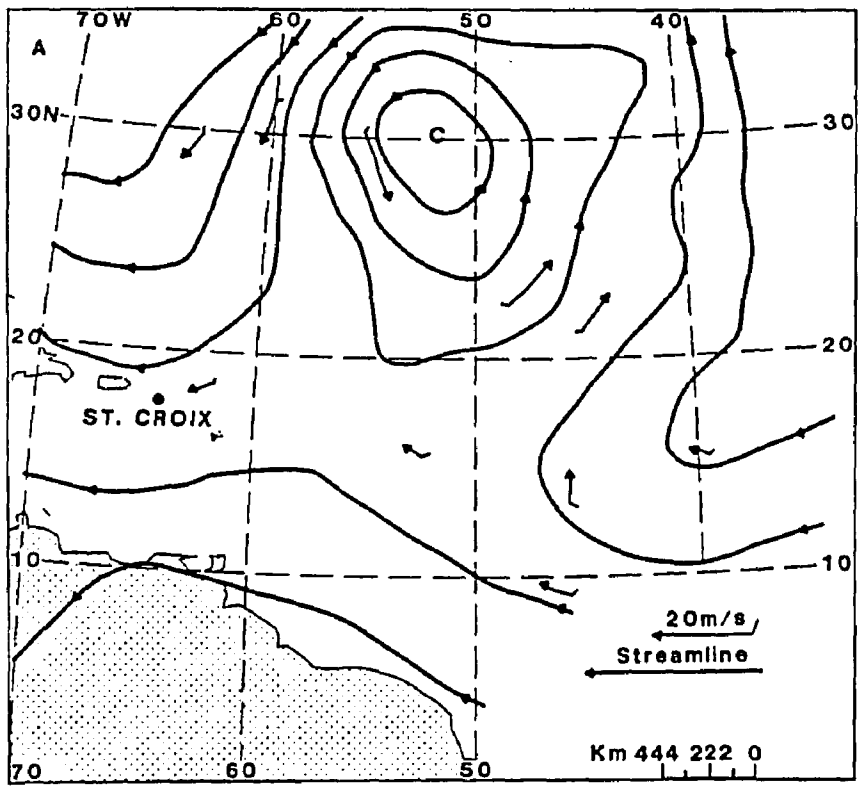


Fig. 4.2. Synoptic weather maps of the tropical Atlantic region during March 31 (A) and April 5 (B) of 1987. The cyclonic (C) circulation is still present in A; in B a large anticyclonic (A) circulation appears with the cyclonic pattern displaced eastward, representing easterly atmospheric waves.

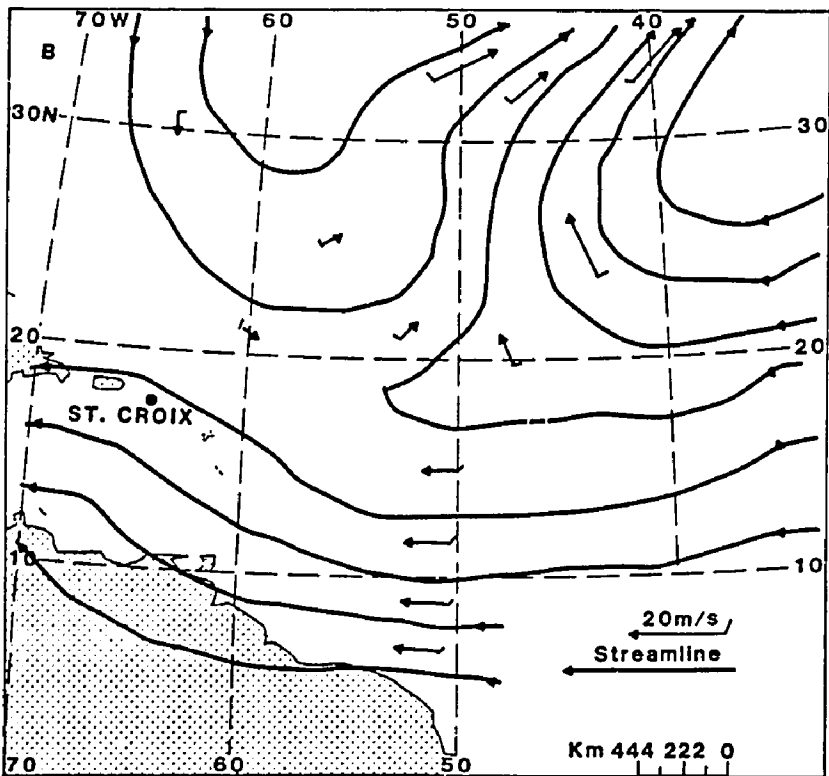
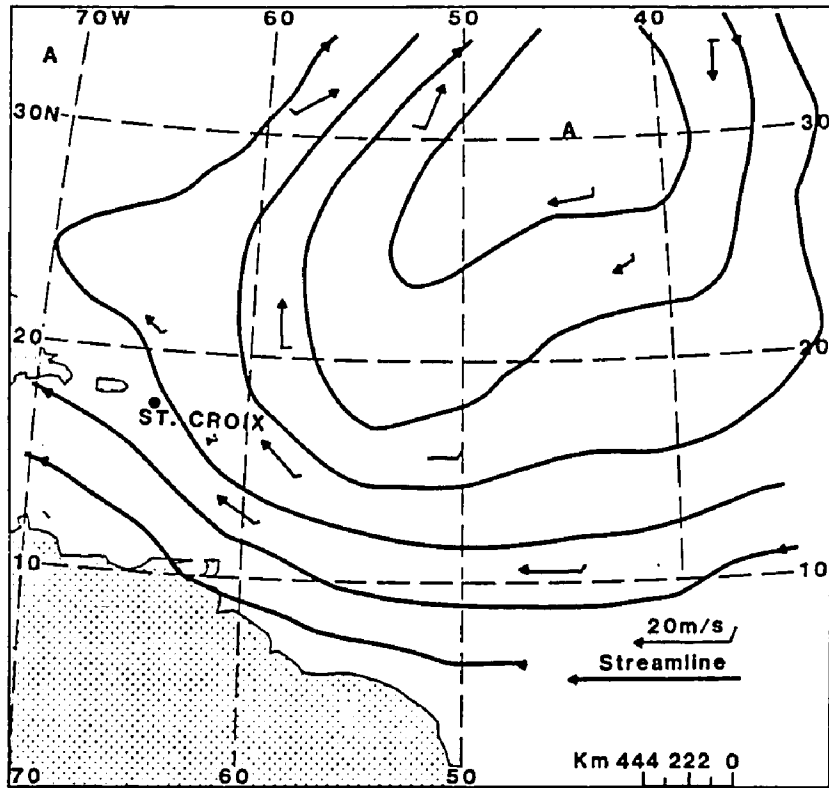


(Figure 4.2b), with speeds ranging from 1 to 5 m·s⁻¹. The fetch with strongest winds during this time was located around latitude 25° N and longitude 60° W. On April 7th, another high pressure center north of Hispaniola dominated the circulation, and winds blew from the NNE- E at a low speed of 1 m·s⁻¹. After this event, an intense high pressure center located near latitude 32° N and longitude 44° W (Figure 4.3a,b) controlled the circulation until the 12th. During the early stages, the winds blew from the SE at 5 m·s⁻¹, then gradually rotated cyclonically to the NW as the center weakened and moved to the NE.

Minimum air temperatures from, the Cotton Valley 2 weather station, 8.5 km west of the study area, had an average of 22.1°C between March 23 and April 12, 1987 (Climatological Data, 1987). The mean sea surface temperature was 26.3°C during March and 27°C in April 1987 (Oceanographic Monthly Summary, 1987). The sea surface anomaly (which is the difference between the monthly mean and the climatological mean sea surface temperature) was + 0.5°C during April. Information was not available for March. A positive anomaly indicated a temperature higher than the climatological mean sea surface temperature.

Surface weather maps allow one to hindcast wave conditions in a specific generating area. The wave generating areas in the North Atlantic consist of a series of cyclonic (low pressure) and anticyclonic (high pressure) centers travelling eastward. These centers act as sources of waves that potentially reach the study site at St. Croix. The moving centers prevent the sea surface from reaching an equilibrium with the winds due to the limited duration of the winds over the fetch. Under these conditions the hindcast can be done using the JONSWAP spectrum (Hasselmann et al., 1973).

Fig. 4.3. Synoptic weather maps of the tropical Atlantic region during April 8 (A) and 11 (B) of 1987. The anticyclonic (A) circulation is still present in A; in B the lower part of both cyclonic and anticyclonic patterns of easterly atmospheric waves is present.



The peak frequency in cps is estimated using the following relationship:

$$f_m = 3.5 * \tilde{X}^{-0.33} * \frac{g}{U}$$

where \tilde{X} is the nondimensional fetch length given by:

$$\tilde{X} = \frac{g X}{U^2}$$

The variable X is the fetch length in meters. Reading the appropriate values of U and X from the synoptic weather maps of the Caribbean, one can calculate the peak wave frequency for a given fetch area. The calculations show that for March 26, 1987, the peak period is calculated between 16-17 s ($U = 18 \text{ m}\cdot\text{s}^{-1}$, $X \sim 944\text{-}1,222 \text{ km}$). The peak period for March 31 and April 1st ($U = 10 \text{ m}\cdot\text{s}^{-1}$, $X \sim 889\text{-}1,833 \text{ km}$) is estimated at 12-16 s. For comparison, the observed wave period for trade wind waves in Grand Cayman is between 6-8 s (Roberts et al., 1975).

Barometric pressure observations made in the Puerto Rico airport (18.5° N , 66.12° W), to the northwest of the study site, were employed to infer trends during the study period. The pressure started at 1010 mb on March 23, rose to 1015 mb by the 29th, and fell to 1011 on April 1st. After this time it rose and then oscillated around 1014 mb with nearly a diurnal period (Fig. 4.4).

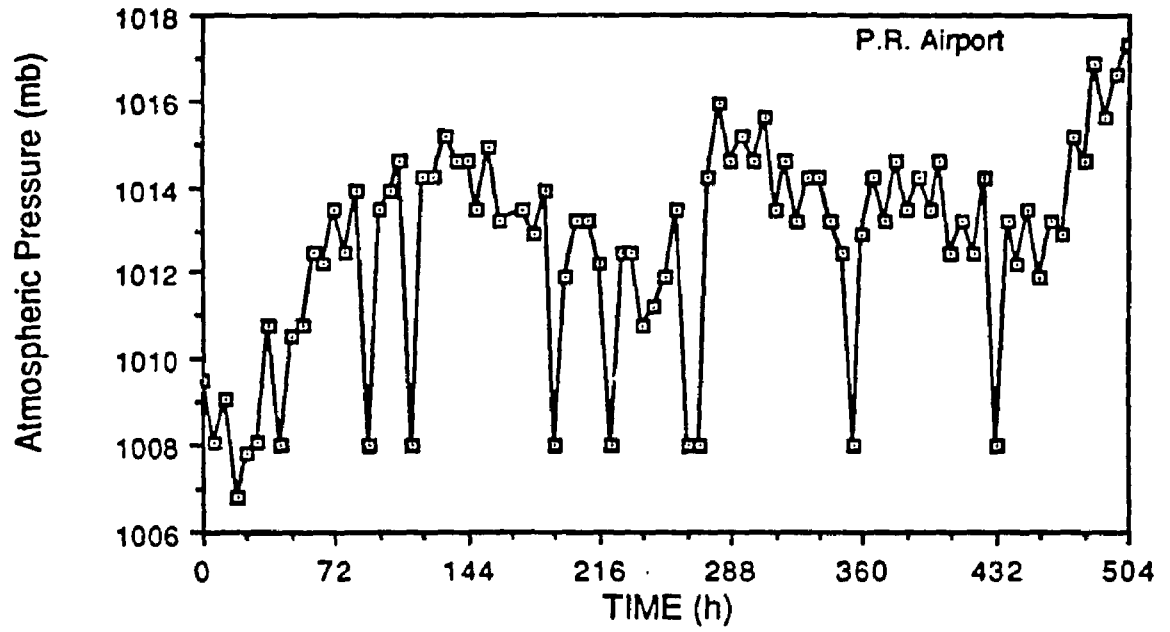


Fig. 4.4. Barometric pressure observed at the Puerto Rico airport showing the passage of atmospheric waves.

5.0 Infragravity and Long-Period Physical Processes

The meteorological and oceanographical processes with time periods of days to minutes constitute the physical background setting for this research and are the central theme of this section. Understanding these oceanographic and meteorological processes is important because they serve as driving agents of water motion around the reef and act as modulating agents for processes of shorter duration. This chapter will discuss and interpret data that relate to meteorological and oceanographical factors. The information is presented in five sections: a discussion of tide measurements, water temperatures, sea level differences, and currents in the forereef channel. Besides presenting the data, the importance of these processes to the reef ecosystem is assessed.

Water Level Measurements

Water level measurements made at the forereef and backreef are presented in Fig. 5.1. Each curve shows 9 complete cycles tidal with one high and one low water per day. Water level data collected on the southern coast of the island also have a diurnal character (Roberts, unpublished data). Previous investigations in the region also have observed a diurnal tide (Ogden, 1974; Kjerfve, 1981). Because the water level time series is short (9.5 days), it is impossible to identify which diurnal component is dominant in this setting. According to the Rayleigh criteria (Pugh, 1987), at least 14 days of measurements are needed to differentiate among the diurnal periods.

A feature present on both tide records was the amplitude modulation. It was induced by the semimonthly north-south motion of the moon (Pugh, 1987). The tidal range was maximum at the beginning of the experiment. The forereef maximum range was 33.1 cm, the lagoon 31.9 cm, in reasonable agreement with previous works (Ogden, 1974). By the end of the measuring period both

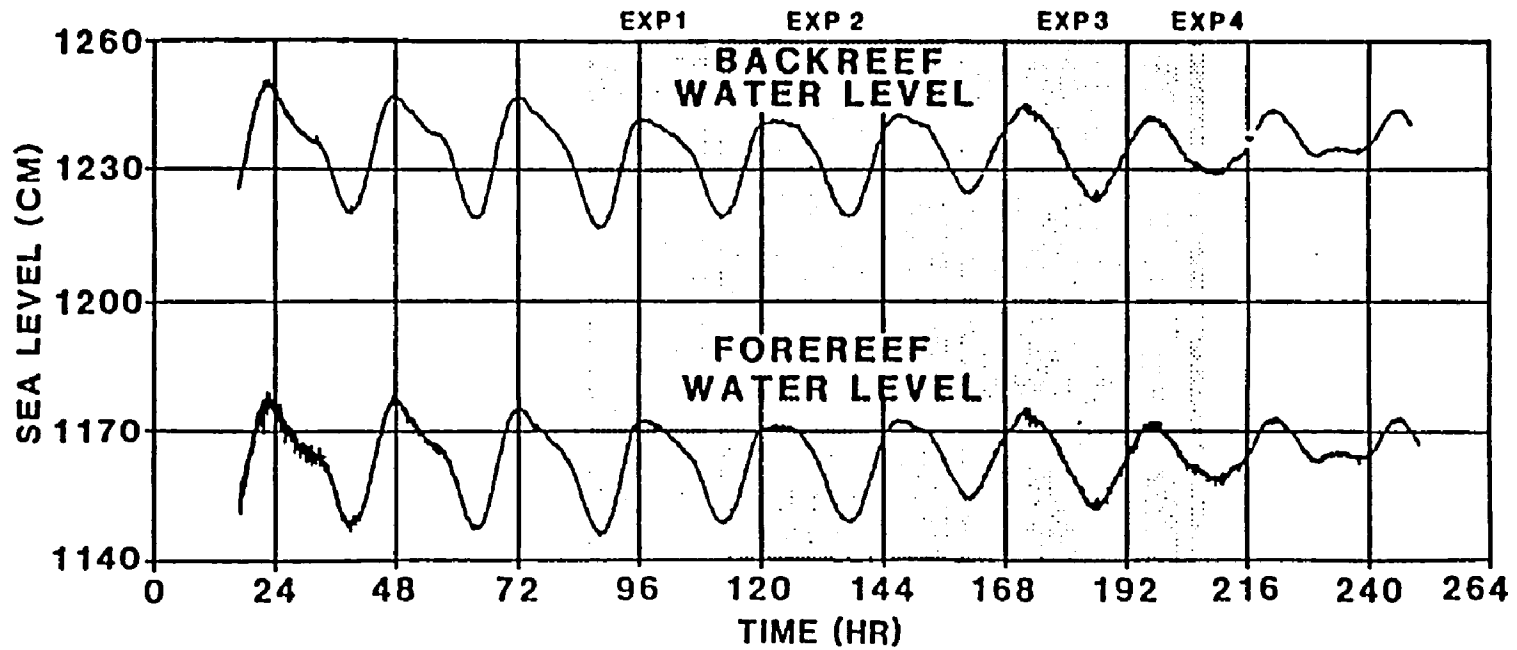


Fig. 5.1. Water level curves showing diurnal tidal variations at the forereef and reef lagoon during the study period.

records reached their minimum range of 11.8 cm. These figures were not corrected for barometric effects. Forereef and backreef curves were similar and appear synchronous. In systems whose geometry and tidal range are such as to give rise to ponding, the lagoon tidal curve becomes highly distorted during low water (Ludington, 1979; Farrow and Brander, 1971). Ponding refers to the trapping of water inside the atoll lagoon as the tide level drops below the atoll rim depth. In these cases, the sea level drop at the lagoon resembles the curve of a basin being emptied through an orifice. If a lagoon has a restricted connection with the open sea, the lag of the tidal curves is large, and the amplitude is modified by friction and shallow water effects (Farrow and Brander, 1971; Pugh and Rayner, 1981). If a relatively free connection exists, comparison of the lagoon water levels and oceanic tides shows few differences (Pugh and Rayner, 1981; Hearn and Parker, 1988). The present data illustrate a small difference in tidal range (1.2 cm), and no deformation of the lagoon tide curve is observed. Both observations agree with those of Hearn and Parker (1988) working in Australia in a system with similar geometry to Tague Reef. Based on their observations, I conclude that a relatively free connection between the lagoon and sea exists and the contribution of reef geometry to deformation of the tidal wave is small.

A detailed examination of Fig. 5.1 reveals the presence of a high frequency fluctuation, which is rather conspicuous at the beginning of the forereef record. A high-pass filtered (1-hour cut-off) version of the data and a blowup of the first 300 min of the lagoon record (Fig. 5.2) confirm the presence of these variations with an amplitude of approximately 1.0 cm and a period close to 30 min. The high-passed lagoon data show that the amplitude was greater at the beginning of the record, decreased at the middle, and increased at the end of the record. The forereef record shows the same variations of

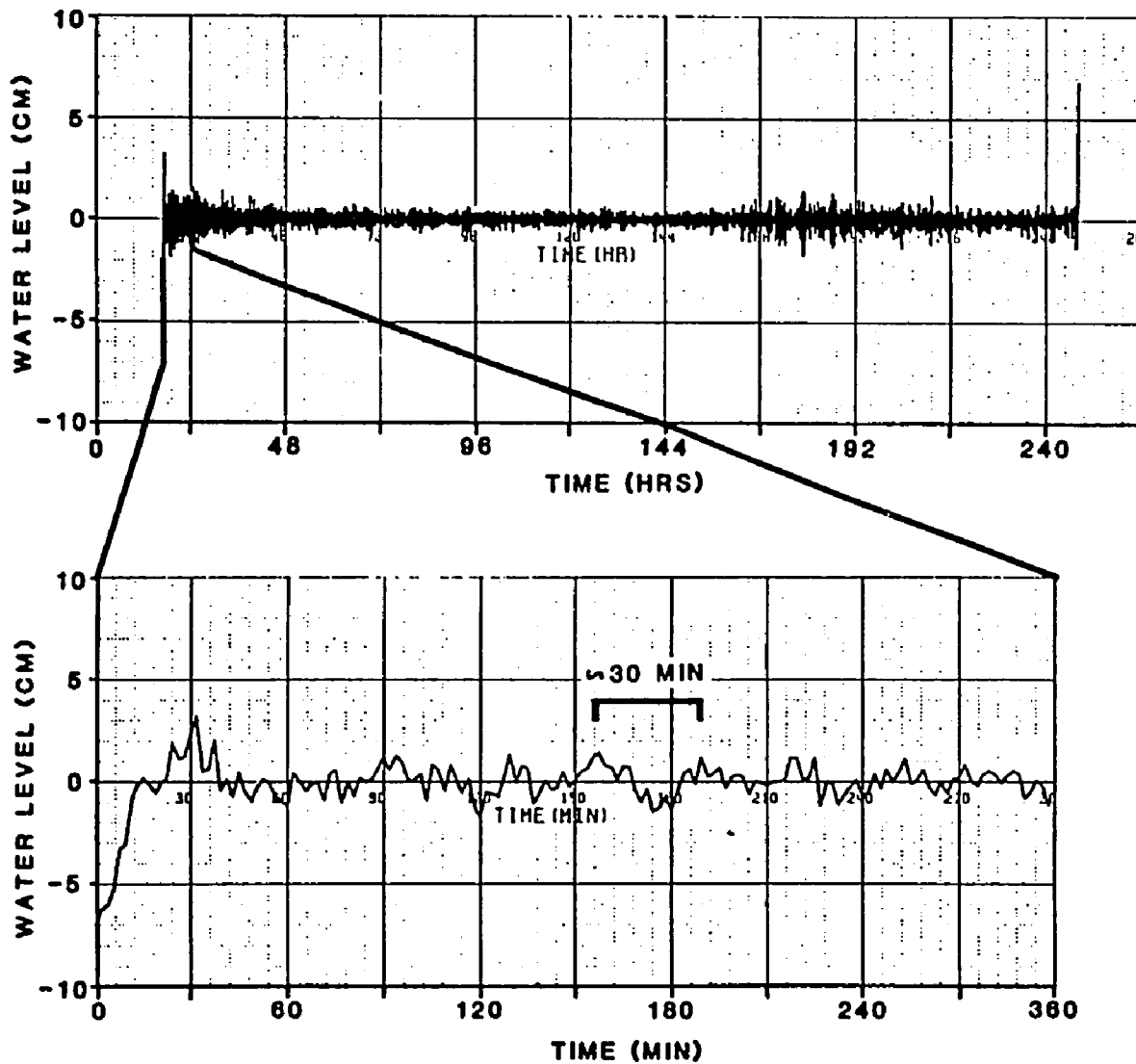


Fig. 5.2. High pass (cut-off 1 min) of the lagoon water level showing infragravity oscillations with a period of 30 min.

amplitude. Similar long period (15-30 min) oscillations of sea level were found by Roberts and Suhayda (1983) working in Nicaragua. However, the amplitude they observed (4-8 cm) was about twice the value observed on this study. This difference in amplitudes cannot be explained at this time. The spectra of lagoon water level variations is presented in Fig. 5.3. Inspection of this curve reveals the presence of three peaks. The first peak contains the diurnal oscillations, whose resolution is very poor because of the short time series. The forereef spectra contain similar peaks. Their amplitude, calculated as the square root of the product of the spectrum value and frequency interval, Δf , can be estimated as 6.9 cm in the lagoon. The second peak represents the semidiurnal tide. Its amplitude is estimated as 2.4 cm in the lagoon. The presence of this component is evident in the asymmetry of the water level curves. The third peak is located in the infragravity band. A spectrum, not shown, from water level measurements collected for nearly four days at Buck Island channel, shows a similar peak at a frequency of 3.6×10^{-2} cpm or a period of 27.7 minutes. The peak height is estimated as 1.7 cm in the channel, 1.8 and 1.6 cm at the forereef and lagoon. Agreement of period and amplitudes at three sites supports the idea of a single signal with a period of 27 minutes and height of 1.7 cm.

Cross-spectra calculations between water level time series were performed with the objective of estimating the related quantities of phase and coherence squared. The coherence squared was calculated using the following expression (Bendat and Piersol, 1986):

$$\gamma^2 = \frac{|G_{XY}|^2}{G_{XX}G_{YY}}$$

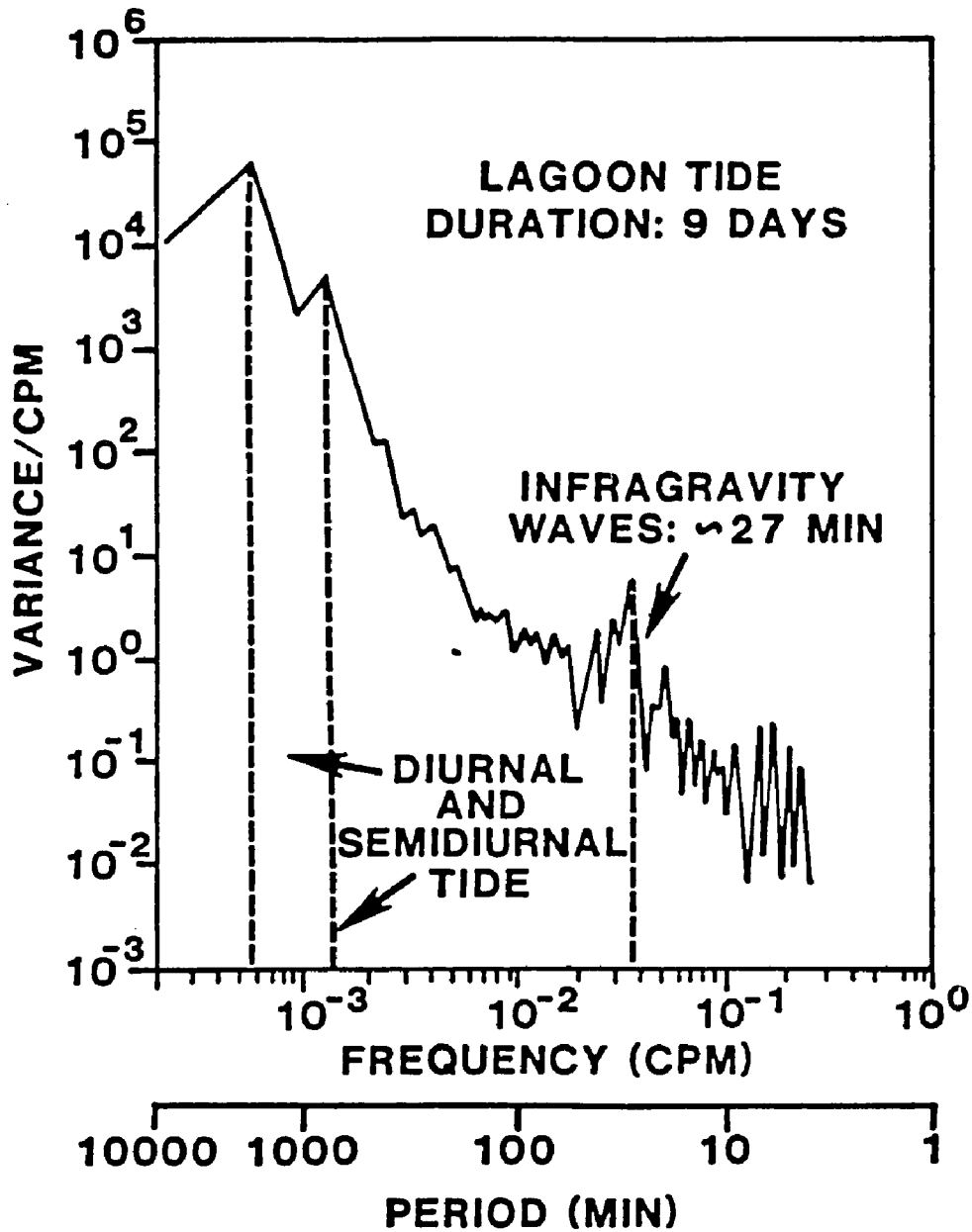


Fig. 5.3. Autospectra of the lagoon water level showing three distinct peaks at diurnal and semidiurnal, and the 27.7 periods. The latter represents the infragravity oscillations present in Fig. 5.2.

where G_{XY} , G_{XX} , and G_{YY} are the one-sided cross spectra and autospectra for signals X and Y. The value of γ^2 is always between 0 and 1. It is a measure of the amount of variance in signal Y that is explained linearly by signal X. A value of 1 indicates that signal Y is totally explained by signal X, a value of 0 indicates that signal Y is not related linearly to signal X. A value between 0 and 1 indicates that signal noise is present in the measurements, the relationship between Y and X is not linear, or other signals influence signal Y. The coherence is used over the forereef to detect frequencies present that may be crossing the reef crest and acting as energy sources for physical processes within the lagoon. The phase angle (θ) is estimated as:

$$\theta = \arctan \frac{Q_{XY}}{C_{XY}}$$

where Q_{XY} and C_{XY} are the imaginary and real parts of the cross-spectrum (Bendat and Piersol, 1986). Calculations were made using 10, 20, and 40 degrees of freedom (df). Values of coherence squared using 40 df are presented in Fig. 5.4A. The 95% significance level is represented by the horizontal line on the figure. Signals contained between 0 and 0.04 cpm, which include the three peaks discussed above, are significantly coherent in all cases. Both tidal peaks have a γ^2_{xy} equal to 1.0 with 10 df. The infragravity waves have a γ^2_{xy} equal to 0.94 with 10 df, and 0.88 with 20 and 40 df. The confidence interval for γ^2_{xy} in the infragravity band indicates that its true value lies between 0.79 and 0.99. Thus, about 90% of the variance in the 27 minutes signal at the lagoon can be explained using the forereef measurements.

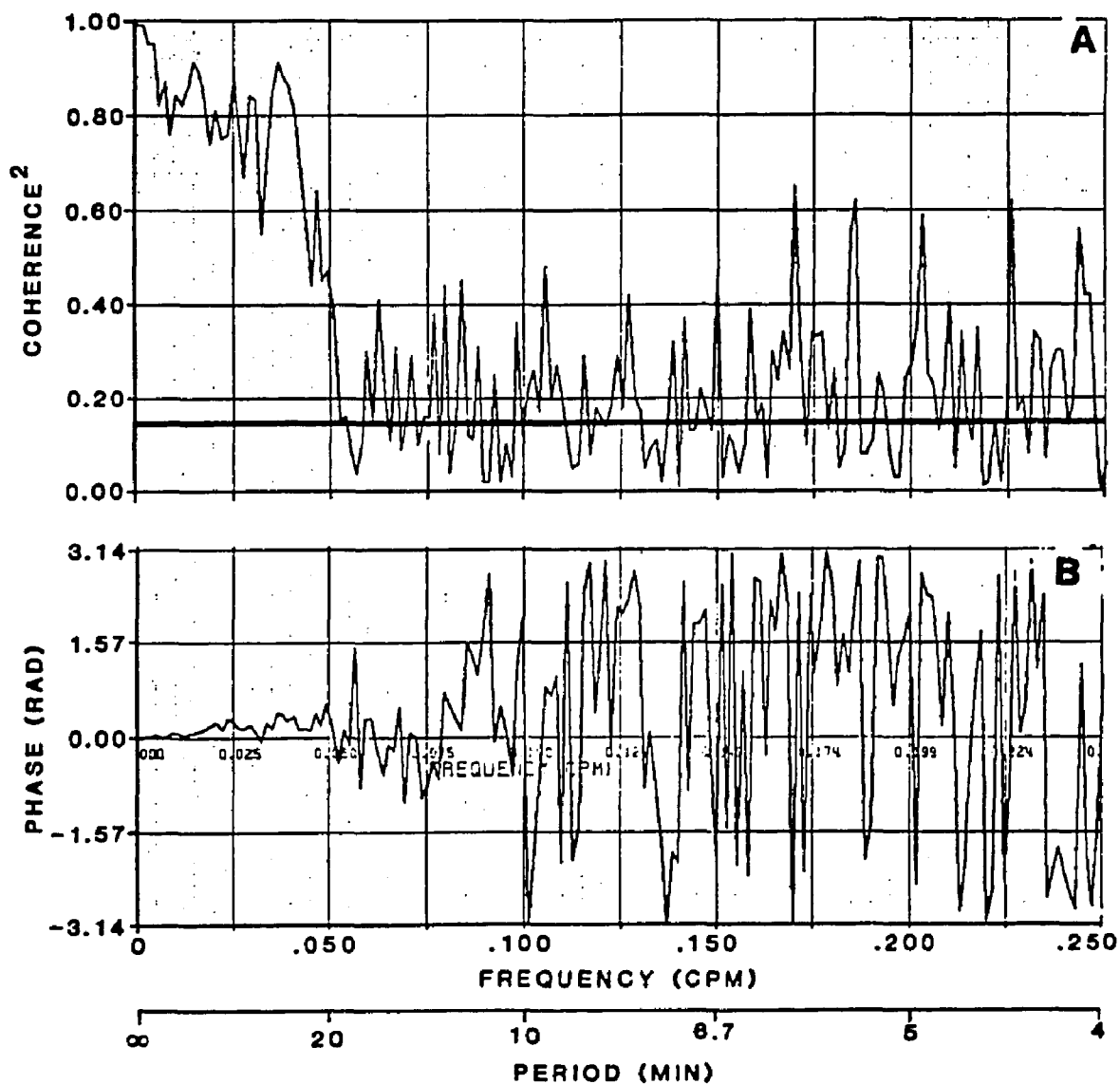


Fig. 5.4. Cross-spectra coherence squared and phase between the water levels at the forereef and lagoon. Notice the high coherence for periods greater than 20 min. The horizontal line represents the 95% significance level.

The phase (θ_{xy}), which is an estimate of the lag or time difference (τ) between both series, was calculated also with 10, 20, and 40 degrees of freedom. The values of θ_{xy} using 40 df are presented in Fig. 5.4B. The phase lag for the diurnal tide and semidiurnal tides is not significantly different from zero because of the short time series used. The 27.7 minute wave has over 450 cycles sampled during the experiment, and its phase lag should be adequately resolved by these techniques. The phase angle is 0.42 radians at 10 degrees of freedom, and the confidence interval indicates that it is significantly different from zero. The time lag calculated from this phase is 1.81 minutes, and the lagoon series leads the forereef series. The time resolution of the tide gages is 1.875 min in this case, making the estimate a borderline case. However, this phase appears physically reasonable. Assuming that infragravity waves are traveling parallel to the coastline, and using the shallow water wave equations, the time lag can be estimated. The difference between the time required for these long waves to travel a known distance through shelf and lagoon waters equals the time lag. This relationship is represented by the following, assuming that they enter the lagoon in phase, by:

$$\tau = t_L - t_F = L \left\{ \frac{1}{\sqrt{gh_L}} - \frac{1}{\sqrt{gh_F}} \right\}$$

where L is the distance traveled by both waves, h_L and h_F are the water depth of the lagoon and shelf, and g is the acceleration due to gravity. Using the average shelf water depth (14.7 m), average lagoon depth (4.9 m), and 3,394 m as the distance from the reef's eastern end to the measuring site gives a time lag of 3.45 min. The true time lag should be smaller than this estimate because the forereef station was near the reef crest and not at the mean shelf depth as

implied by the calculations. That the time lags should be smaller than 3 min can be visualized by imagining a shallow wave traveling through a channel that is divided by a sloping step at the center into halves of different depth. The resulting constant phase lines or wave crests will form an S pattern with the time lag decreasing across the sloping step. It must be pointed out that this model should hold equally well for the tides; however, the data do not allow a comparison in this case.

To explain the infragravity oscillation, the straight ledge model developed by Snodgrass et al. (1962) is applied to the northern shelf of St. Croix. This model assumes a stationary wave in the offshore direction and a traveling wave along the shelf. According to Summerfield (1969) this model implies a trapping of energy on the shelf by reflection at the shoreline and internal reflection at the shelf edge. The across-shelf wavelength estimated from the model is 23.7 km and represents four times the width of the shelf, 5.9 km. Thus, this value is reasonable to explain this oscillation as a resonance of long waves impinging on the northern shelf of St. Croix.

Water Temperature

Water temperatures, within the limitations discussed in Appendix A, at the forereef and lagoon are presented in Fig. 5.5. The most striking features of both curves are the daily fluctuations and the temperature difference between forereef and lagoon waters. Highest daily temperature and the maximum difference between stations occur at 1400 hours. The minimum temperature and thermal equilibrium between both stations occur near 0400 hours. The time of maximum and minimum temperature coincides with low and high tide conditions. In this case, tides augment the effects of incident radiation since low tides coincide with maximum insolation. Thus, heat is distributed in a shallower water column. Not all heat gain during the day is released because

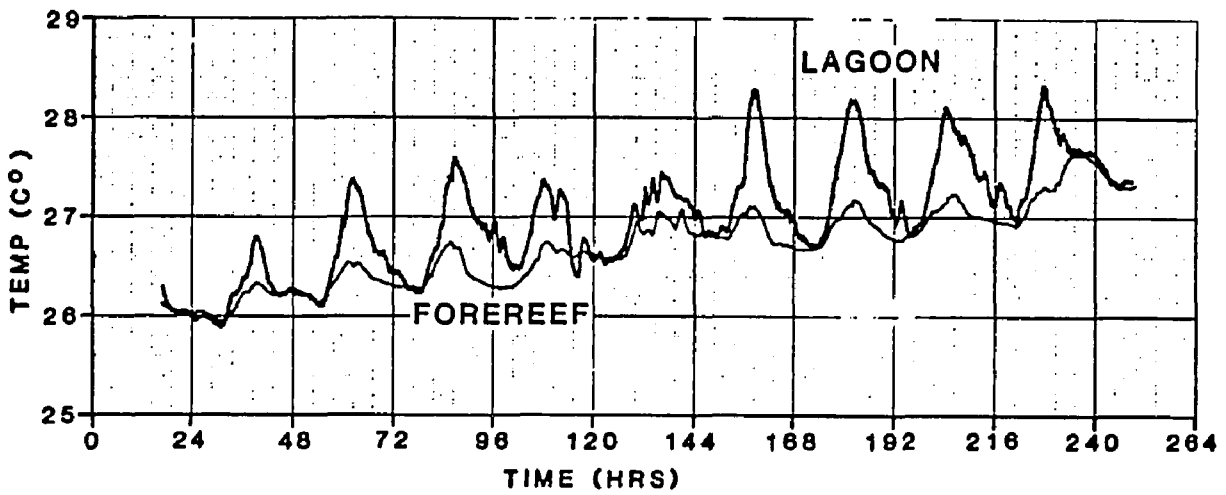


Fig. 5.5. Water temperatures from the tide gages at the forereef and lagoon showing diurnal oscillations. Notice that the lagoon waters are always warmer than forereef waters.

a net temperature increase occurs during the measuring period. This temperature increase may reflect the beginning of the summer heating season.

A mean temperature of 26.7°C (range 27.7°C to 25.9°C) characterizes the forereef. Lagoon waters had a mean temperature of 27.0°C (range 28.3°C to 25.9°C). The daily temperature range at the forereef was 0.4°C and 1.2°C on the lagoon, and the average daily temperature difference across the reef was 0.8°C. A simplified heat balance between input radiation and absorbed heat (von Arx, 1962) can be expressed in the following way for the temperature range, ΔT :

$$\Delta T = \frac{R}{\rho h C_p}$$

where R is the incident solar radiation per day, ρ is the water density at the in-situ temperature and salinity of 35.7 ppt, h is the water depth, and $C_p = 0.932 \text{ cal}\cdot(\text{g}\cdot^\circ\text{C})^{-1}$ the specific heat at constant pressure. Substituting the values of $h = 1,470 \text{ cm}$, $\rho = 1.023 \text{ g}\cdot\text{cm}^{-3}$, and $R = 7.17 \times 10^2 \text{ cal}\cdot\text{cm}^{-2}$ at latitude 17° N (Handbook of Physics and Chemistry, 1976) gives $\Delta T = 0.51 \text{ }^\circ\text{C}$ at the forereef. Values for the reef lagoon are $h = 490 \text{ cm}$, $\rho = 1.022 \text{ g}\cdot\text{cm}^{-3}$, and for the same values of radiation and C_p , give $\Delta T = 1.54^\circ\text{C}$. The agreement between observed and calculated values is excellent considering that some heat is lost by evaporation and other processes at the water surface. The maximum horizontal temperature gradient calculated from these values is 1.0 °C, which agrees very well with the observed value of 0.8 °C. Temperature gradients between the open sea and lagoon water have been documented in several studies (Pugh and Rayner, 1981; Andrews et al., 1984; Kjerfve 1978). Kjerfve (1978) states that heat is exported from the lagoon during day time and imported at night by advective processes. In atolls, heating of waters on calm days gives rise to lagoon stratification (Andrews et al., 1984), which traps cooler

bottom waters. The tide imports new cold water during flood and removes warm lagoon water during ebb. Pugh and Rayner (1981) used the warm lagoon waters as tracers to study the flushing mechanism in atolls. Their study indicated that the instantaneous horizontal gradient at the atoll is inversely proportional to the tidal range in lagoons of restricted connection with the sea.

Agreement between calculated and observed temperature changes around the reef, and especially at the forereef, gives support to the inference that forereef water characteristics are controlled by shelf processes and not by the local water depth.

The physical implications of these horizontal and temporal temperature gradients are reflected in the water density field. Forereef water is denser than lagoon water during daytime. At the reef crest, intense mixing of lagoon and forereef waters by wave breaking turbulence occurs. The resulting crest water, having a density greater than the lagoon water, flows down the backreef slope and settles in the lagoon bottom. The presence of cooler temperatures near the bottom, noted during dives made in the lagoon during the study, provides credibility to this hypothesis. Therefore, lagoon water is replenished from the bottom upwards, and vertical density gradients can develop under low wind conditions. Consequently, nutrient and sediment flows into the lagoon can be affected by the vertical stratification. Episodes of thermal stratification in the lagoon have been observed (Robinson Lance, personal communication). These processes may have some ecological consequences since the denser water has been intensively modified as it transits the reef crest (Hamner and Wolanski, in press).

In-Situ Winds

In-situ observations of wind velocity at the reef crest are presented in Fig. 5.6 (for the actual location of the anemometer see Fig. 2.1). The time series

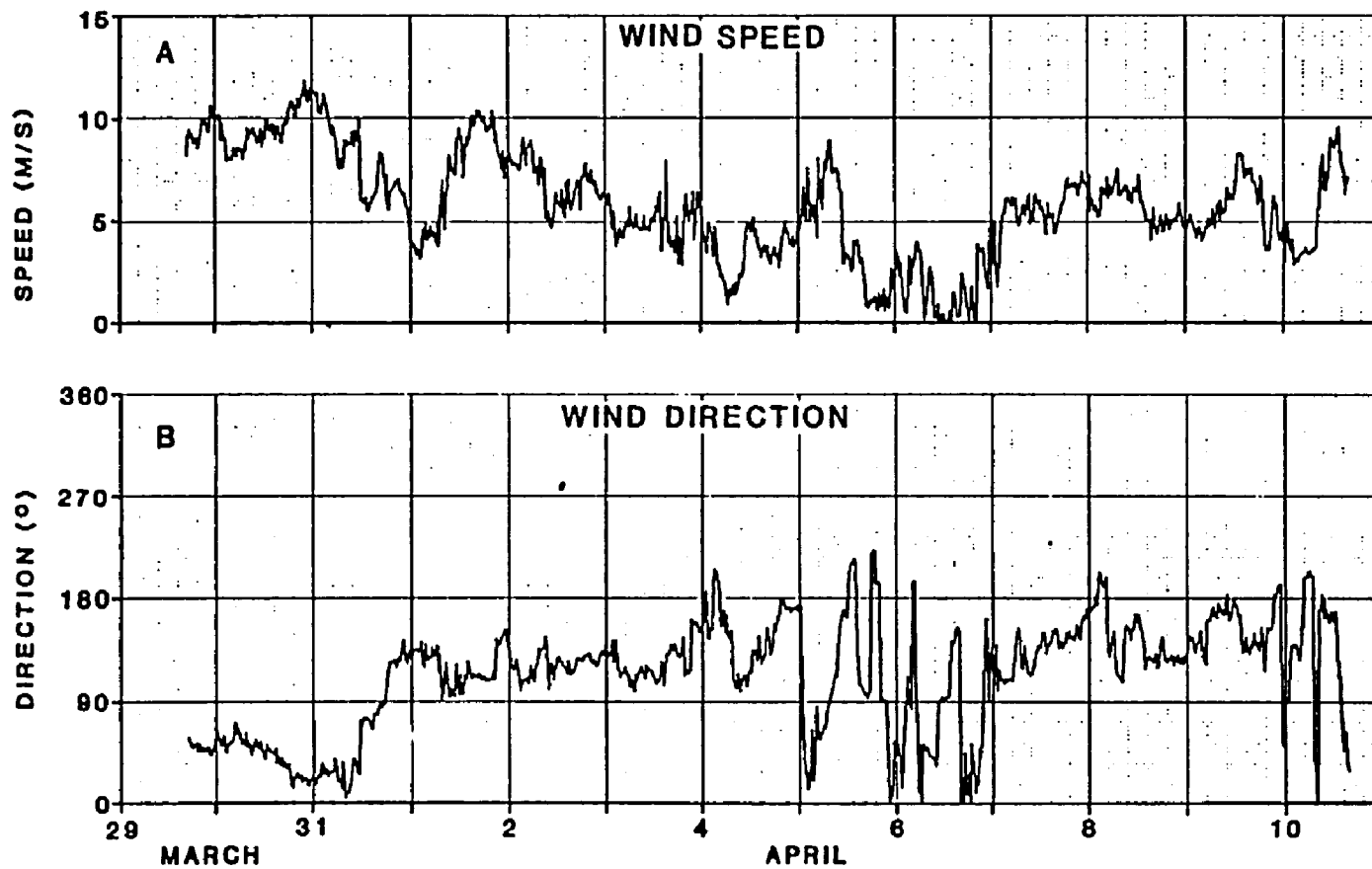


Fig. 5.6. Wind speed and direction measured at the reef crest during the study period.

started on March 29, 1987, and lasted over twelve days (see Chapter 3). Winds (Fig. 5.6B) started to blow from the NE with a speed of about $10 \text{ m}\cdot\text{s}^{-1}$, then shifted to ESE on the 31st with an average speed of about $6 \text{ m}\cdot\text{s}^{-1}$ for four days. On April 5, the winds became highly variable for two days; on the 7th, direction changed from ESE to S with speeds around $6 \text{ m}\cdot\text{s}^{-1}$ for three days. Finally, on the 10th the wind direction fluctuated from N to S and increased in speed to about $9 \text{ m}\cdot\text{s}^{-1}$ until the end of the experiment. Comparison with the meteorological conditions discussed in Chapter 4 reveals that the major wind events were recorded in the local measurements, and agreement is reasonable. Wind velocity (speed and direction) was decomposed into along-reef (u) and cross-reef (v) components, in a coordinate system rotated 26.5° to the east of magnetic north. These components are presented in Fig. 5.7. The u -component (Fig. 5.7A) blew toward the west through most of the measuring period with variable speed. One episode of wind shift is clearly visible. The episode occurs at the beginning of the measuring period with wind blowing from the north and turning to the east. The v -component (Fig. 5.7B) started turning strongly shorewards and alternated between offshore and onshore for the remainder of the experiment. The time speed averages are $-3.9 \text{ m}\cdot\text{s}^{-1}$ and $-0.64 \text{ m}\cdot\text{s}^{-1}$ for the u and v components. The net shoreward speed of the v -component results from the high speed ($11 \text{ m}\cdot\text{s}^{-1}$) at the beginning of the record. Fourier analysis of both components is presented in Fig. 5.8. The u -component spectrum (Fig. 5.8A) indicates a monotonic linear decay with possible peaks at 28 and 10 hours, but most of the energy lies at lower frequencies. The spectrum of the v -component, Fig. 5.8B, illustrates a possible peak in the low frequency band, between 30 and 21 hours. This peak can be interpreted as a sea-land breeze system and, because of the small size of the

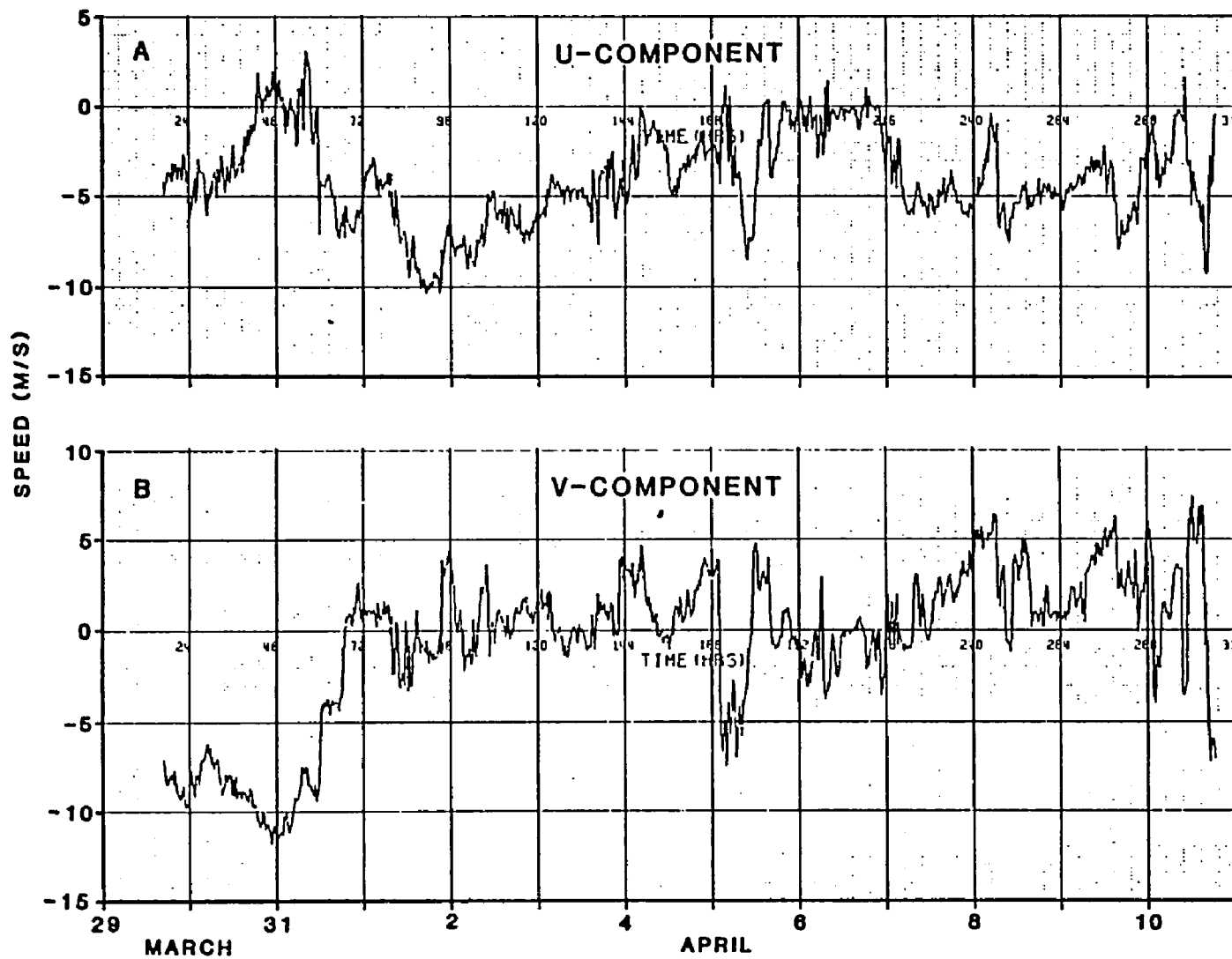


Fig. 5.7. Alongshore (U) and cross-shelf (V) components of the wind vectors using the coordinated system shown in Fig. 2.1.

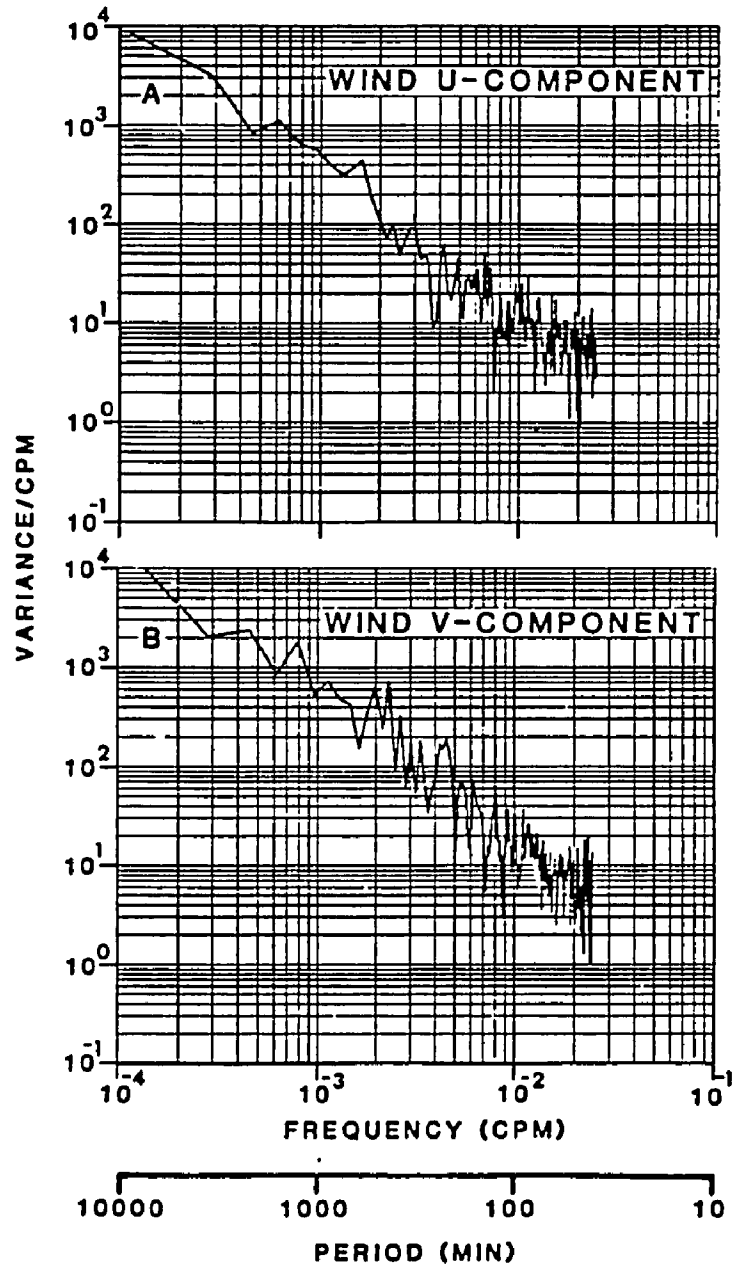


Fig. 5.8. Autospectra of the wind components with 6 degrees of freedom. The frequency step is 0.000172 cpm.

island and short time series, may be masked by the general wind circulation and not properly resolved by this technique.

Water Level Differences

Relative sea level differences across the reef crest are presented in Fig. 5.9. The striking feature of this plot is the presence of high frequency fluctuations that have the appearance of noise superimposed on long waves. The amplitude of these fluctuations is 2-3 cm at the beginning of the record and decreases to near 1 cm towards the end of the experiment. Long oscillations of the record have a period of 24 hours, and a comparison with the tide curves (Fig. 5.1) shows that each cycle of sea level differences matches identically with the tidal cycles. The cause of this 24-hour surface slope oscillation is not clear at this time; however, phase lags, or tidal amplitude attenuation between the lagoon and forereef are possible explanations. If infragravity waves are assumed to be sinusoidal curves of equal amplitude (a conclusion reached above) lagged in time across the reef crest, sea level differences can be calculated. Assume:

$$\eta_F = a \sin(\omega t),$$

$$\eta_L = a \sin(\omega t + \theta_{xy}).$$

If the phase lag is small, then the sea level differences are given by:

$$\Delta\eta = a\theta_{xy} \cos(\omega t).$$

These calculations indicate that sea level differences should have the same frequency as the infragravity waves, an amplitude directly proportional to the phase lag, and a 90° phase shift with respect to the forereef water level. The frequency spectrum of the relative sea level differences with 20 degrees of freedom is presented in Fig. 5.10. The figure shows that significant energy is located in the tidal band. A smaller, significant peak occurs at 27 min. This peak corresponds to the infragravity signal observed in the tide records.

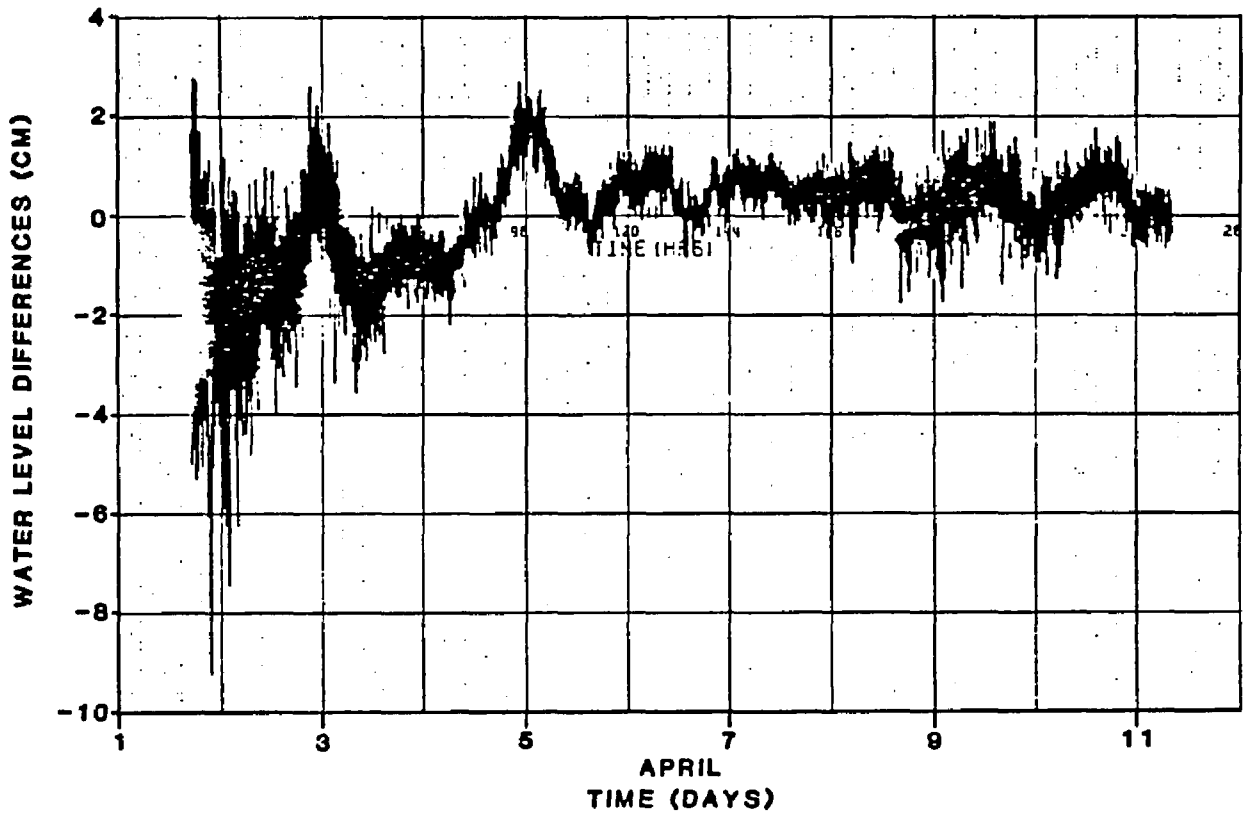


Fig. 5.9. Relative water level differences across the reef crest during the study period.

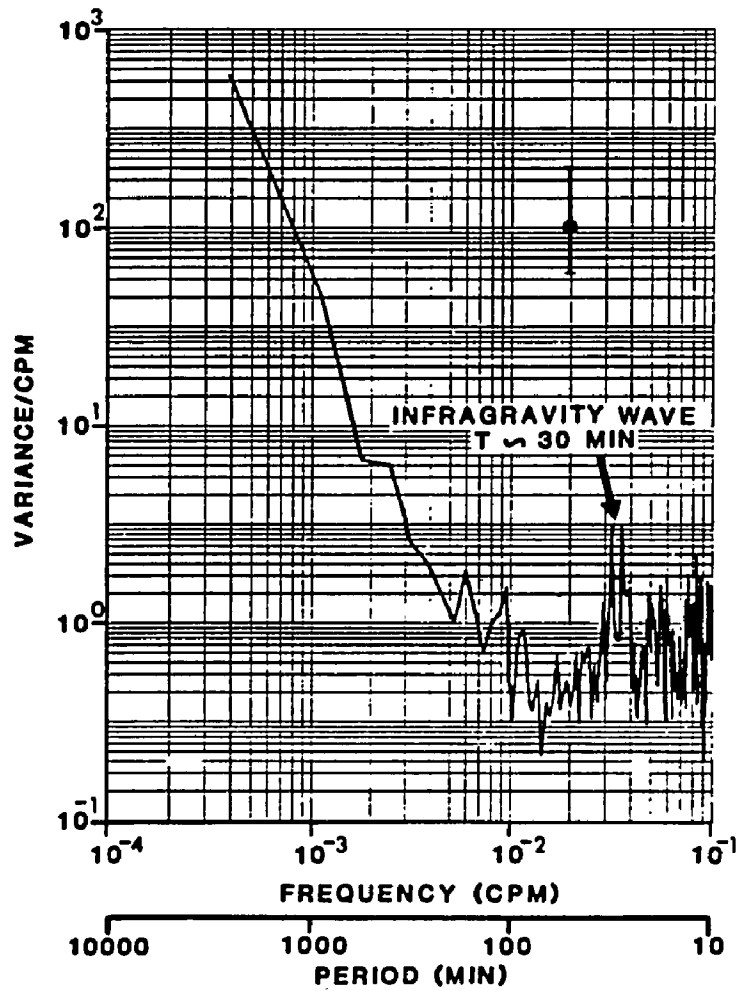


Fig. 5.10. Autospectra of the water level differences with 20 degrees of freedom. The frequency step is 0.00071473 cpm.

Calculation of the theoretical spectra for the sea level differences ($G_{\Delta\eta}$) and forereef water levels (G_F) based on this model suggest that a peak should exist at the same frequency.

The ratio of these spectra estimates equals:

$$\frac{G_{\Delta\eta}}{G_F} = \theta_{XY}^2$$

Substitution of the spectral values, $G_{\Delta\eta}=3$ and $G_F=17.9$, results in a phase lag of 0.42 radians. The calculated phase from the cross spectra is 0.39 radians. The agreement is excellent and provides supporting evidence to the hypothesis that sea level differences are due to alongshore phase lags. The phase lags result from differences in wave propagation over the forereef and in the lagoon. Another piece of evidence supporting the alongshore propagation of infragravity waves can be obtained from the phase lag between forereef tide record and water level differences. These calculations show that the phase lag is indeed close to 90° . Water level differences across the reef include effects of ponding (Ludington, 1979), surf beat oscillations (Seelig, 1983), and wave set-up (Tait, 1972; Gerritsen, 1981). Ponding and surf beat oscillations depend on tide characteristics, reef geometry, incident wave energy, and water depth at the reef crest. The sea level differences also depend on the width of the lagoon (Seelig, 1983). Gerritsen (1981) found that frictional effects reduce the amount of wave set-up, which contributes to sea level differences. The effects of long-period oscillations on set-up, considered by Gerritsen (1981), suggest the possibility that resonance on the shelf can contribute to and amplify the water level differences across the reef. Thus, the observed water level differences represent the sum of these processes. These water level differences in turn

drive currents that contribute to the flushing and material transport across the reef.

Long-term Current Measurements

Long-term current measurements were made at the forereef in Buck Island Channel, Fig. 5.11. The speed record, Fig. 5.11A, exhibits semidiurnal fluctuations, and the direction records was bidirectional, Fig. 5.11B. The maximum observed speed was $20 \text{ cm}\cdot\text{s}^{-1}$ and the most frequent speed was close to $10 \text{ cm}\cdot\text{s}^{-1}$. Current direction varied consistently between 120 and 288 degrees, with the westward flow lasting twice as long as the eastward flow. Velocity vectors (Fig. 5.12) were decomposed into a u-component (flowing along the reef) and a v-component (flowing across the reef) by rotating the coordinate system 26.6° to the east (Fig. 2.1). The u-component, Fig. 5.12A, was considerably stronger than the v-component. A net westward flow, indicated by the negative values, averaged $3.13 \text{ cm}\cdot\text{s}^{-1}$. Spectral analysis of this component, Fig. 5.13A, resolved one peak at the semidiurnal frequency and a monotonic decrease toward higher frequencies. The speed amplitude estimated from the spectrum at the semidiurnal frequency was $9.1 \text{ cm}\cdot\text{s}^{-1}$. The v-component time series (Fig. 5.12B) displayed high frequency oscillations of small speed. The time average was $0.21 \text{ cm}\cdot\text{s}^{-1}$ and directed lagoonwards. Variance values for the across-reef (v) component were one order of magnitude smaller than for the along-reef (u) component. The spectrum (Fig. 5.13B) peaked at the diurnal period. However, a large portion of the variance still occurred at semidiurnal periods. Working on the south coast of St. Croix, Roberts et al. (1981a,b) found that currents varied on semidiurnal and fortnightly time scales and responded to abnormal weather events. Tidal forcing of the currents outside the reef was observed by Greer and Kjerfve (1982) while working on Carrie Bow reef. Australian workers (Pickard, 1986;

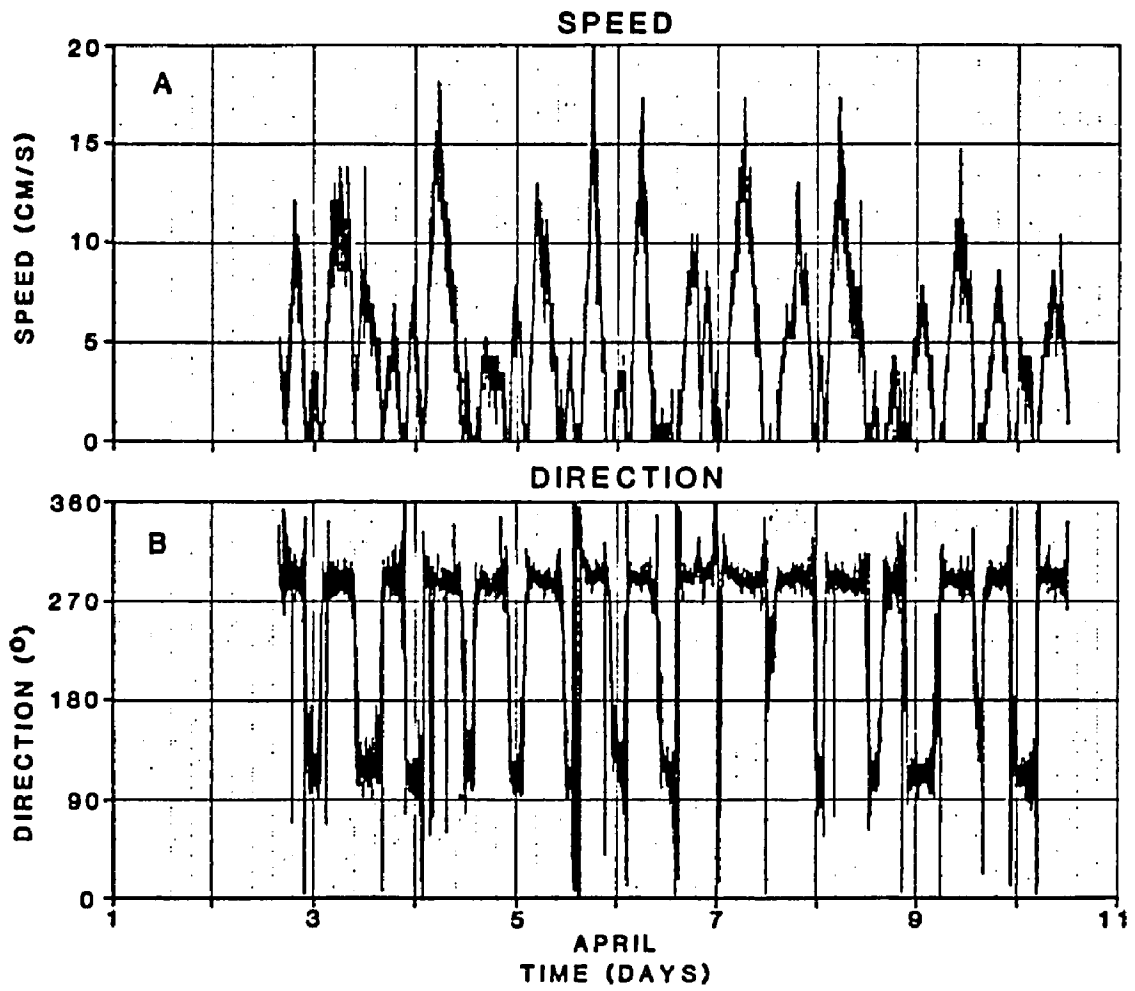


Fig. 5.11. Speed and direction of the Buck Island channel currents measured during the study period.

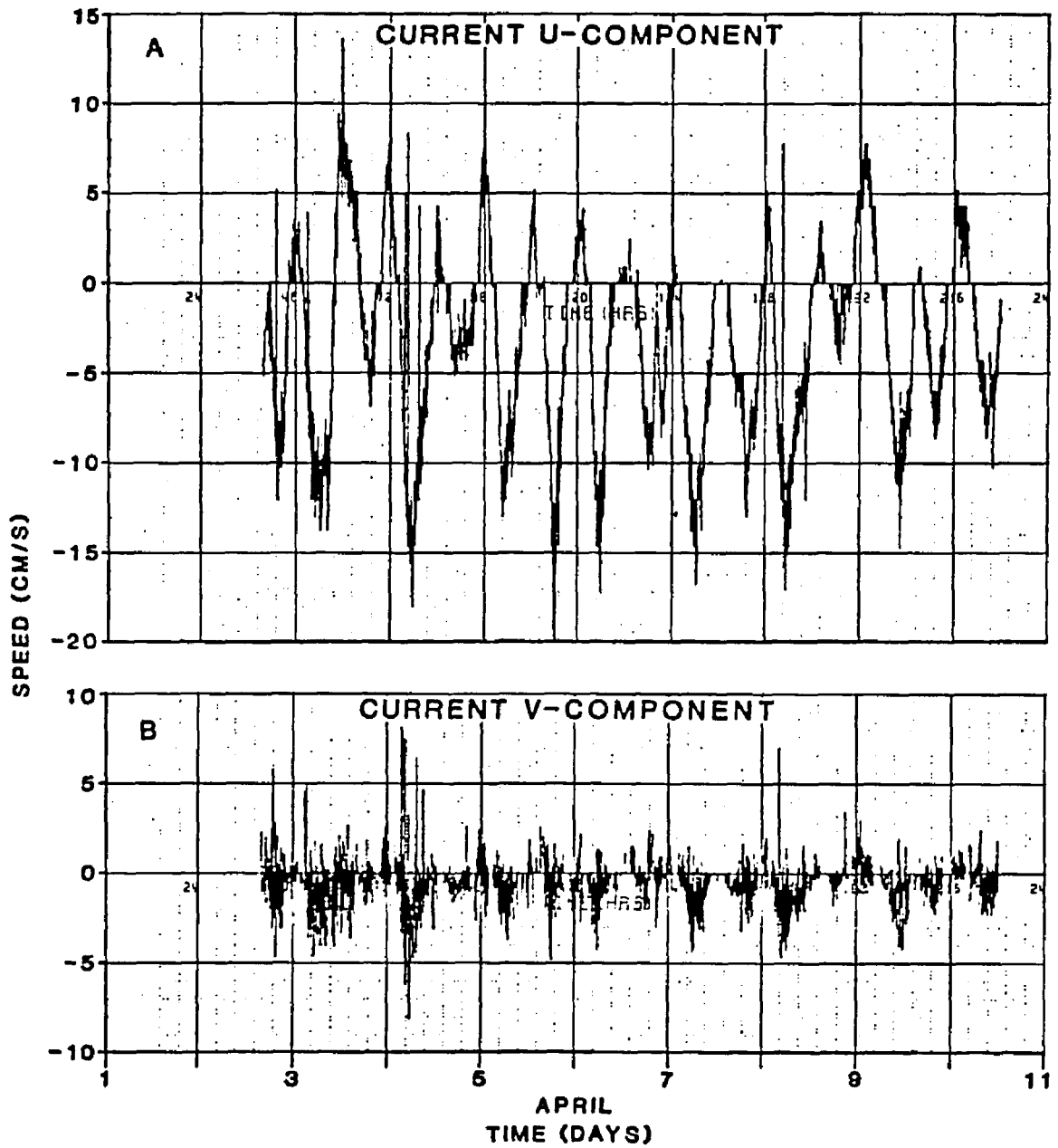


Fig. 5.12. Alongshore (U) and cross-shelf (V) components of the current vectors using the coordinated system shown in Fig. 2.1.

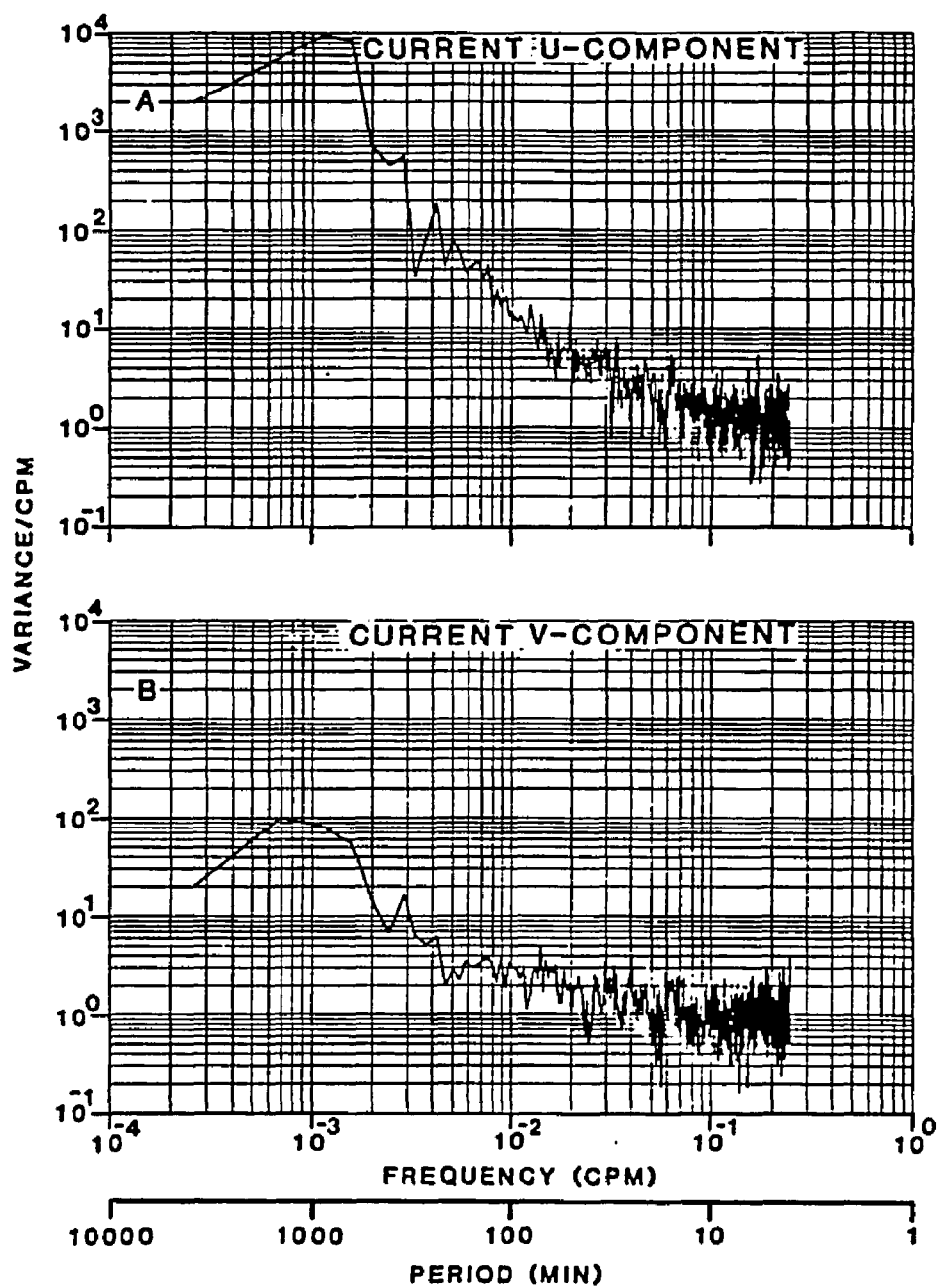


Fig. 5.13. Autospectra of the current components with 10 degrees of freedom. The frequency step is 0.0004396 cpm.

Wolanski and Pickard, 1983) found similar current patterns but in places with a considerably larger tidal range. The physical implications of these tidal currents are very important in creating water level differences and mass transport across the reef crest. Huthnance (1985) has shown that reefs are effectively transparent to tidal waves unless the reef crest is very broad (> 25 km). Sea level difference across the reef can be computed by:

$$\Delta\eta = V^2 \frac{Kd}{gh}$$

where h is the reef crest water depth, K is a friction coefficient, d is the width of the reef, g is the acceleration of gravity, and V is the current speed crossing the reef. This relationship reflects a balance between surface slope and bottom friction. The bottom friction is modelled by a quadratic law. Assuming that (a) the Endeco measurement is representative of a vertical average, (b) no stratification exist, (c) no friction occurs except across the reef, and (d) steady state exists, the above model can be applied in this study. Substituting the v -component time average corrected for depth changes ($4.8 \text{ cm}\cdot\text{s}^{-1}$), $h = 1.2 \text{ m}$, $d = 80 \text{ m}$, and using a K value of 0.003 (Huthnance, 1985), the sea level difference is 0.05 mm. This result indicates that currents in Buck Island Channel do not contribute significantly to sea level differences across the reef in this system. The mass transport across the reef per meter of crest width assuming a uniform current profile at the mooring station in Buck Island Channel, is 57 liters per second, resulting in a reef crest current speed of $4.8 \text{ cm}\cdot\text{s}^{-1}$, obtained from considerations of mass conservation. The cross reef current observations at the crest (Chapter 7) and in the lagoon (almost imperceptible to our sensors) are smaller than this value of $4.8 \text{ cm}\cdot\text{s}^{-1}$.

The latter results show that assuming a uniform current profile at Buck Island Channel is not correct. However, these calculations indicate an order of magnitude for the mass transport across the reef crest which, it will be seen later (Chapters 7), is of the correct order.

6.0 Wave Processes

Understanding changes in waves as they transit the reef and the physical processes that influence these changes comprises a major objective of this research. In previous chapters, results concerning several physical processes (sea level fluctuations, wind, and currents) that directly influence or modulate wave processes were presented. This chapter will focus on interpretation of measurements of waves traveling across the reef and of wave energy transformation. To fulfill this objective, four field experiments were conducted; however, only the representative Experiments 3 and 4 will be discussed in detail. Results from other experiments are presented in Appendix B. This chapter is divided into a discussion of methods and techniques of data analysis and separate discussions of results from Experiments 3 and 4. Wave attenuation by and transmission across the reef, tidal influence on wave attenuation and transmission, and the variability of these processes with frequency form the central themes of these discussions. The summary section presents the results of a model to predict wave height and energy dissipation based in part on an understanding of the reef system derived from field experiments.

Data Analysis

The general procedures of the data analysis were introduced in Chapter 3. In this section, specific techniques and details of the procedures will be discussed as applied specifically to wave data.

Spectra of wave pressure records were computed using a Winograd Fast Fourier Transform algorithm. Smoothing of the spectral curve was done in the frequency domain by averaging n contiguous estimates. After several trials, results suggested that smoothing with $n=8$ provided acceptable curves. The

spectral estimates calculated in this way had 16 degrees of freedom and a Nyquist frequency of 0.5 Hz. Conversion of the pressure spectrum to water level was done following the procedures of Kim and Simons (1974). The correction factor employed was expressed as:

$$K(f) = \left\{ \frac{\cosh\left\{2\pi\left(\frac{h-z_s}{\lambda}\right)\right\}}{\cosh\left\{2\pi\left(\frac{h}{\lambda}\right)\right\}} \right\}^2$$

where h is the total water depth, z_s is depth at which the sensor was positioned, and λ is the wavelength at the given water depth. The wavelength was calculated from knowledge of water depth and wave period and the relationship given by linear wave theory.

From each spectrum several parameters were calculated. The dominant wave period was calculated as the reciprocal of the peak frequency. Significant wave height was calculated using the relationship between total variance of the record and energy of the wave spectrum. This relationship is given by:

$$H_s = 4\sqrt{\int G(f)df}$$

where $G(f)$ is the double-sided spectral function. The integral was approximated numerically by a summation from 0.01 cps to 0.25 cps. The lower limit was chosen because it was assumed that waves with periods greater than 100 s do not contribute significantly to the energy spectrum. The upper limit of 0.25 cps was selected because beyond this frequency the

distortion introduced by the correction factor renders the spectrum unusable. It must be pointed out that this relationship between energy and significant wave height is a better approximation in deep water (U.S. Corps of Eng., 1984).

These wave height estimates represent the wave energy available in the record and are reliable indicators of energy changes between the chosen frequency intervals as waves transit the reef.

Two quantities related to wave heights are the transmission coefficient and energy reduction. The transmission coefficient (K_T), which is a measure of the wave energy that transits the reef to the lagoon, is calculated by the following expression:

$$K_T = \frac{H_L}{H_F}$$

where H_L and H_F are the wave heights at the lagoon and forereef. Relative energy reduction is calculated by:

$$\Delta E = \frac{H_2^2 - H_1^2}{H_1^2}$$

where H_2 and H_1 are the transmitted and incident wave heights.

The bandwidth (v) is a measure of the spectrum width. Bandwidth is defined as:

$$v = \sqrt{\frac{\mu_0 \mu_4 - \mu_2^2}{\mu_0 \mu_4}}$$

where the μ 's represent the different moments of the spectrum (Phillips,1982). In particular, μ_0 represents the area or energy under the spectrum. Longuet-Higgins (1980) shows that bandwidth is an important parameter that influences the statistical distribution of wave heights and quantities derived from the wave spectrum. If the spectrum has one narrow peak, v approaches a value of 0; if there are several peaks, v tends toward 1. Bandwidth is employed to study the spectrum changes as waves transit over the reef.

Two other quantities useful to this study are the coherence squared (γ^2) and phase angle (θ), which are functions of frequency and defined in the previous chapter. Knowledge of the phase allows calculation of the travel time (τ) of the wave signal between the different stations. The travel time, τ , can also be estimated if the signal speed and travel distance are known. For shallow linear water waves, the phase velocity, which is the speed at which the pattern travels, is given by:

$$c = \sqrt{gh}.$$

The travel time is then computed by:

$$\tau = \int \frac{dx}{\sqrt{gh}}.$$

In these formulas g is the acceleration due to gravity and h is the water depth, a function of distance.

To study changes in wave energy as a function of frequency, a time-delay spectrum model is used. The model is expressed as (Bendat and Piersol, 1986):

$$G_{XY} = \alpha G_{XX} \exp(i2\pi f\tau)$$

where the G's retain their previous meaning, f is the frequency, τ is the time delay, which is a function of frequency, and α , also a function of frequency, is the attenuation coefficient. The attenuation coefficient will be less than one if energy at a given frequency is dissipated, and greater than one if the energy increases. The attenuation coefficient is estimated from the spectrum values using the following expression:

$$\alpha = \frac{|G(f)_{XY}|}{G(f)_{XX}}$$

During calculation of the attenuation coefficient in this model, reflection effects are included assuming that the reef is a ridge with vertical sides. The ridge model causes an overestimate of reflection and conservative estimates of α .

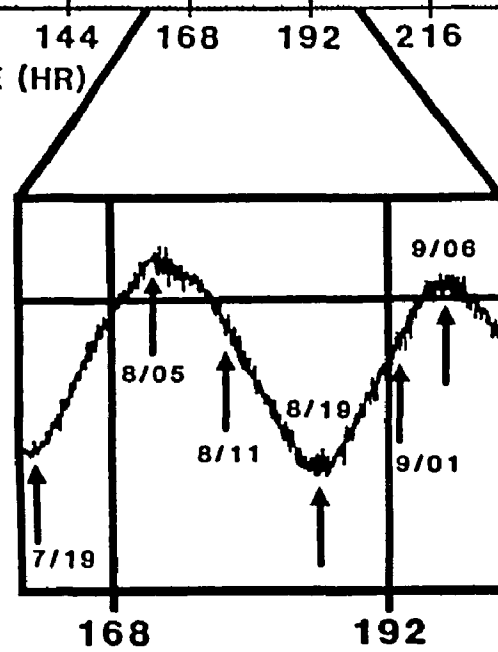
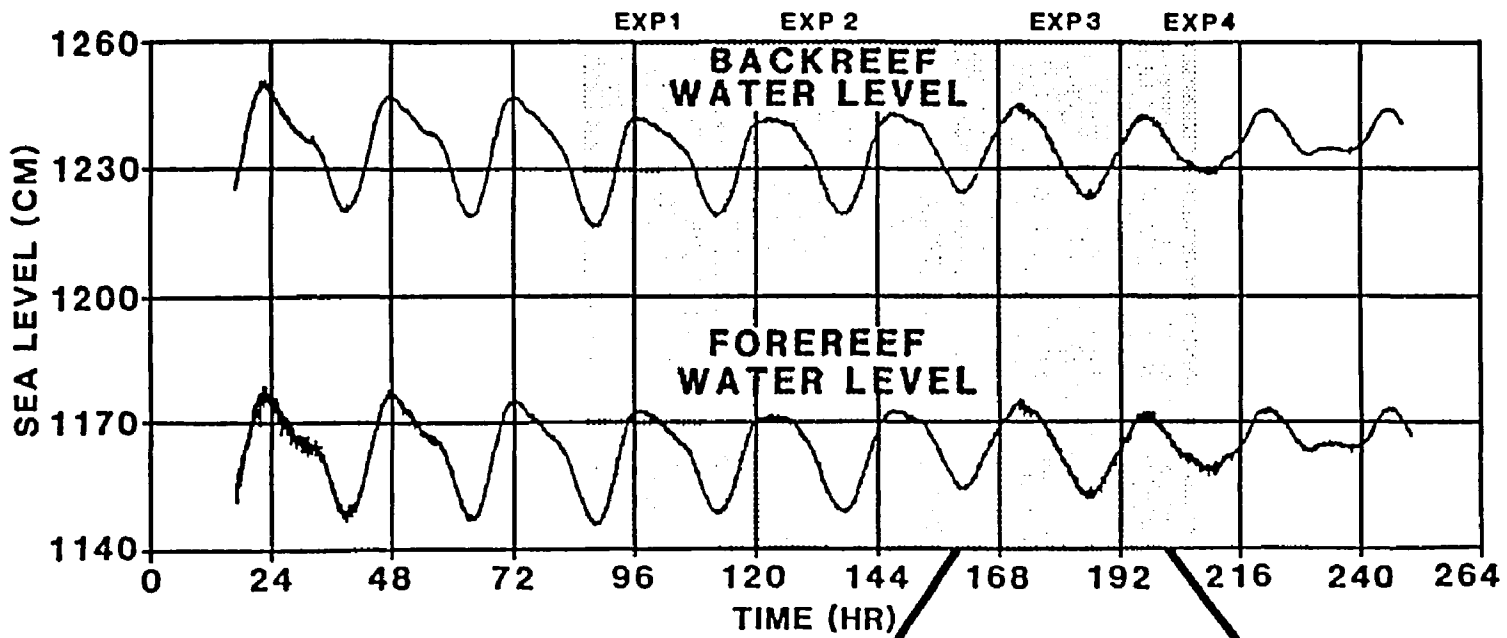
Experiment 3

This section will discuss wave data, emphasizing wave modifications as they transit across the reef and the modulation of these changes by the tides. Wave data for this experiment were collected in 20 min bursts during 49 hours or two tidal cycles. Measurements were made along a transect across the reef using the instrument arrangement shown in Fig. 3.3. Wave sensors were located at the forereef, crest, and backreef. The following discussion is based on all wave data collected, but illustrations presented are derived from 6 data

sets collected at different times throughout the experiment. These data sets constitute records collected on April 7 at 1800; April 8 at 0500, 1100, and 1900; and April 9 at 0100 and 0600 hours. They represent conditions through all phases of the tide (Fig. 6.1) and typical sea states encountered during the experiment.

Wave spectra from data sets along the reef profile during high and flood tide conditions are presented in Fig. 6.2. Spectra for low and ebb tide conditions are illustrated in Fig. 6.3. Note that several spectra are double peaked. This shape indicates that two wave trains were reaching the reef at these times. Wave spectra during the two previous experiments have only a single peak (see Figs. B1, B2 for Experiment 1 and Figs. B3, B4 for Experiment 2 in Appendix B) indicating that only one wave train was reaching the reef. Examination of all wave spectra computed during the course of this investigation reveals that a peak between 0.08-0.10 cps (12-10 s) prevailed through the first two experiments and started decaying at the beginning of Experiment 3. By April 8 at 2200 hours it had completely disappeared. At the same time, the peak between the frequencies 0.055-0.077 cps (18-13 s) started arriving, and by April 9 at 0100 hours it was the only wave train reaching the reef. Other noteworthy aspects of Figs. 6.2 and 6.3 are the changes in energy levels as the waves travel across the reef and the differences in energy change between high and low tide. Wave spectra at 8/05 and 9/01 in Fig. 6.2 and spectra at 7/18 in Fig. 6.3 illustrate that some frequencies lose and others gain energy. Calculations of relative changes of the spectral peak energy indicate an average of 62% peak reduction from forereef to crest during this experiment (77% and 69% during Experiments 1 and 2). This large reduction is, in part, due to wave breaking, which occurs just before waves reach the reef crest site. The reduction from forereef to backreef is 80% during this experiment (94%

Fig. 6.1. Tidal curves with inset showing the tide stage of wave data sets selected for discussion during Experiment 3 and 4.



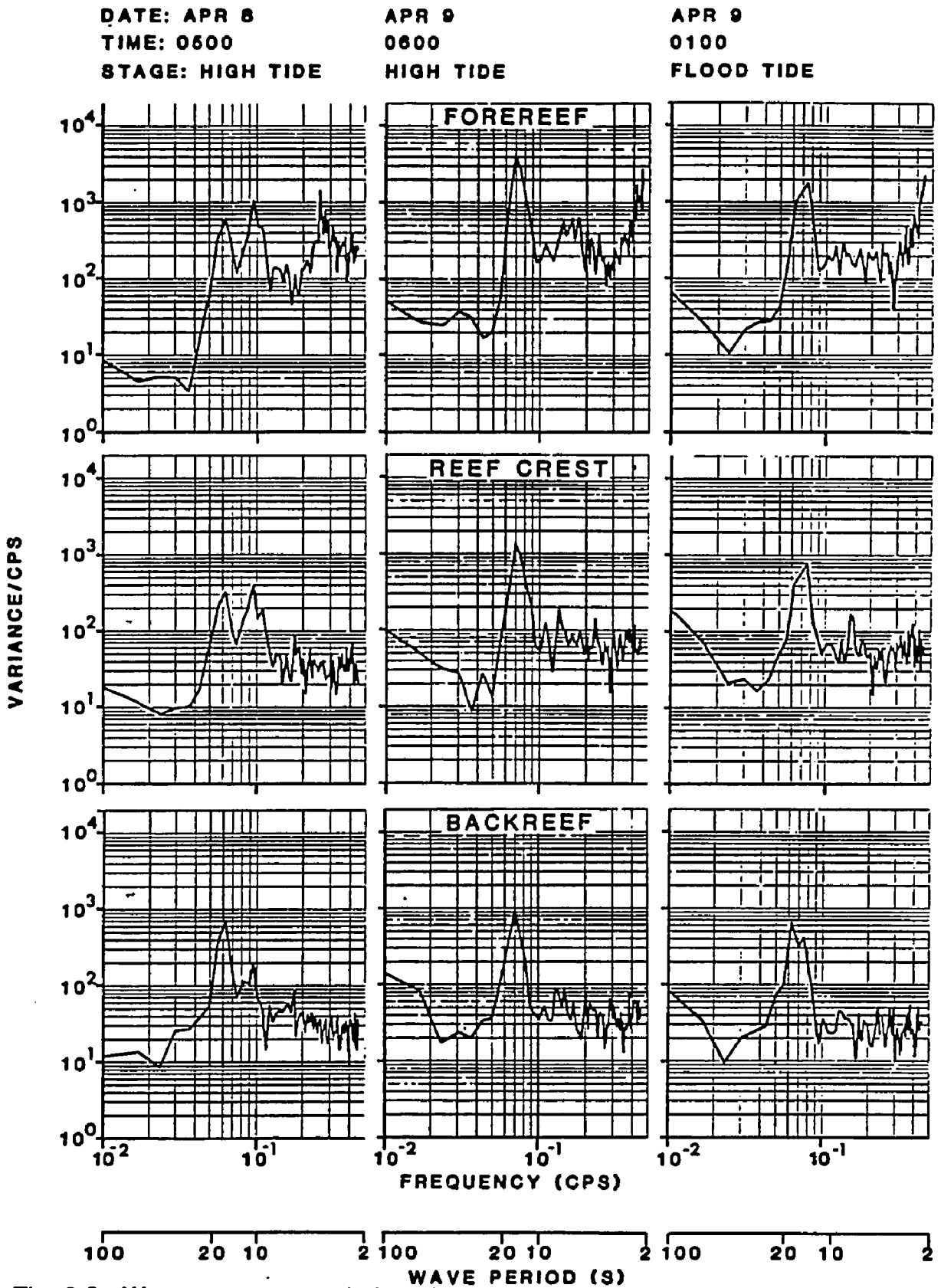


Fig. 6.2. Wave autospectra during high and flood tide during Experiment 3 across the reef profile with 16 degrees of freedom.

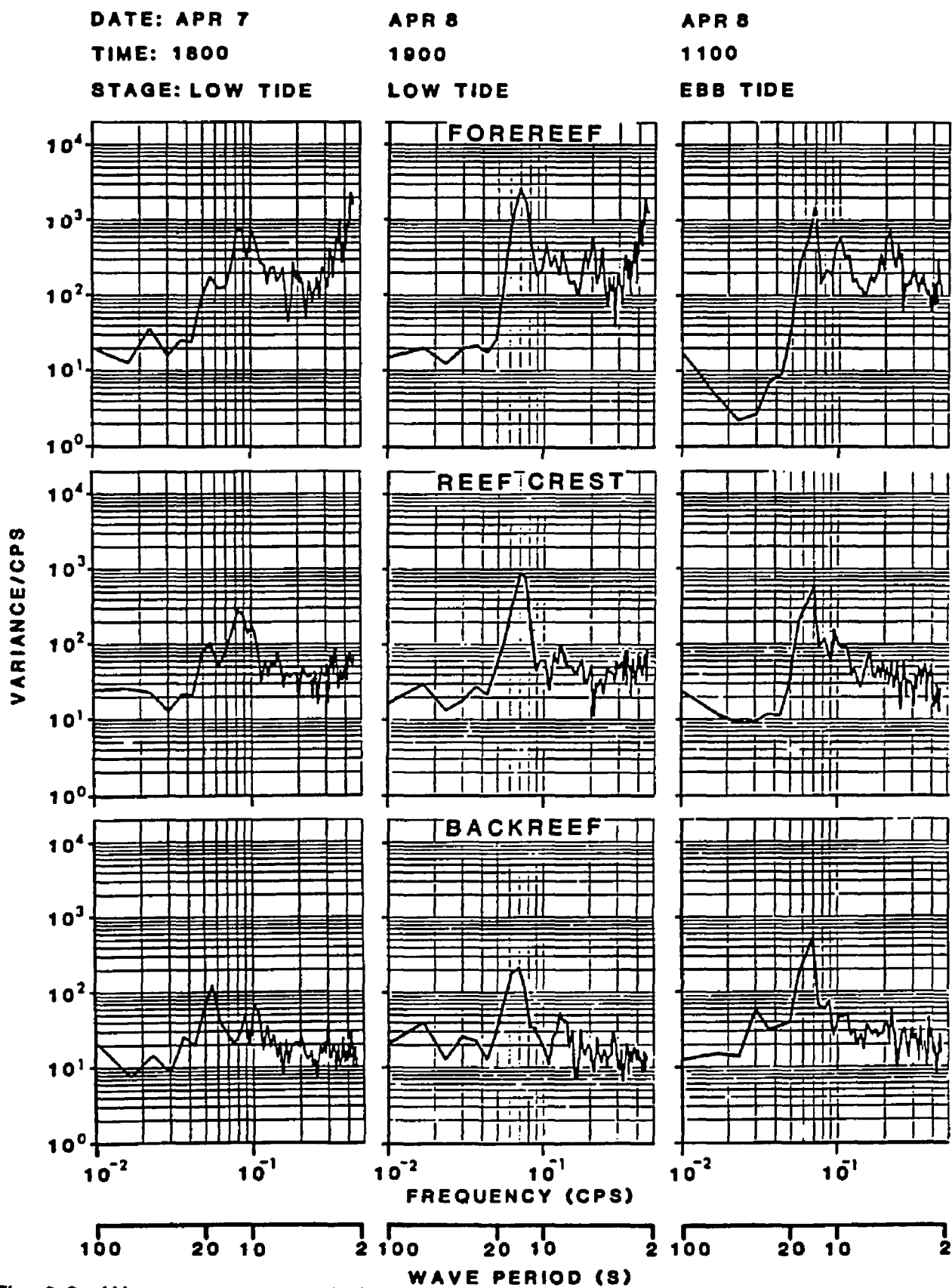


Fig. 6.3. Wave autospectra during low and ebb tide during Experiment 3 across the reef profile with 16 degrees of freedom.

from forereef to lagoon during Experiment 1). A trend towards higher values of peak reduction at low tide is found in data sets from all experiments. The frequencies that experience an energy increase are generally in the higher end of the spectrum and very close to the first harmonic of the peak. Also, the peak at 0.077 cps shows an increase of energy towards the backreef. In summary, a trend of decreasing energy as waves transit across the reef and modulation of energy dissipation by the tide are evident. However, these relationships cannot be generalized for all frequencies present in the spectrum. These energy changes imply that reefs may selectively attenuate some spectral components compared to others, or some energy levels with respect to others.

Characteristic wave periods are difficult to evaluate in this experiment because of the presence of two peaks. Based on the higher peak, the dominant period at the forereef and crest started at 10 s, increased to 16 s by April 8, decreased to 13-14 s (April 8), and then remained unchanged throughout the experiment. The dominant backreef wave period varied between 13 and 18 s throughout the entire experiment. A trend towards longer wave periods in the backreef is evident in Experiment 3 data (Figs. 6.2 and 6.3). This tendency for longer wave periods in the lagoon is not observed in Experiments 1 and 2. The sequence of events leading to the increase of wave periods is as follows: the reef selectively attenuates waves associated with the peak of 0.08 cps as they transit across the reef, and waves associated with the frequency of 0.077 cps travel into the lagoon relatively unchanged, shifting the spectrum to lower frequencies, thus moving the wave period towards higher values.

Average bandwidth of wave spectra is 0.55 at the forereef, 0.77 at the crest, and 0.80 at the backreef. An increase of bandwidth towards the backreef indicates that energy from the peak is being dissipated and some energy is being transferred to other components, creating in this way a flatter spectrum.

This trend of increasing the bandwidth towards the lagoon is also evident in Experiments 1 and 2. Between the forereef and crest, the bandwidth increases from 0.61 to 0.73 during Experiment 1 and from 0.50 to 0.74 during Experiment 2. Physically, this bandwidth change means that, in the reef crest region, wave harmonics are being excited and coupled with the attenuation to create a flatter spectrum. The harmonic excitation occurs by nonlinear mechanisms such as second harmonic generation, nonlinear energy transfer, or quadratic friction.

Wave height time series at each station are presented in Fig. 6.4. All three stations show an increase in wave heights towards the end of the experiment, this increase in wave heights represents a change in the characteristics of waves reaching the reef. Forereef data reveal an oscillation with a period near 6 hours (see also data for Experiments 1 and 2 in Figs. B5 and B8). This period is probably associated with overtides. At the reef crest station some of the variations present at the forereef are filtered out, and the wave height decreases. At the backreef station most of the variability present on the two previous stations is filtered out, and a well-defined cycle of 24 hours is observed. Wave height decreases from forereef to backreef in all experiments. High wave conditions at the backreef correlate with high tide, and low wave conditions correspond to low tide. Also, data from the station closest to the lagoon, curve B in Fig. 6.4, indicate the greatest modulation by the tides. Average wave height at the forereef station is 32.6 cm (range 44.0 to 23.7 cm). At the crest station, average wave height is 19.1 cm (range 25.5 to 13.7 cm). The backreef station has an average wave height of 14.9 cm (range 20.5 to 10.0). Reduction of average wave height between forereef and crest is 41 %, and 54% from forereef to backreef.

The coefficient of wave transmission throughout this experiment is shown in Fig. 6.5. Notice the strong tidal modulation of the curve. High

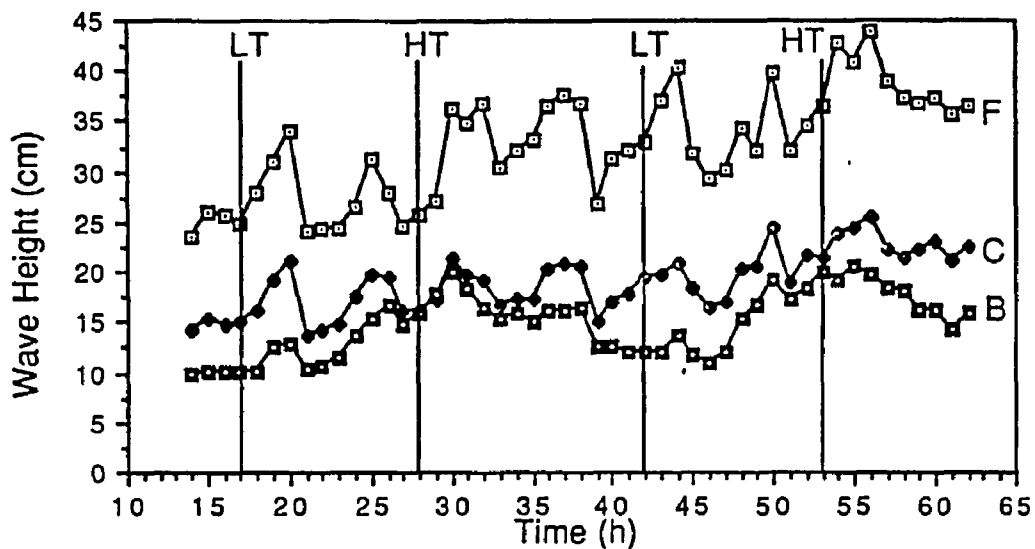


Fig. 6.4. Wave height time series at the foreereef(F), crest(C), and backreef(B) during Experiment 3. (HT= high tide, LT= low tide)

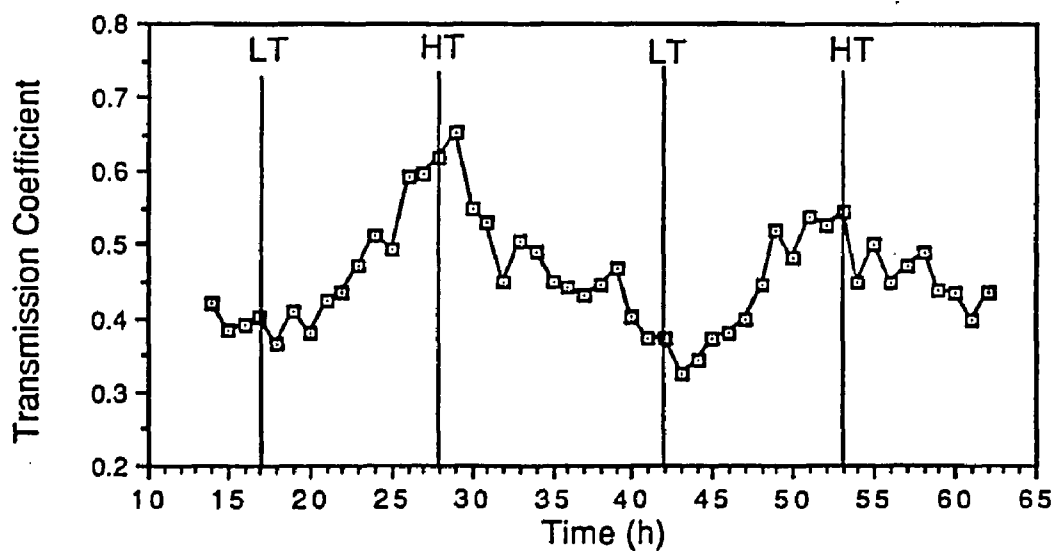


Fig. 6.5. Wave transmission coefficients during Experiment 3. (HT= high tide, LT= low tide)

transmission and low transmission are correlated with high and low tide conditions. Average wave transmission is 0.46, with a high of 0.65 and a low of 0.32. The other estimates of wave transmission made in this study are those of Experiment 1 (Fig. B6). Well-developed oscillations of about 6 hours are present in these results. Average transmission was 0.33 (range 0.49 to 0.14), and agreement with Experiment 3 is not so good. Studies of submerged wave breakers have shown that wave transmission increases as the water depth above the crest increases (Ahrens, 1987). It was therefore expected that wave transmission would be maximized during high tide and minimized at low tide. These results show that, even in a reef system developing under low tidal range conditions (0.3 m), wave transmission across the reef is modulated at tidal frequencies.

Relative energy dissipation, ΔE , from forereef to crest and forereef to backreef is presented in Fig. 6.6. Average energy dissipation from forereef to crest (curve F-C) during this experiment is 65% (range 80% to 44%). The average dissipation between forereef and backreef (F-B) is 78% (range 90% to 58%). The forereef to crest energy reduction values are in good agreement with Experiments 1 and 2, 71% and 65%. The forereef to backreef value is close to the result of Experiment 1, 88% between forereef and lagoon. In Fig. 6.6, which represents data from Experiment 3, tidal modulation is more pronounced. Around 15% more energy is dissipated at low than at high tides between forereef and crest, and 20% more between forereef and backreef. A difference of 13% in the average energy reduction exists between these curves. Energy reduction during Experiment 1 (Fig. B7) does not exhibit the tidal modulation; instead it shows the 6-hour oscillation. The energy reduction during Experiment 2, Fig. B9, shows a weak tidal modulation, but this is expected since data collected at the reef crest does not exhibit tidal modulation.

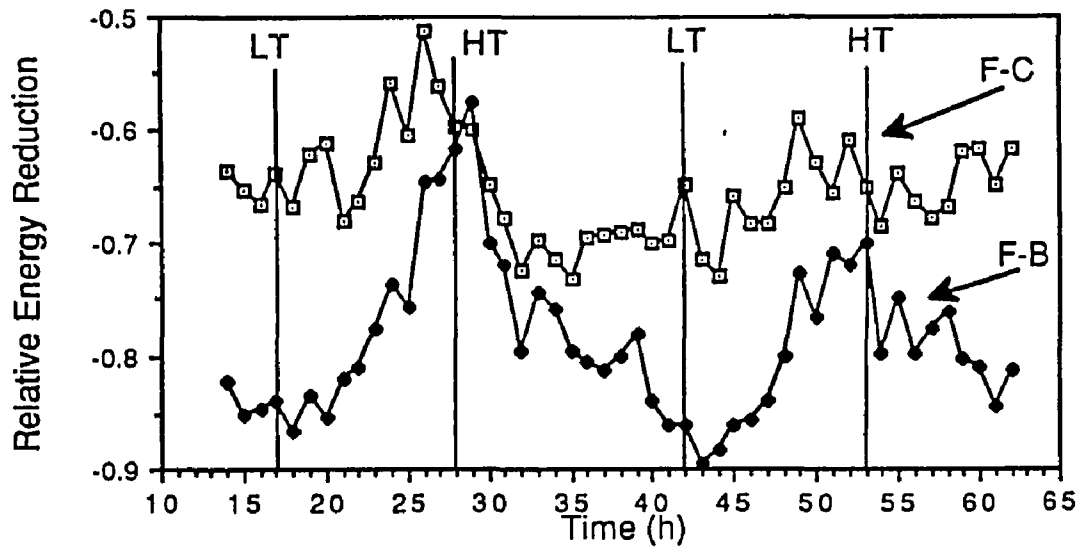


Fig. 6.6. Relative wave energy change from forereef to crest (F-C) and forereef to backreef (F-B) during Experiment 3. (HT= high tide, LT= low tide)

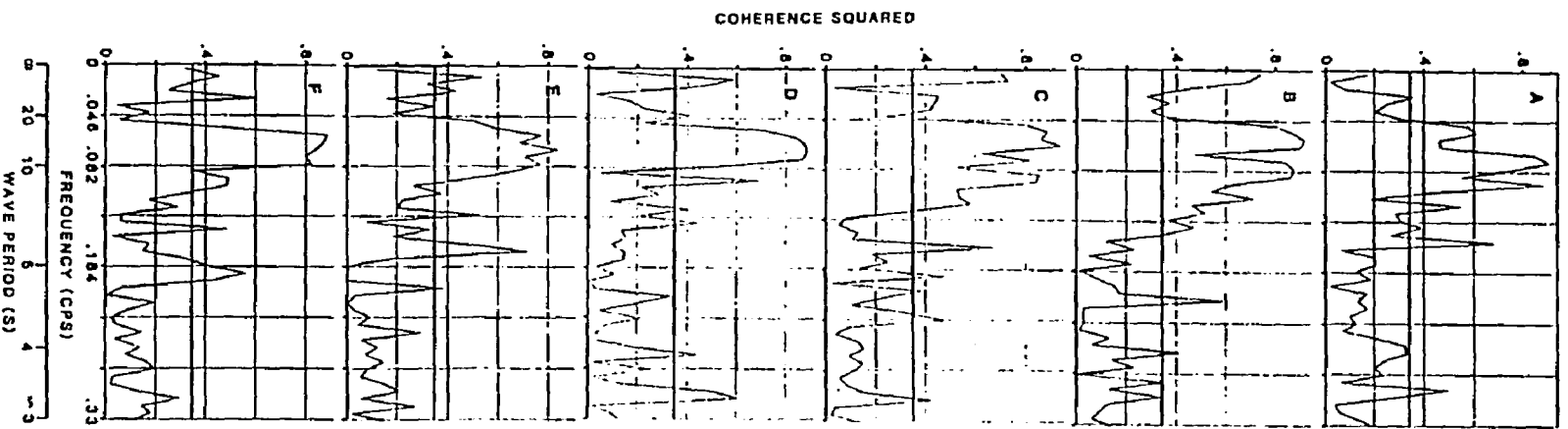
These trends confirm the fact that wave energy dissipation increases lagoonward.

Coherence squared was computed with 16 degrees of freedom (95% significance level of 0.35) using the formulae presented in the data analysis section. The calculated coherence squared between forereef and crest waves is illustrated in Fig. 6.7. A broad region between the frequencies of 0.055 and 0.10 cps (18-10 s) exhibits high coherence with values near 0.8 or greater. Similar results between forereef and crest waves were obtained during Experiments 1 and 2. The coherence between forereef and backreef waves is significant from 0.055 to 0.1 cps. The crest and backreef waves are significantly coherent between 0.055 and 0.01 cps. The coherence, however, is higher (0.7 to 0.8). This higher coherence between crest and backreef waves is similar to results from Experiment 1, where crest waves show more coherence than forereef waves with lagoon waves. Physically, this trend means that forereef waves are better predictors of crest waves, and these in turn are better predictors of backreef wave conditions. High coherence values at the peak frequencies have been observed also by Lee and Black (1978).

Even though the phase angle is not presented, it is employed to calculate the travel time(τ) as explained in the data analysis section. The average travel time from forereef to crest, as calculated from the phase angle for Experiment 3 is 15.2 s, and 14.8 and 15.5 s for Experiments 1 and 2. These estimates have relative errors of 5%, 8%, and 5% when compared to 16 s. The 16 s represents the travel time of waves from forereef to reef crest and is obtained from the integral evaluation presented in the data analysis section.

To analyze the variation of wave attenuation as a function of frequency, the time delay model discussed in the data analysis section was employed. The model output consists of the attenuation coefficients for each frequency.

Fig. 6.7. Coherence squared between forereef and crest waves for April 7, 1800; April 8, 0500, 1100, and 1900; April 9, 0100, and 0600 hours.



Results from the model evaluation for the forereef-crest wave pair are shown in Fig. 6.8. In the low frequency region ($f < 0.05$ cps) the model illustrates moderated attenuation of the signals, indicated by a coefficient (α) value near or larger than 1.0. Wave theory shows that scattering by an object takes place if the length of the obstacle is comparable to the wavelength of the incident waves. The reef crest width is about 100 m long, and the waves traveling over the crest have wavelengths of this order, given the water depths and wave periods prevailing during the study. Thus waves with periods larger than gravity waves will have longer wavelengths and be little or not affected by the reef. The attenuation coefficient then will be of the order of unity at least. If the nonlinear transfer of energy to lower frequencies is considered, then it is conceivable to observe attenuation coefficients greater than 1. The frequency region that corresponds to the peak present in the wave spectra (0.05-0.1 cps) has an average attenuation coefficient value of 0.62. The region between 0.1 and 0.15 cps has an attenuation (α) value of 0.35; between 0.15 and 0.2 cps the attenuation (α) has a value of 0.22. These estimates of the attenuation coefficient (α) are similar to results from Experiments 1 and 2. For the forereef-backreef pair, Fig. 6.9 shows the models results. The attenuation coefficient (α) has an average of 0.41 between 0.05 and 0.1 cps, 0.2 between 0.10 and 0.15 cps, and 0.13 between 0.15 and 0.20 cps.

The crest-backreef pair, not shown, has values of 0.62, 0.46, and 0.37 for the respective frequency bands. These values demonstrate that low frequencies can effectively transmit more energy than wind waves across the reef. Physically, this relationship means that periodic motions like tides and infragravity waves (periods of 24 hours to 1 min) can cross the reef without been modified significantly by its presence. Gravity waves, on the other hand, if of the right frequency, can be significantly

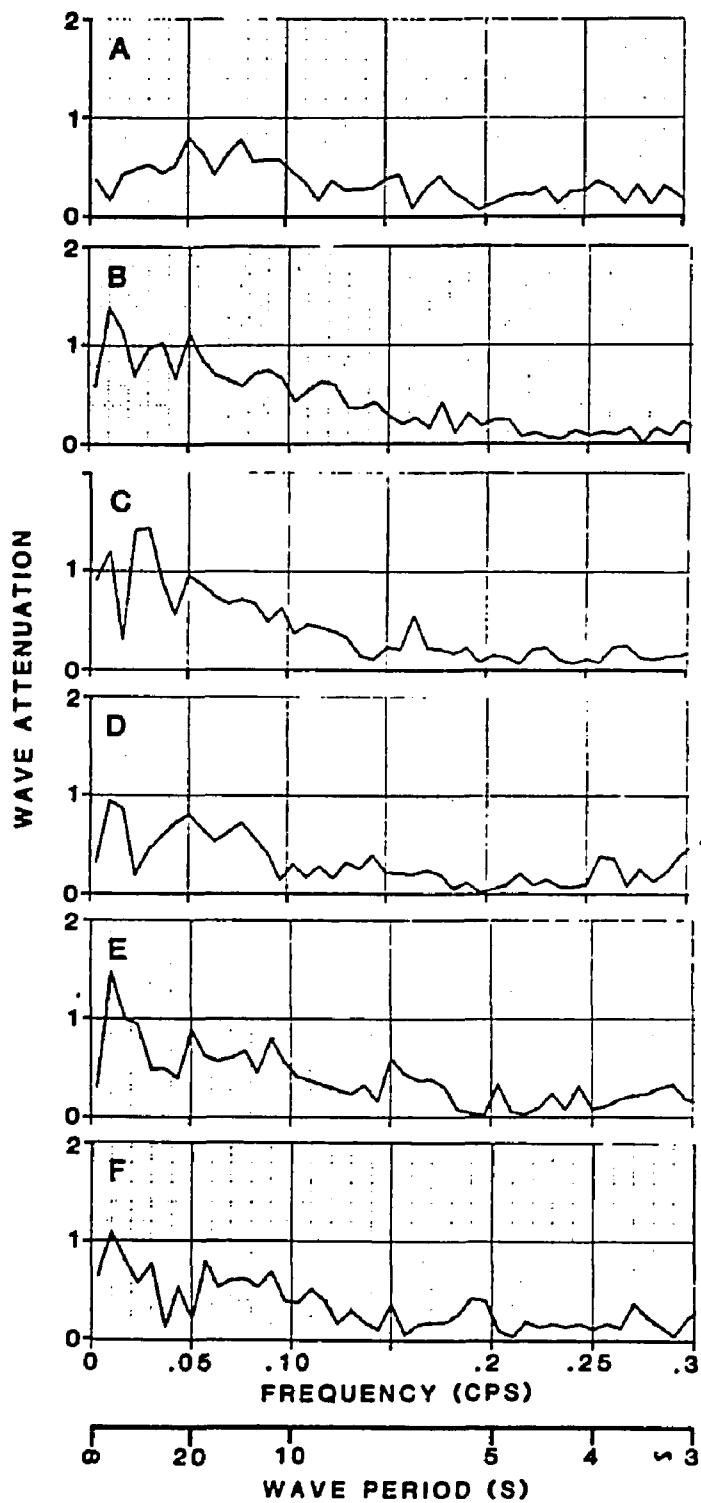


Fig. 6.8. Wave attenuation from forereef to crest as function of frequency during April 7, 1800; April 8, 0500, 1100, and 1900; April 9, 0100, and 0600 hours.

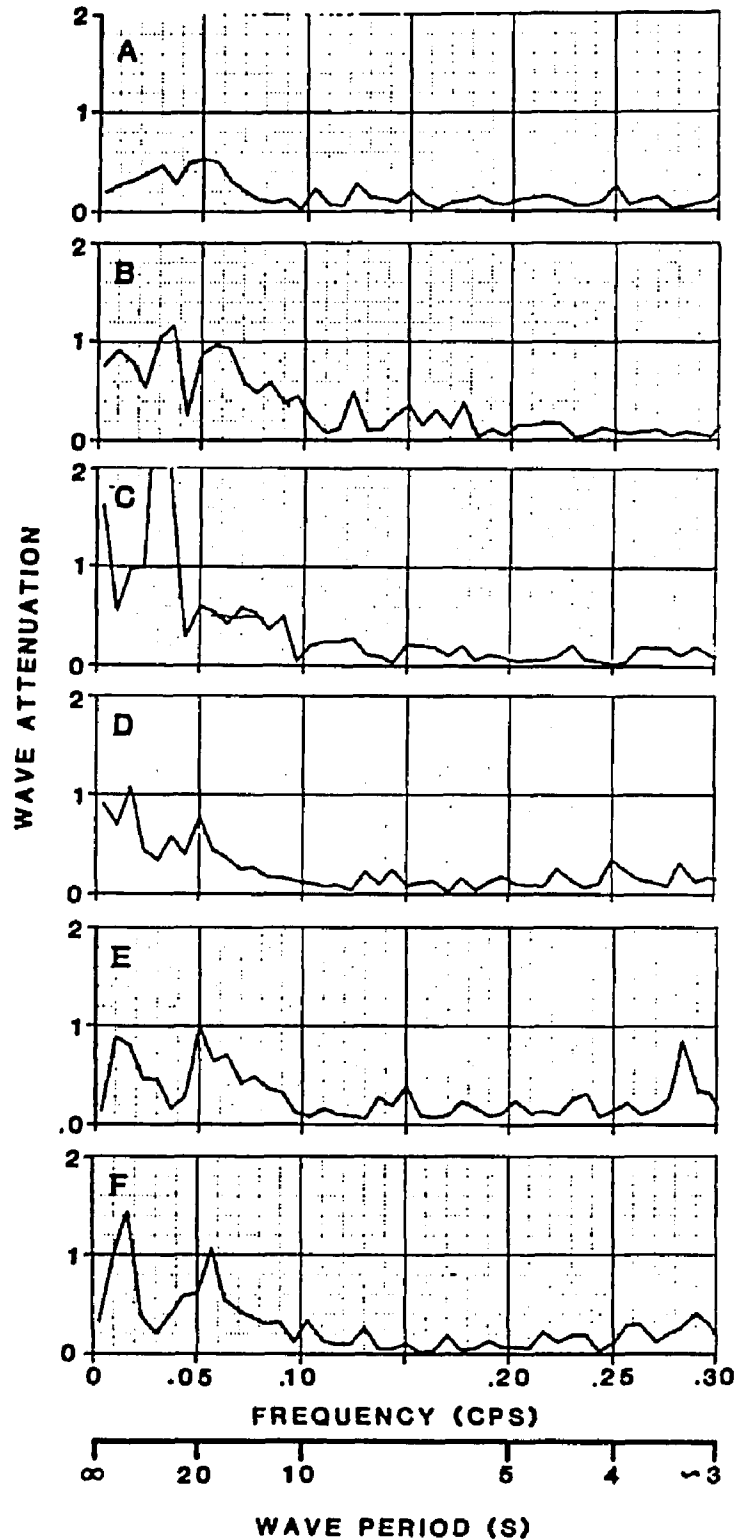


Fig. 6.9. Wave attenuation from forereef to backreef as function of frequency during April 7, 1800; April 8, 0500, 1100, and 1900; April 9, 0100 and 0600 hours.

reduced in height and energy by the reef. These relationships help explain the common observation that reef lagoons contain fine sediments. Calmer waters allow them to be deposited and to accumulate.

Experiment 4

The objective of Experiment 4 was to study water level oscillations over the reef with periods over 1 min. This information can not be obtained from the short records that were being collected in the previous experiments. To obtain the necessary data, continuous records of 1 hr and 55 min were collected in this experiment. The instrument array was similar to the one used during Experiment 3. Typical wave spectra at the forereef, crest, and backreef stations are presented in Fig. 6.10. Each spectrum has 20 degrees of freedom. There are two main peaks, one is located at a frequency of 0.07 cps (14 s North Atlantic swell) at all three stations, and a second peak occurs at a frequency of 0.15 cps (≈ 7 s), which may represent the first harmonic or the typical Caribbean swell. Energy reduction is 64% from forereef to crest, and 82% from forereef to backreef. The wave period corresponding to the main peak is 14 s from forereef to backreef. Average bandwidth at the forereef station is 0.61, and at the crest and backreef stations 0.81. Again, the wave spectra flatten and become more uniform towards the reef lagoon.

Wave height at the forereef station is 32.7 cm, at the crest 19.6 cm, and at the backreef 13.2 cm. Reduction of wave height is 40% between forereef and crest, and 60% from forereef to backreef. Both estimates are in excellent agreement with values of wave height reduction found in previous experiments. The transmission coefficient of 0.40 also agrees with those found in previous experiments.

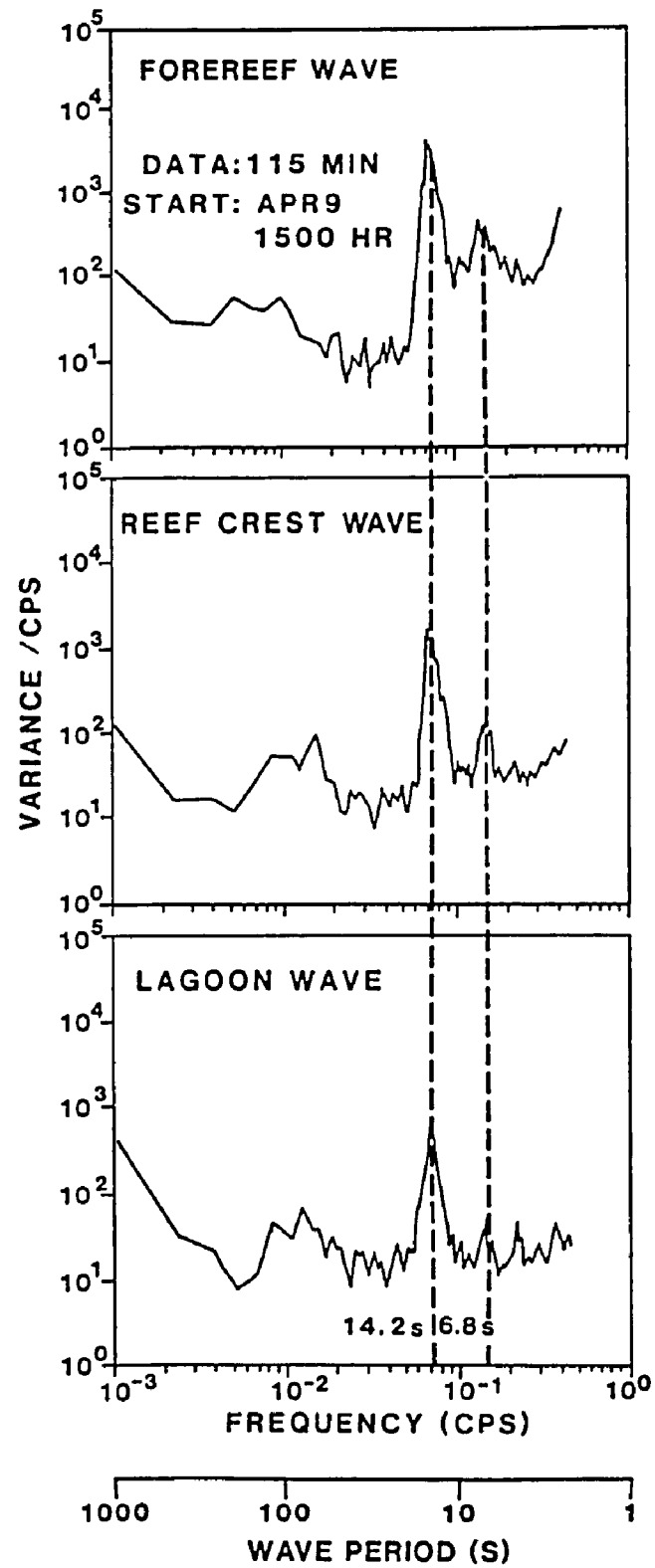


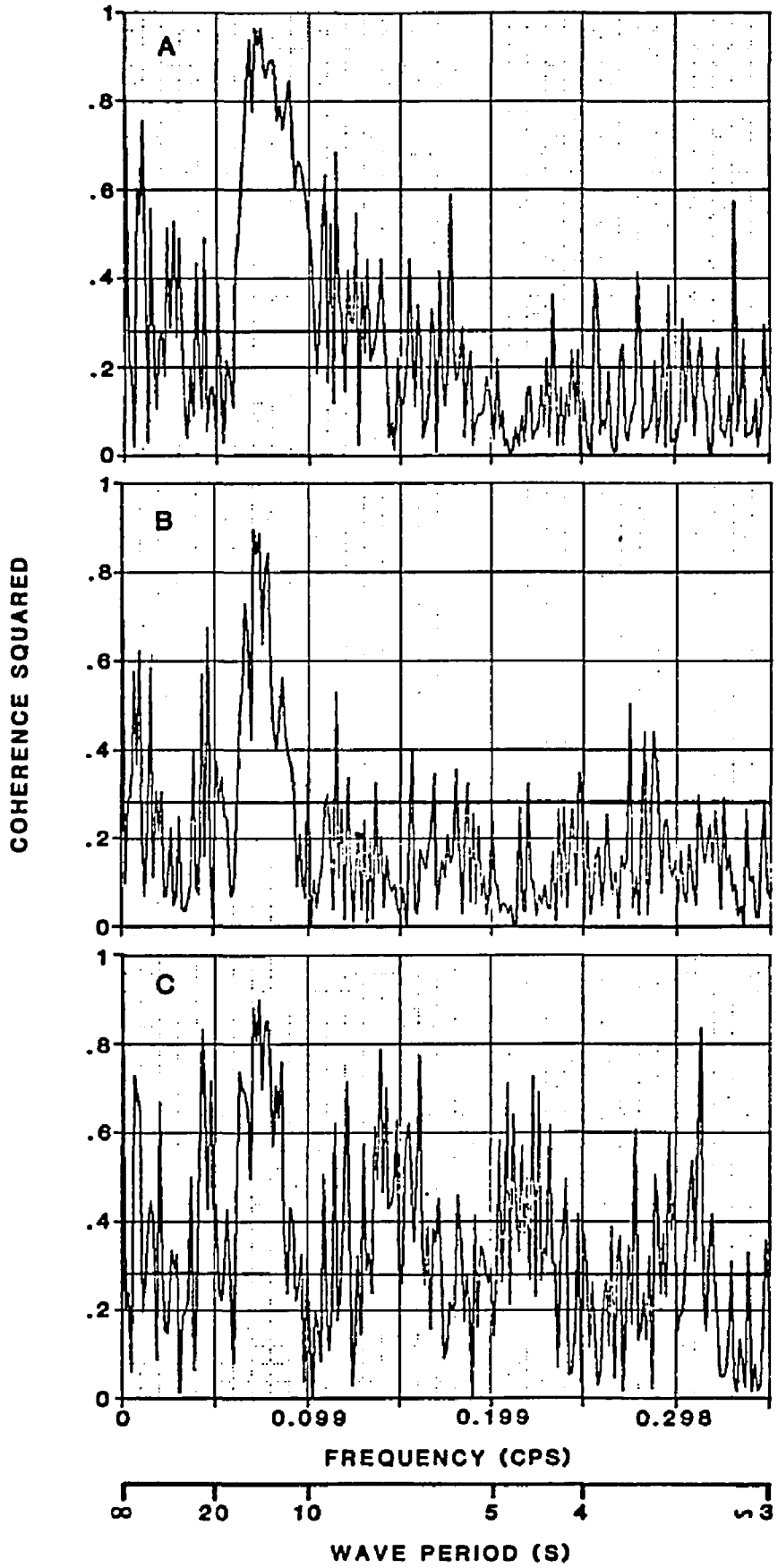
Fig. 6.10. Wave autospectra across the reef profile during Experiment 4 with 20 degrees of freedom.

Coherence squared plots for this experiment are presented in Fig. 6.11. Coherence values for the the forereef- crest pair are illustrated in Fig. 6.11A, the forereef-backreef pair in Fig. 6.11B, and the crest-backreef pair in Fig. 6.11C. All plots indicate a region of significant coherence of 0.9 between the frequencies of 0.055 and 0.10 cps. Another region of high coherence around 0.149 cps exists between crest and backreef sites (Fig. 6.11C). Average travel time from forereef to lagoon calculated from the phase angle, is 13.3 s (relative error of 17% when compared to the travel time of 16 s). Summarizing, the energy and wave reduction, transmission coefficients, bandwidth, and wave coherence estimates for waves measured during a long period of continuous data collection are similar to the ones observed during the previous experiments and allow the discrimination of long period oscillations.

The time delay model is also applied to the data from this experiment. Results of the model evaluation for the forereef-crest wave pair reveal, that in the low frequency region ($f < 0.05$ cps), waves are not as severely attenuated as shown by an α near or larger than 1.0. The frequency region between 0.05 and 0.1 cps has an α value of 0.60, and the region between 0.1 and 0.15 cps has an α value of 0.30. For the forereef-backreef pair, the coefficient has an average value of 0.40 between 0.05 and 0.1 cps, 0.1 between 0.10 and 0.15 cps, and 0.1 between 0.15 and 0.20 cps. The crest-backreef pair has values of ~ 0.60 , ~ 0.40 , and ~ 0.30 for the respective frequency bands. These results provide confirmation of the inference that low frequency waves (periods of 24 hours to 1 min) can effectively transmit more energy across the reef than wind waves (periods 30 to 1 s).

Because the recording period for this experiment was long, ~ 2 hours, the 27-minute oscillations observed in the tide records should have been recorded in the wave records collected. However, wave spectra for this experiment fail to

Fig. 6.11. Coherence squared between the forereef and crest (A), forereef and backreef (B), and crest and backreef (C) waves during Experiment 4. The horizontal line represents the 95% significance level.



show a peak at this frequency. The reason for the absence of the peak at 27 minutes in the spectra is that fewer than 5 cycles were present in the records. A low-pass (cut-off 1 min) version of these records (Fig. 6.12) shows 4 cycles of 25 minutes at the backreef and crest, and less well-defined cycles at the forereef station. The presence of these oscillations in these records shows that they are present across the whole reef and not just at the lagoon and Buck Island Channel. Larger amplitudes of these waves in the lagoon are apparent from the data presented in Fig. 6.12, and reflection from the shoreline is a possible explanation. The importance of these oscillations is that they serve as modulating agents for the gravity waves, since they can change the water depth at the reef crest. In this way, long-period waves perhaps control the extent of energy dissipation by wave breaking and bottom friction. They can also contribute to the net transport of water since they can effectively move water across the reef.

Numerical Prediction of Wave Height

Models for predicting wave height found in the scientific literature can be classified in two categories: energy conservative and dissipating models. The conservative models, as the name implies, are based on the conservation of energy and are therefore valid up to the breaking point. These models predict the wave height changes caused by refraction and shoaling. Dissipation models allow for energy dissipation either by bottom friction or turbulence. Models that assume that bottom friction dissipates energy generally use a quadratic law to calculate the bottom stress. Models by Bretschneider and Reid (1954) and Hasselman et al. (1973) fall into this category. Two major disadvantages of these models are that they don't work beyond the breaking point and they need a friction coefficient, which is an empirical parameter. Studies of oscillatory boundary layers have shown that the bottom friction

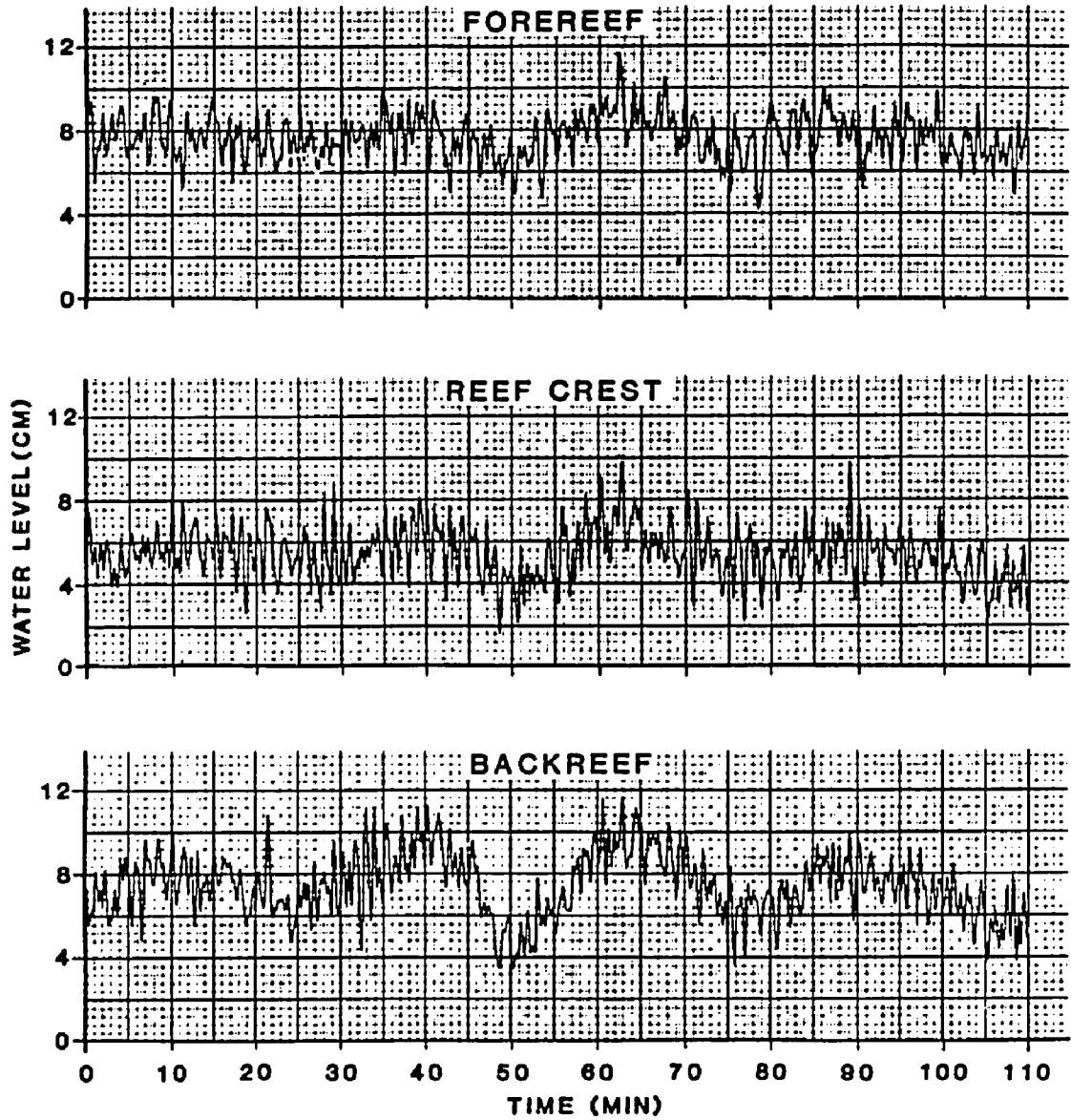


Fig. 6.12. Water level, low passed (cut-off 1 min), at the foreereef, crest, and backreef during Experiment 4 illustrating the 30-min oscillation.

coefficient could be predicted from a knowledge of the wave orbital amplitude and the roughness of the bottom. Johns (1983) shows that this functional relationship is a consequence of the quadratic law used to calculate the bottom stress. Kamphuis (1975), Jonsson (1966, 1980), and others present diagrams to estimate the frictional coefficient from a knowledge of the bottom roughness and wave parameters. Such diagrams are based on empirical or semiempirical studies under laboratory conditions. Friction coefficients obtained this way demonstrate consistency among studies, which consistency provides some confidence for their use. It is fair to say that many other formulas exist for predicting the friction coefficient, but all are either empirical or suffer the same shortcomings as the ones mentioned above. Other studies of channel flows have shown that geometry of the roughness elements and size are important in determining friction coefficient values (Sabir 1962; U.S. Dept. of Transportation 1984, 1975). In general, larger roughness elements have larger friction coefficients. These considerations require that each case be treated individually and special care be used in determining the bottom roughness and geometry.

Another type of model considers the interaction of wave boundary layers and currents. Examples are given by Grant and Madsen (1979) and Fredsøe (1984). In this case, the interactions have the effect of increasing the friction coefficients. There are also models that include the dissipation of energy by turbulence in the wave breaking region. These are, in general, a variation of the bore analogy or solution of the equations of motion for turbulence using some kind of closure scheme. Models in this category include Lin and Hwang (1986), Horikawa and Kuo (1966), Shiau and Wang (1977), Basco and Svendsen (1984), Thornton and Guza (1983), Dally et al. (1984), and Gerritsen (1981) among many others. The major advantage of these models is the

capability to follow the wave through the breaking point and surf zone. A major disadvantage is the necessity of determining at least three parameters for the model. Many other models exist that are based on the combination of dissipating mechanisms, shoaling, and refraction. In most cases the models have to be solved using numerical techniques. In this study, the model of Thornton and Guza (1983) is used. The criteria for its selection were (1) it considers dissipation by turbulence during wave breaking and bottom friction; (2) the effects of shoaling and refraction are included in the equations; and (3) dissipation of energy is based on the wave height distribution and not on a monochromatic wave height. Other factors that influenced the selection were the facts that wave fields approach steady state and the current fields were orthogonal to the direction of wave propagation, as discussed in Chapter 5. Finally, a similar scheme based on bottom friction and turbulent dissipation using the bore analogy was employed by Gerritsen (1981) for his work in Hawaii. The starting point is the steady wave energy equation:

$$\frac{d(Ec_{gx})}{dx} = -(\epsilon_f + \epsilon_b)$$

where E is the wave energy density given by linear theory, c_{gx} is the group velocity in a direction perpendicular to the reef, and ϵ_b and ϵ_f are the energy dissipation functions of turbulence and friction respectively. The expression for the average turbulent dissipation per unit area is:

$$\epsilon_b = \frac{3\sqrt{\pi}\rho g f B^3 H_{rms}^5}{16 \gamma^2 h^3} \left[1 - \frac{1}{\left(1 + \left(\frac{H_{rms}}{\gamma h}\right)^2\right)^{5/2}} \right]$$

where g is the gravitational acceleration, h is the water depth, f is the peak

frequency, B is a breaker coefficient that accounts for the differences in breaker type and is considered a function of the proportion of foam in the face of the breaker, ρ is the water density, γ is the wave height to depth ratio at breaking, and H_{rms} is the root mean squared wave height. The average frictional dissipation per unit area is:

$$\epsilon_f = \frac{\rho C_f}{16 \sqrt{\pi}} \left[\frac{2\pi f H_{rms}}{\sinh(kh)} \right]^3$$

where c_f is the bottom friction coefficient, $\sinh(kh)$ is the hyperbolic sine, and k is the wave number calculated as the reciprocal of the wavelength. These equations are solved using a simple forward step scheme (Thornton and Guza, 1983) with eleven steps across the reef, Fig. 6.13. Of the three parameters necessary for the model, the authors recommend a value of 1.5 for B . The friction coefficients are calculated using the work of Kamphuis (1975) with the assumption that if a_{1m}/k_n is less than 1.0, then $C_f = 1$. The a_{1m} is the linear wave theory radius of the particle orbit at the bottom, and k_n is the roughness of the sea floor. This assumption is made considering that Jonsson (1980) uses a similar approximation but with a value of 0.30 if a_{1m} / k_n is less than 1.57. Another justification for this assumption is based on the friction coefficients obtained by Gerritsen (1981) and Kono and Tsukayama (1980) working on coral reefs, which have values of around 0.7. The roughness value k_n is calculated in the following way, which is believed by the author to be a new method. From the work of Loya (1978), the rugosity across the reef crest is calculated. Rugosity is defined as the length of a chain following the reef bottom over the chain length parallel to the reef bottom over the same transit. This is a technique from line transects methods and measures the reef floor coverage. The length following the reef floor is a measure of the arc length and

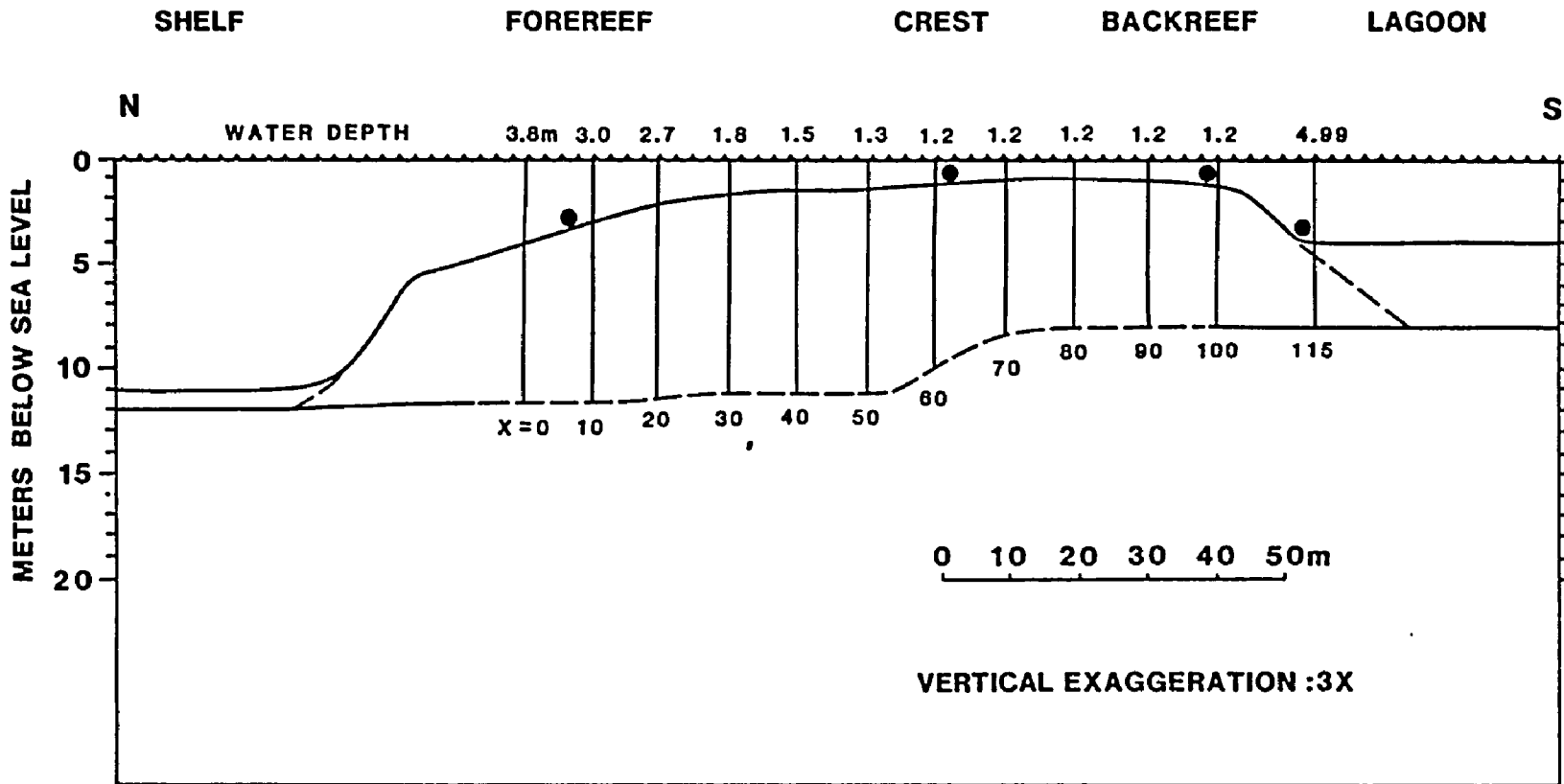


Fig. 6.13. Grid across the reef profile used during the numerical calculations of energy dissipation.

from calculus this can be approximated by:

$$L = n\Delta x \sqrt{1 + \left(\frac{\Delta y}{\Delta x}\right)^2},$$

but the $n\Delta x$ factor equals the arc length above the floor of the reef. Dividing by this factor gives the rugosity factor, since by definition it is the ratio of both arc lengths. Squaring and solving for Δy , one obtains an estimate of the roughness. The value of k_n , assuming the separation of coral colonies $\Delta x = 0.5$ m, is 0.52 m. This value is used across the reef profile.

The third parameter needed for the model was the wave height to depth ratio (γ) at breaking point. Direct measurements necessary to estimate γ were not made. It was decided that measurements at the reef crest provide a close estimate of γ since this station was close to the breaking point.

An improvement of the model was made by including wave reflection from the reef. The reflection coefficient at each step was approximated using the following expression (Mei, 1984):

$$K_r = \frac{\sqrt{h_1} - \sqrt{h_2}}{\sqrt{h_1} + \sqrt{h_2}}$$

where h_1 is the depth of the incident side and h_2 is the depth of the transmission side. Refraction was not included but a simple calculation was performed to study its effects. The calculations indicated a 10% reduction of the wave heights from the wave height model.

Predicted wave heights based on this model across the reef transit during Experiment 3 are shown in Fig. 6.14. The cases presented represent all phases of the tide. Wave height increases for the first 30 m, levels off during the next 10 m, and then decreases steadily until reaching the end of the transit.

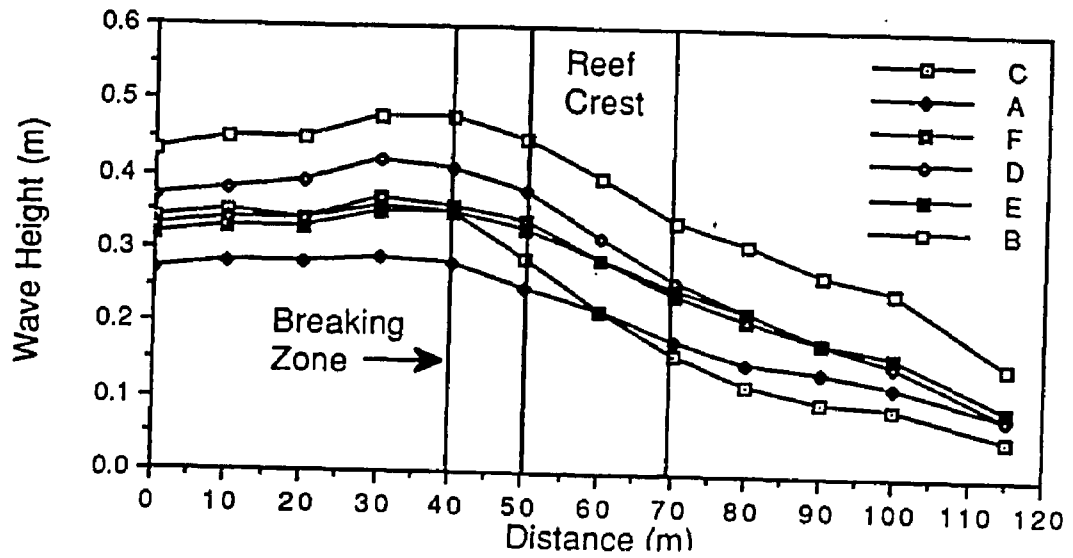


Fig. 6.14. Predicted wave height across the reef profile. High tide A,B; low tide C,D; flood E; and ebb F during Experiment 3.

Similar wave height profiles are obtained for Experiments 1 and 2, (Fig. B14 and 15 in Appendix B). Wave height profiles, Figs. B14 and 15, group themselves according to the tide phases; however, this was not the case during Experiment 3. Changes of wave height across the reef are important, but they provide no information as to the physics involved in the energy dissipation. In order to determine which mechanism is contributing most to the dissipation of wave energy, the estimates of bottom friction and wave breaking are plotted across the reef transit, Figs. 6.15 and 6.16. During the first 30 m, shoaling effects dominate, and the wave height increases even though energy is being dissipated by bottom friction. Between 40 and 60 m frictional and turbulent dissipation increase sharply, reaching their maximum, and wave heights start to decline. This decrease in wave height continues across the reef crest and into the backreef because of continuing energy losses by bottom friction. Of particular interest is the fact that, during low tide, turbulent dissipation consistently approaches the level of frictional dissipation (Fig. 6.16), making the total energy dissipation greater. These results agree with those found in the previous experiments (Figs. B10 through B13 in Appendix B). This relationship explains the tidal modulation of wave heights. It is significant that bottom frictional energy dissipation is not small as on beaches (Thornton and Guza, 1983), and cannot be neglected in coral reefs.

Average friction coefficients during each experiment across the reef profile are presented in Table 6.1. Notice that during Experiments 1 and 2 the friction coefficients estimates are similar. However, during Experiment 3 the friction coefficients decrease considerably even though the roughness elements and tidal characteristics remain unchanged. The only parameters that changed were the wave period and height, which increased. The reduction of the frictional coefficients is related to the fact that longer waves,

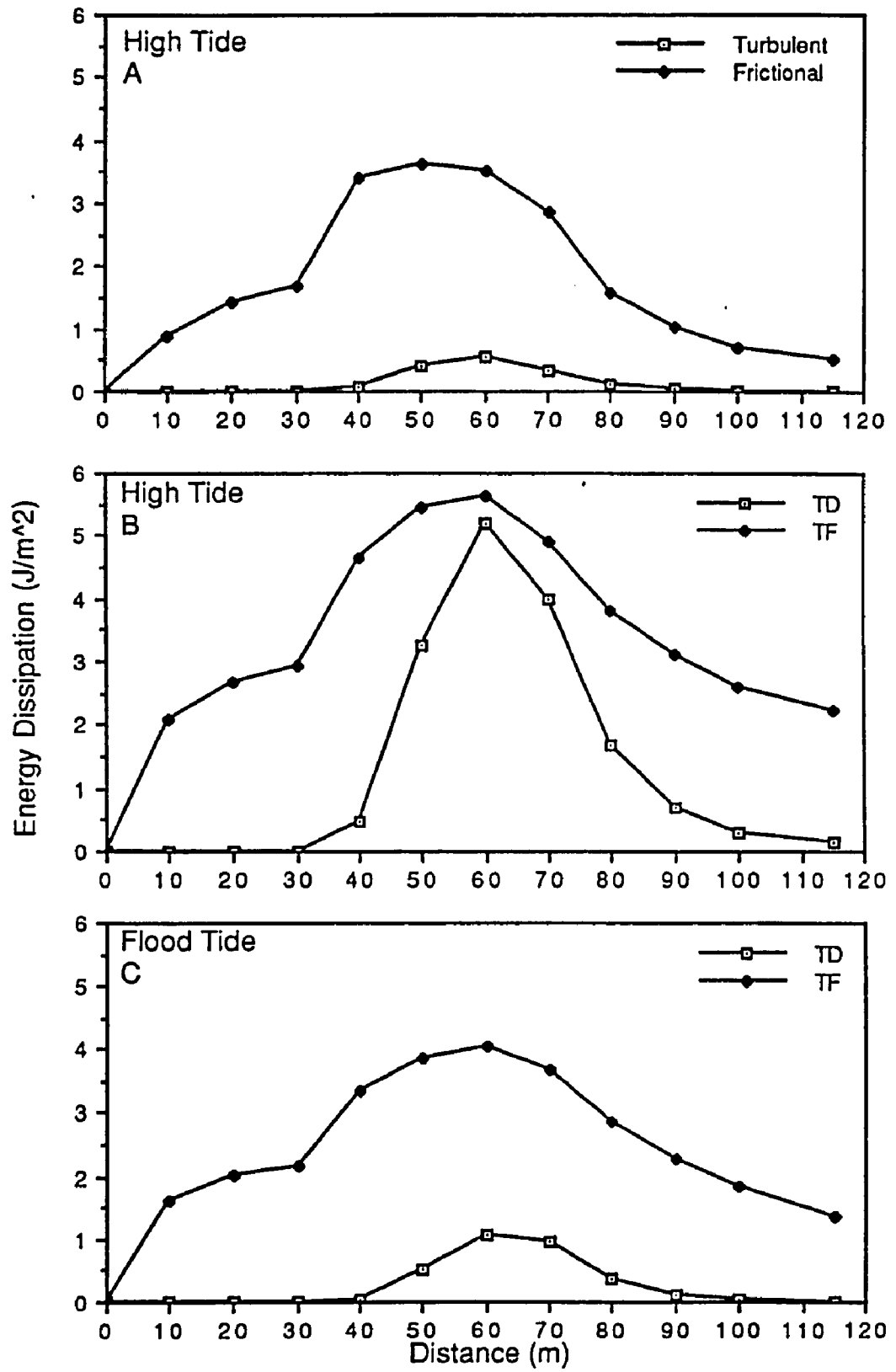


Fig. 6.15. Energy dissipation by bottom friction (TF) and turbulence dissipation (TD) across the reef. High tide A,B; flood C during Experiment 3.

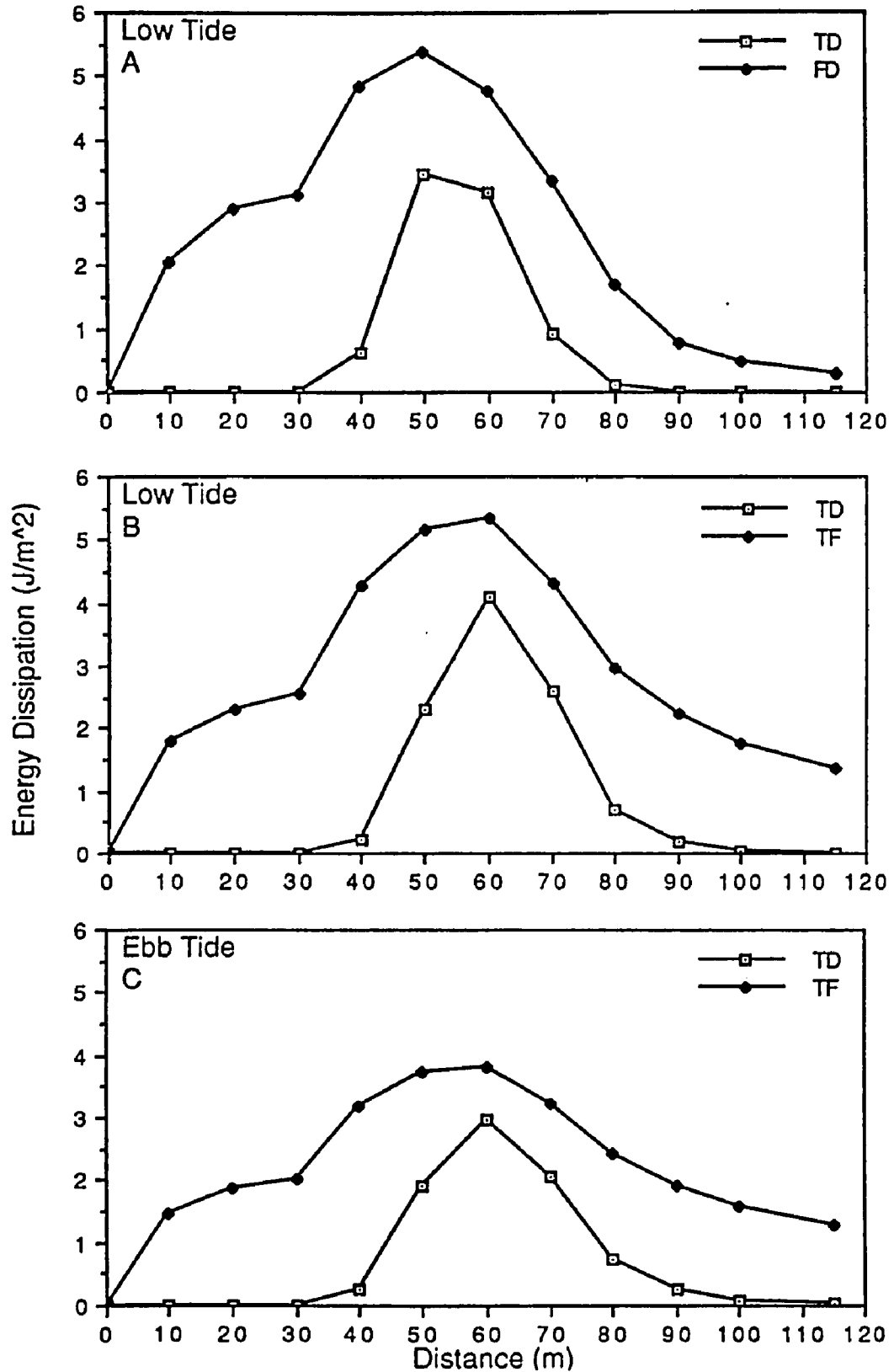


Fig. 6.16. Energy dissipation by bottom friction (TF) and turbulence dissipation (TD) across the reef. Low tide A,B; ebb C during Experiment 3.

Table 6.1. Average friction coefficients for each experiment and reef interval.

Interval	Exp. 1	Exp. 2	Exp. 3
1	1.00	1.00	0.83
2	1.00	1.00	0.70
3	1.00	1.00	0.67
4	0.82	0.88	0.50
5	0.74	0.84	0.45
6	0.82	0.89	0.45
7	0.94	0.99	0.54
8	1.00	1.00	0.63
9	1.00	1.00	0.70
10	1.00	1.00	0.77
11	1.00	1.00	0.87

which were present during Experiment 3, respond to roughness elements of the reef, which differ from coral heads. Roberts et al. (1975) showed that spur and groove topography of the forereef were the roughness elements. The reflection coefficient at each interval was less than 10%, except at the lagoon, where it fluctuated in all cases between 30 and 40%.

To evaluate the model's performance a comparison of the predicted heights with observed wave heights at the reef crest was carried out. Results with and without refractive effects are presented in Figs. 6.17 and 6.18. The model tends to overestimate wave heights in both instances; however, an improvement is observed when refraction is included in the model. Even though most of the assumptions behind the model are met in this study, underestimation of energy dissipation by the model causes wave heights to be large. Possible reasons for this overestimating of wave heights are (1) bottom friction is not well described by using the same roughness across the reef; (2) γ is obtained from measurements at the reef crest, and (3) refraction is neglected. The effect of using a single roughness value across the reef is to prevent the model to adjust to possible changes of

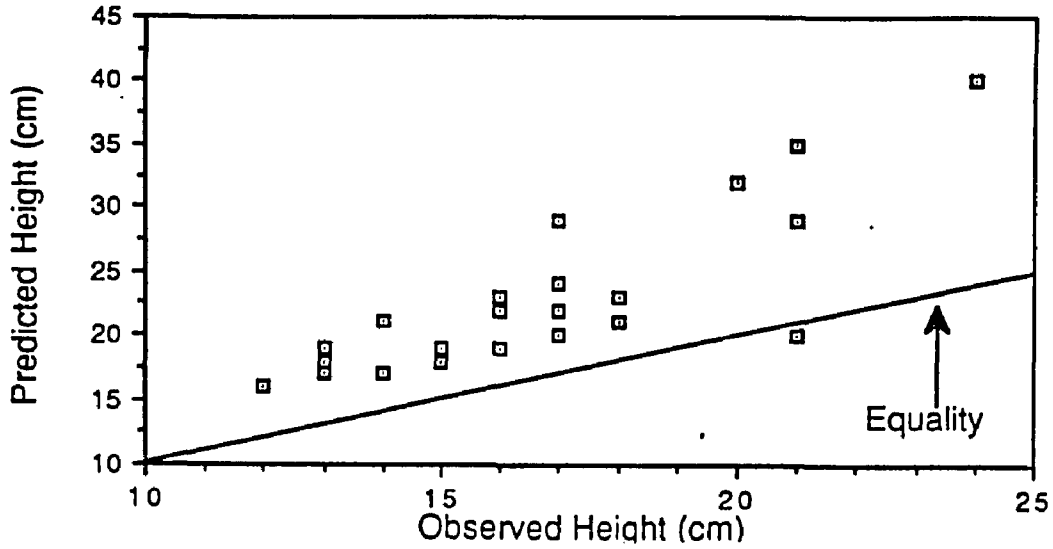


Fig. 6.17. Comparison of predicted and observed wave heights at the reef crest with no refraction.

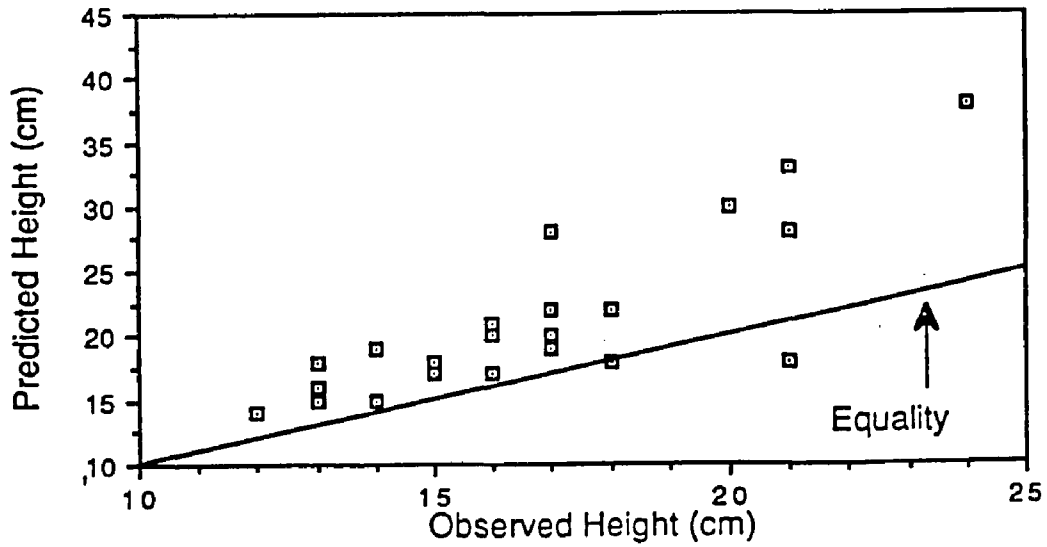


Fig. 6.18. Comparison of predicted and observed wave heights at the reef crest with 30° refraction.

interaction scales between waves and topography. This inability to change scales of interaction gives rise to lower friction coefficients, which dissipate less energy. The lack of measured values of B also favors underestimation of energy dissipation. However, the physical insights obtained from the model more than compensate for its poor performance.

Therefore, both field data and model results indicate that wave energy, as inferred from wave height, decreases as waves transit across the reef. Average energy reduction between forereef and crest is 67%, and 83% from forereef to backreef. Water depth changes at the reef crest forced by tides and other infragravity oscillations modulate these changes. An average of 15% more energy reduction occurs during low tide from forereef to crest and 20% more from forereef to backreef. The tide modulating effects are more pronounced at the backreef and lagoon stations than at the reef crest. The numerical calculations demonstrate that wave energy dissipation by wave breaking and bottom friction are of the same magnitude. The wave prediction scheme overestimates the wave height by an average of 37%. Besides the need to consider more dynamical processes, this error is due to inaccuracies in determining various input parameters needed for the model.

7.0 Currents and Mass Transport

Mass transport across reefs is of vital importance to studies of ecology, sedimentation, and programs of reef management and conservation. The variability, magnitude, and physical processes that drive reef currents and mass transport form the central themes of this chapter. Data were collected during four experiments. However, discussion of results and illustrations is based on data from three experiments. Data sets were selected to investigate vertical current shear at the reef crest, currents at different sites over the reef (forereef, crest, backreef, and lagoon), and frequency dependence of the currents. Criteria for data selection were (1) presence of information on the vertical structure of currents, (2) presence of long period oscillations in the currents, and (3) tide phase. This chapter is divided into a discussion of vertical current profiles at the reef crest, and comparisons of forereef to backreef current. Finally, calculations of mass transport by waves at the crest are discussed.

Vertical Current Profile

A vertical array of current meters placed at the reef crest (Fig. 3.1) was operated for three tidal cycles. Two ducted current meters were installed 0.95 and 0.65 m above the reef floor. The objective of this instrument arrangement was to study vertical shear and possible current reversals within the water column. Unfortunately, the upper meter malfunctioned after the first tidal cycle. The discussion of vertical current shear is therefore based on measurements made during the first tidal cycle. Spectra of current measurements from both instruments during high and flood tide conditions are illustrated in Fig. 7.1. A peak between 0.08 -0.1 cps (12.5-10 s) is evident in records from both meters. The variance levels are around $1,800 \text{ (cm}\cdot\text{s}^{-1})^2\text{cps}^{-1}$ except at the top meter on April 5 at 0100 hours. Calculation of characteristic speeds using the spectra

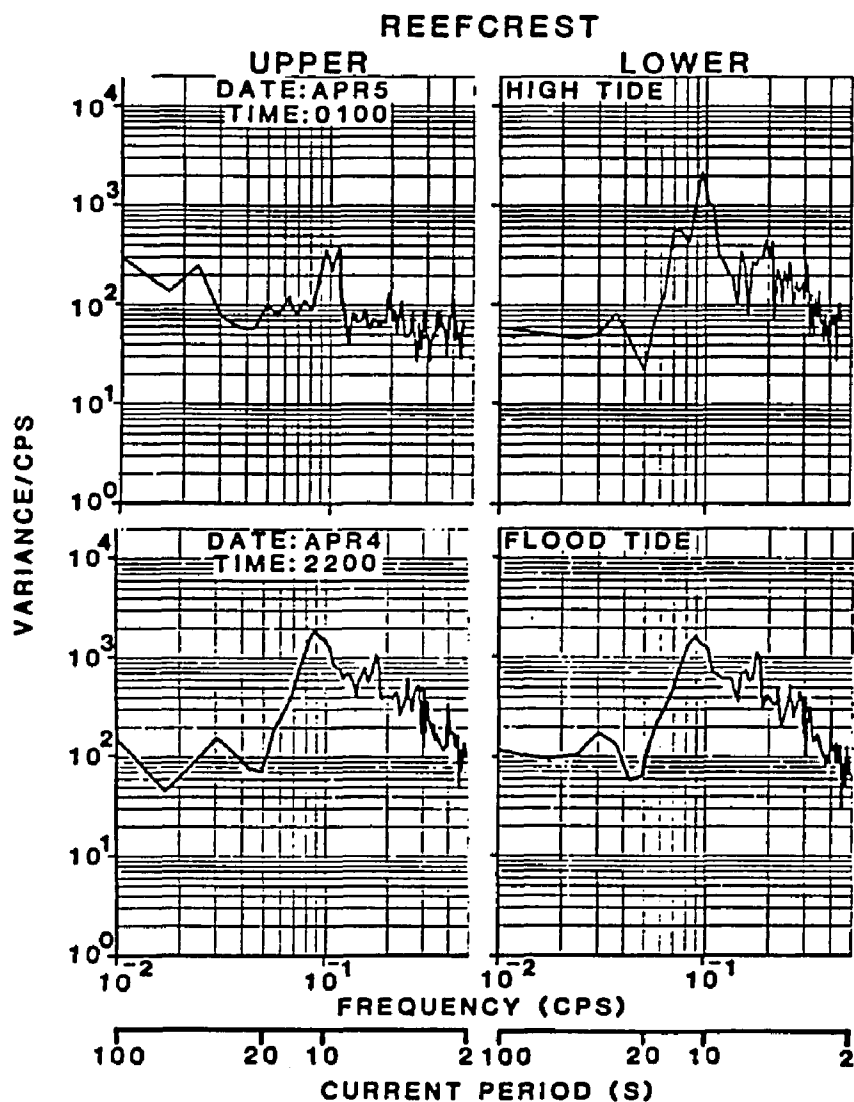


Fig. 7.1. Current autospectra from measurements at the reef crest by 2 ducted current meters oriented in an onreef-offreef direction and stacked vertically (at 0.95 and 0.65 m above the reef floor). During Experiment 1 data on which the above autospectra were generated were collected at high and flood tide with 16 degrees of freedom.

were done by multiplying the spectral estimate by the frequency step, 0.006667 cps and taking the square root. Speed amplitude estimates based on these spectral peaks are between 4.3 and 10.5 $\text{cm}\cdot\text{s}^{-1}$. Spectra corresponding to low and ebb tide conditions are presented in Fig. 7.2. The dominant peak again is between 0.08 and 0.1 cps (12.5-10 s). Variance levels during these tide conditions, however, are somewhat lower 1,200 $(\text{cm}\cdot\text{s}^{-1})^2\text{cps}^{-1}$. The speed amplitude estimates during low tide conditions are 6.8-8.9 $\text{cm}\cdot\text{s}^{-1}$. Shapes of these spectra are similar to wave spectra observed at this location (Figs. B1 and B2). Notice that speed amplitudes at high tide are higher than at low tide and correlate with the wave height changes as expected.

Analysis of the current records indicates that, in general, the speeds vary around 20 $\text{cm}\cdot\text{s}^{-1}$ in the offshore and onshore directions at both meters. Maximum speed values are 50 $\text{cm}\cdot\text{s}^{-1}$ directed onshore and 30 $\text{cm}\cdot\text{s}^{-1}$ directed offshore at both levels. The net currents have values around 1 $\text{cm}\cdot\text{s}^{-1}$ directed onshore with tidal modulation, as will be discussed later.

Coherence squared between the waves and currents at the lower current meter is presented in Fig. 7.3. Coherence at frequencies smaller than 0.046 cps (period ~22 s) is always nonsignificant, indicating that low frequency currents are not linearly related to the wave field at the same frequencies. At frequencies larger than 0.046 cps, the coherence values generally increase to near 1.0, indicating that waves and currents are linearly related. Coherence between waves and currents in the upper layer is similar to those of Fig. 7.3.

The close agreement of the speed amplitudes and averages, as well as with direction, indicates that the vertical shear of currents at the reef crest is either small or was not detected during this experiment.

Fig. 7.2. Current autospectra with 16 degrees of freedom, from measurements at the reef crest by two ducted current meters oriented in an onreef-offreef direction and stacked vertically (at 0.95 and 0.65 m above the reef floor). During Experiment 1, data on which the above autospectra were generated were collected at low and ebb tide.

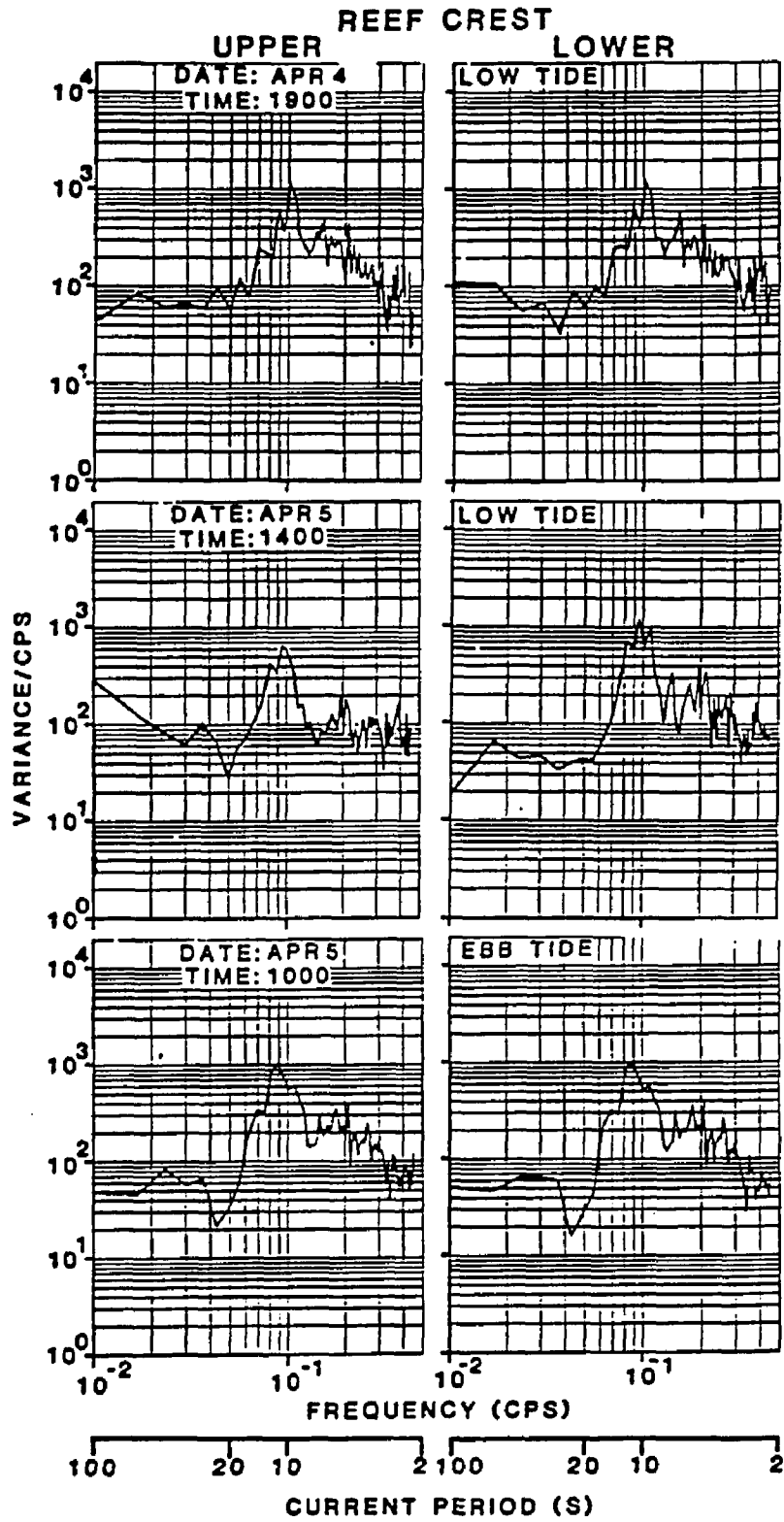
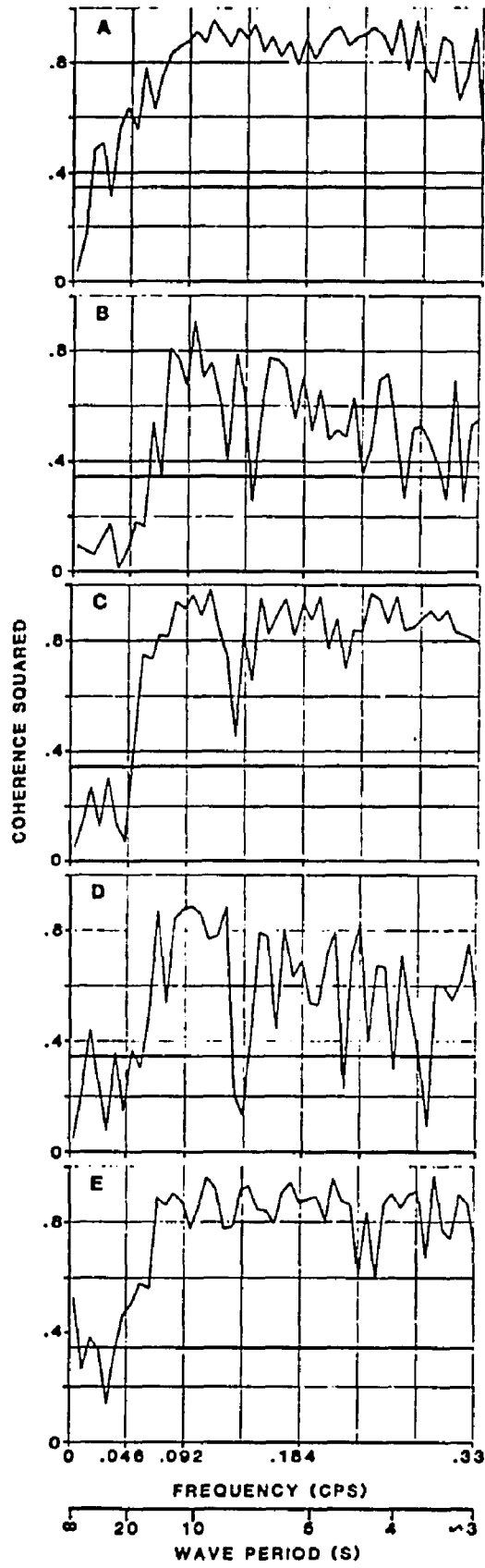


Fig. 7.3. Coherence squared between waves and currents of April 4, 1900(A) and 2200(B); April 5, 0100(C),1000(D), and 1400(E) at the reef crest during Experiment 1 with 16 degrees of freedom.



Currents Across the Reef Profile

The objective of this section is to study the transverse variability of currents from forereef to lagoon. The ducted current meter arrangement is illustrated in Fig. 3.3. Measurements were collected for two tidal cycles during a 20 min burst every hour. The lagoon measurements were made during Experiment 1. The meter location is illustrated in Fig. 3.1. This meter operated for one tidal cycle only. Current spectra at the forereef and backreef stations during high and flood tide conditions are presented in Fig. 7.4. A peak near 0.075 cps (13 s) is evident at both stations. Notice the reduction of the variance levels towards the backreef, which reduction is similar to the trend observed in the wave heights. Low and ebb tide conditions illustrated in Fig. 7.5 show a similar trend of the speed spectra and similar shape. Current spectra illustrated in Figs. 7.4 (high tide) and 7.5 (low tide) are mirror images of the corresponding wave spectra shown in Figs. 6.2 and 6.3. Forereef speed amplitudes estimated from these spectra peaks are 6.9-13.1 $\text{cm}\cdot\text{s}^{-1}$ for high tide and 10.3-10.6 $\text{cm}\cdot\text{s}^{-1}$ at low tide. The backreef estimated speeds are 4.2-7.0 $\text{cm}\cdot\text{s}^{-1}$ at high tide and 1.9-4.1 $\text{cm}\cdot\text{s}^{-1}$ at low tide. The speed amplitude was calculated as described in the previous section. Current observations from the reef crest are not discussed because during Experiment 2 the reef crest current meter malfunctioned.

Lagoon measurements, however, were made, and results were unexpected. The lagoon water depth at the lagoon meter site was almost 5 m, and the currents were low and irregular throughout the entire observation period. There are two possible explanations for these observations. The first is that under small waves the currents are weak and a sudden depth increase reduces the

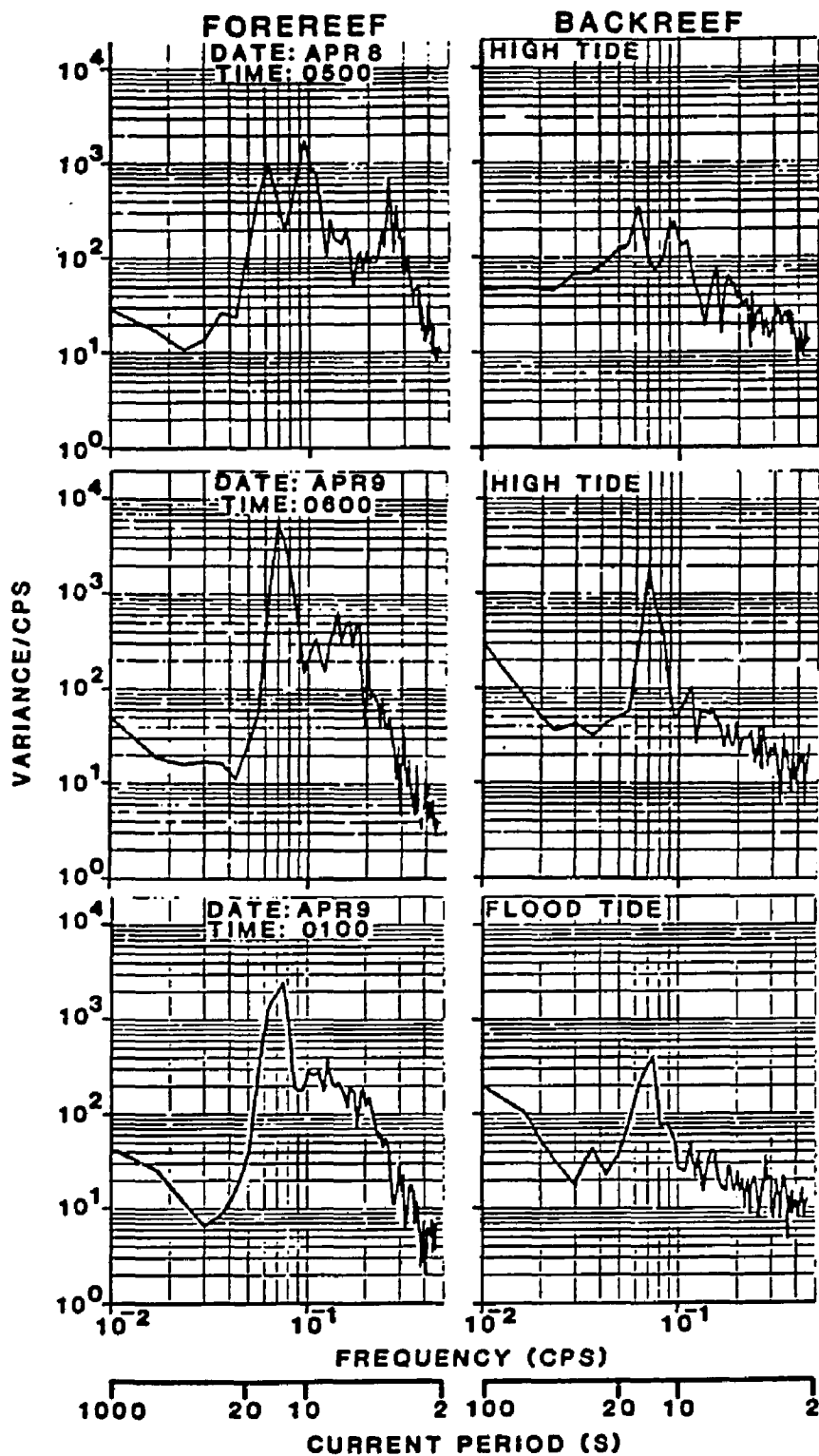


Fig. 7.4. Current autospectra from measurements at the forereef and backreef during Experiment 3 at high and flood tide with 16 degrees of freedom.

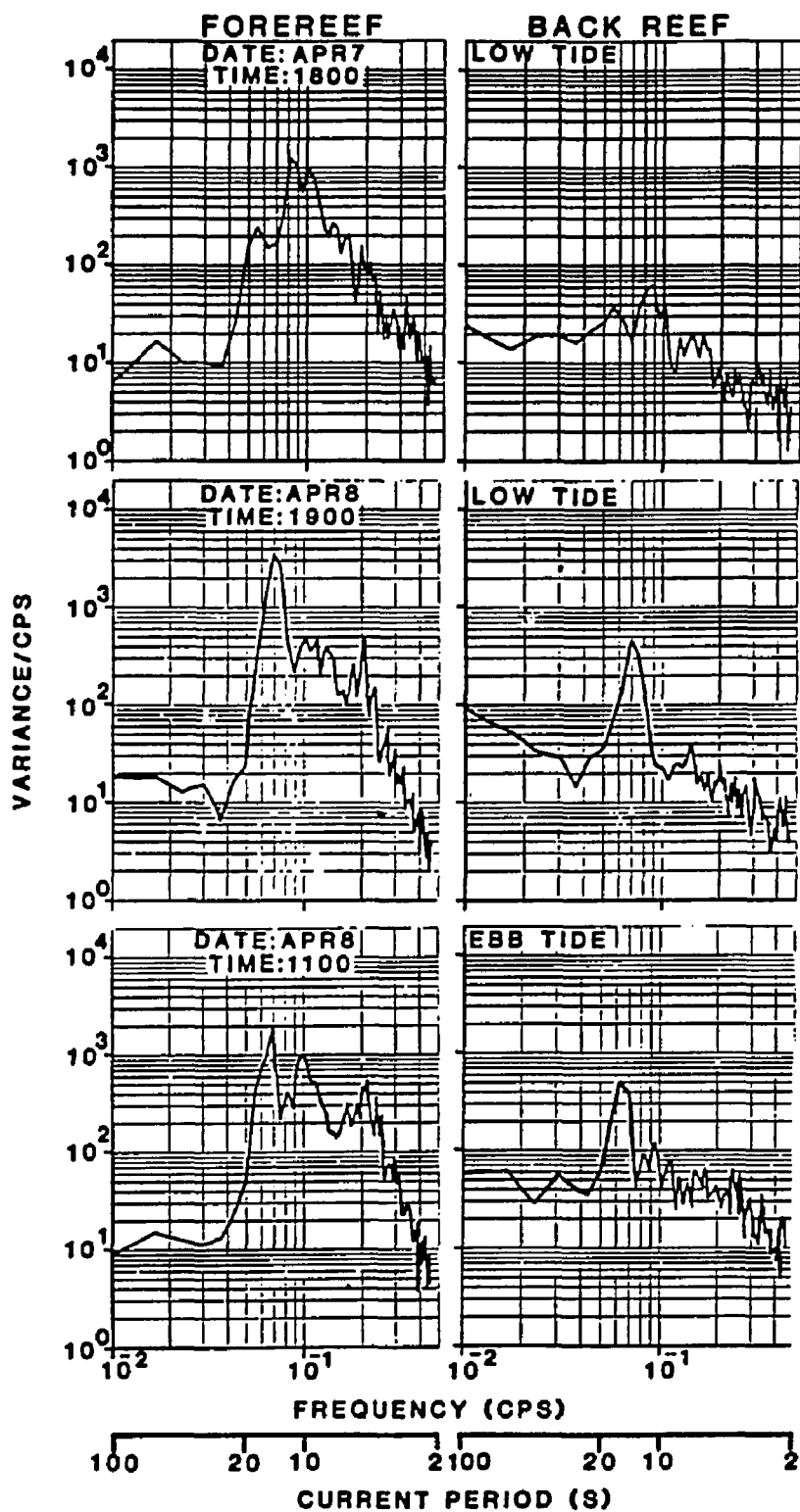


Fig. 7.5. Current autospectra from measurements at the forereef and backreef during Experiment 3 at low and ebb tide with 16 degrees of freedom.

speed dramatically because of mass continuity. The second possibility is that reef crest water behaves like a jet issuing from the crest and passes over the current meter that was installed near the lagoon floor.

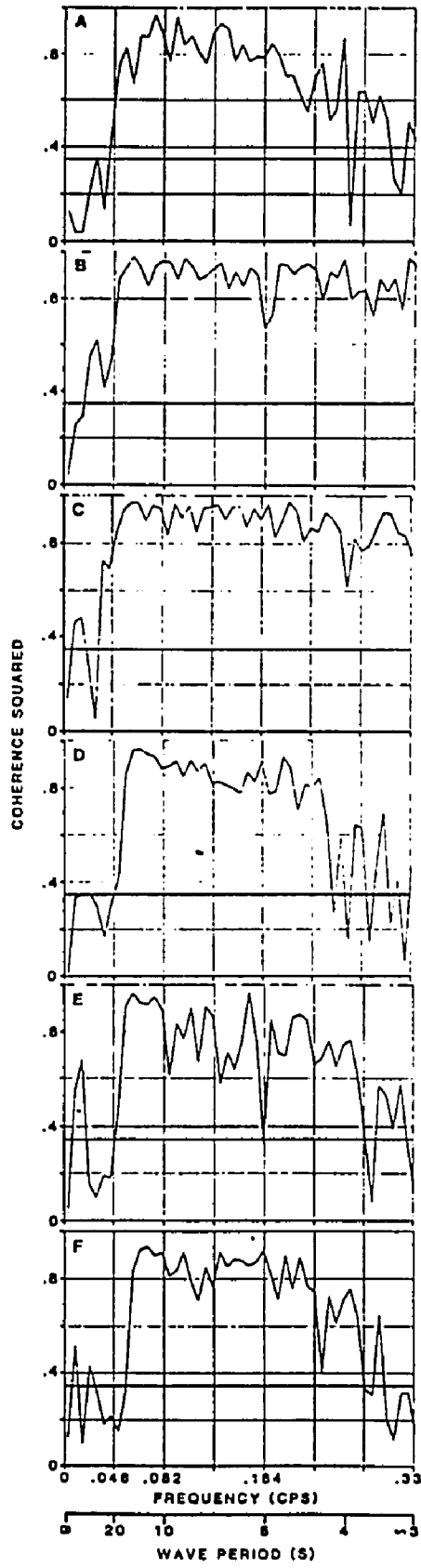
The most frequent speed at the forereef is near $20 \text{ cm}\cdot\text{s}^{-1}$. At the backreef it is about $10 \text{ cm}\cdot\text{s}^{-1}$. Maximum offshore speeds are around $45 \text{ cm}\cdot\text{s}^{-1}$ at the forereef and $20 \text{ cm}\cdot\text{s}^{-1}$ at the backreef during the observation period. Maximum measured onshore speeds are $39 \text{ cm}\cdot\text{s}^{-1}$ at the forereef and $30 \text{ cm}\cdot\text{s}^{-1}$ at the backreef. Mean speeds over the 20-minute measurements are around $1 \text{ cm}\cdot\text{s}^{-1}$ directed onshore. The time series of these mean currents over two tidal cycles indicate tidal modulation.

Coherence squared between waves and currents at the forereef station is presented in Fig. 7.6. Again, frequencies smaller than 0.046 cps are not correlated with the waves, and frequencies larger than 0.046 cps are significantly correlated with the waves. This high coherence between waves and currents across the reef profile suggests that waves are driving the currents with periods less than 22 s. Note also that there is very little wave energy at frequencies less than 0.046 cps.

Experiment 4

The objective of Experiment 4 was to study long-term wave current variability (periods between 30 and 1 min). Therefore, the 20-min burst sampling used in other experiments was replaced with continuous measurements over a period of 1 hour and 55 minutes. Swells of 12-15 s and wave heights around 0.30 m were the most energetic signals during this study. Wind conditions represented typical Caribbean trade winds. The instrument array for this experiment was similar to that used for Experiment 3. Current spectra at the forereef and backreef sites (Fig. 7.7) indicate that most current energy is concentrated near a frequency of 0.07 cps (14 s) at both stations;

Fig. 7.6. Coherence squared between waves and currents of April 7, 1800(A), April 8, 0500(B), 1100(C), 1900(D), April 9, 0100(E), 0600(F) at the forereef during Experiment 3.



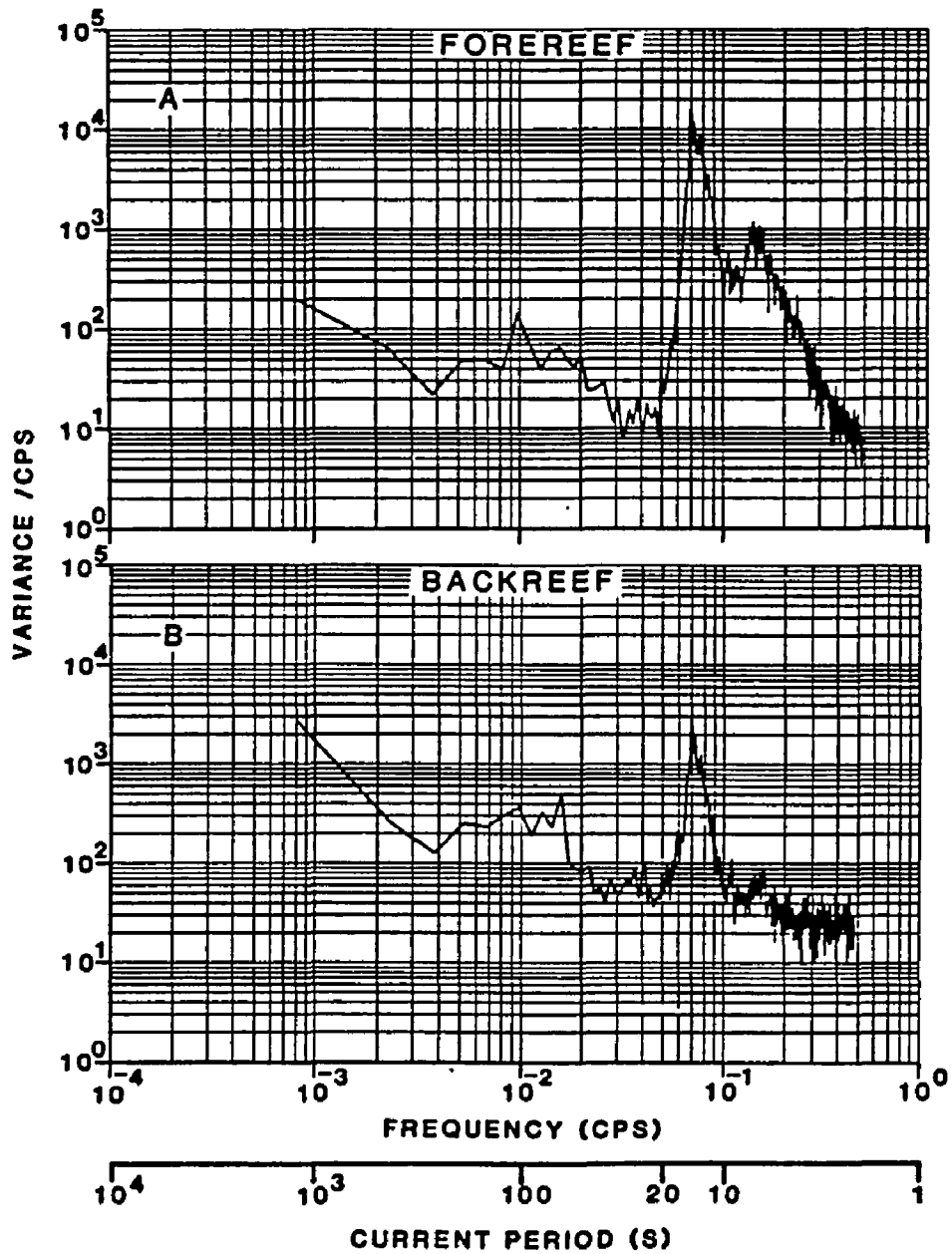


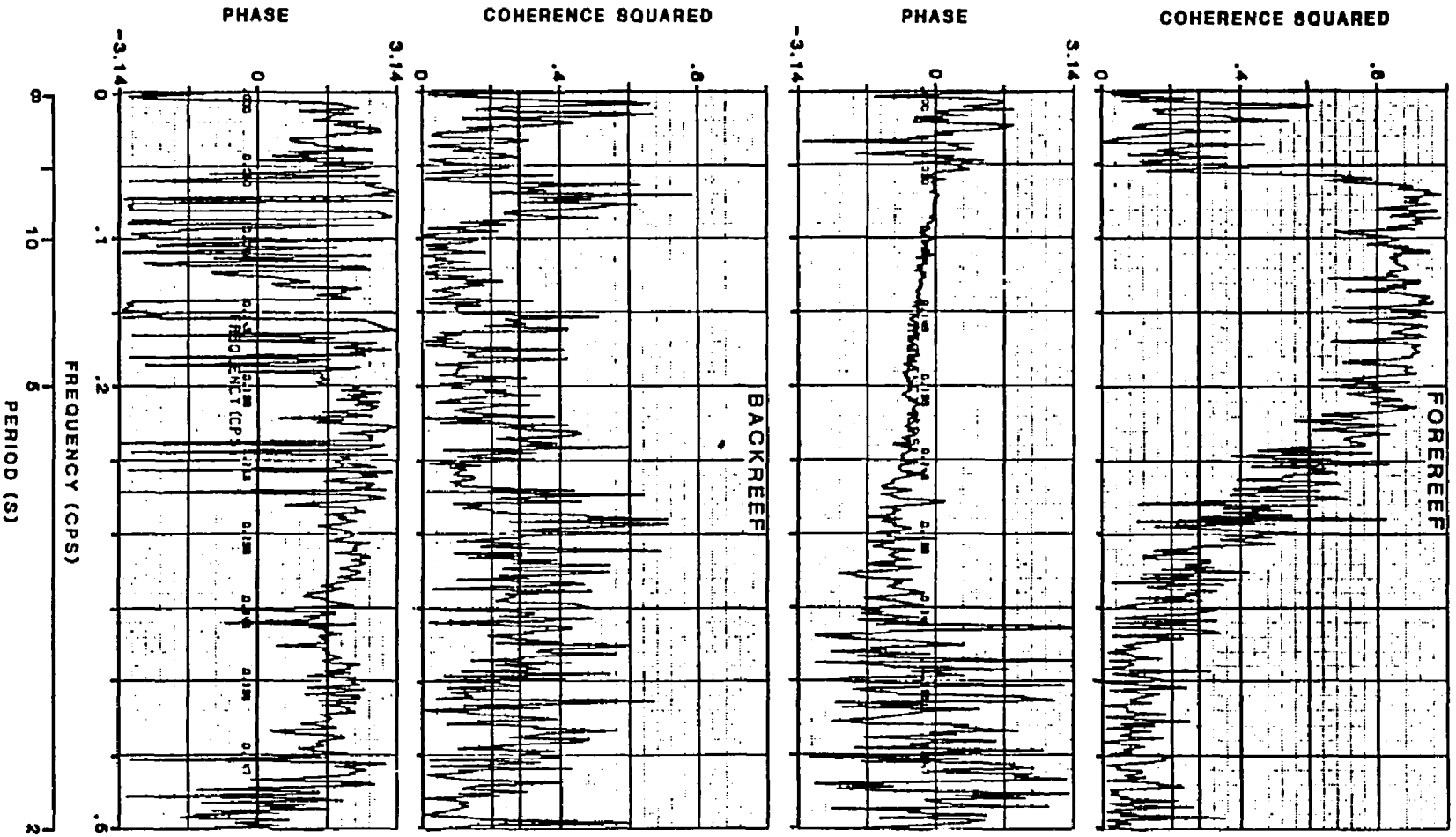
Fig. 7.7. Current autospectra from measurements at the forereef and backreef made during Experiment 4 with 20 degrees of freedom..

another peak near 0.15 cps (6.7 s) is present at the forereef but not in the backreef data. Again, variance reduction between stations is evident. Current speeds at the 14 s period, based on the spectra, are $5.2 \text{ cm}\cdot\text{s}^{-1}$ at the forereef and $1.9 \text{ cm}\cdot\text{s}^{-1}$ at the backreef stations. Maximum offshore speeds are $44 \text{ cm}\cdot\text{s}^{-1}$ at the forereef and $18 \text{ cm}\cdot\text{s}^{-1}$ at the backreef. Onshore maximum speeds at the forereef are $45 \text{ cm}\cdot\text{s}^{-1}$ and $30 \text{ cm}\cdot\text{s}^{-1}$ at the backreef stations. Mean currents are near $2 \text{ cm}\cdot\text{s}^{-1}$ at the forereef and $3 \text{ cm}\cdot\text{s}^{-1}$ at the backreef, both directed onshore.

Coherence squared and phase between waves and currents at both forereef and backreef data collection sites are presented in Fig. 7.8. The coherence squared at the forereef is similar to that of the previous experiment and will not be described here. Phase shows a linear trend with a negative slope in the frequencies of interest (0.01-0.5 cps). This relationship means that waves and currents are linearly related. Coherence squared between waves and currents of the backreef station shows significant coherence only near the frequency of the main peak (0.07 cps), and even then not high values. The phase oscillates around 180° . Up to this point the information presented has shown that energy at frequencies of gravity waves and tides directly influences currents. However, no indication of the infragravity signal has been found in the currents analysis. It was decided to explore this possible interaction using other techniques.

A low-pass filtered version of both current records with a cut-off of 60 s (Fig. 7.9) was made to check for the presence of long-period oscillations. The forereef record illustrated fluctuations with magnitudes near $4 \text{ cm}\cdot\text{s}^{-1}$ and a time average of $1.97 \text{ cm}\cdot\text{s}^{-1}$, both directed onshore, with no flow reversals. The current meter was 1.0 m above the sea floor in a water depth of 3.8 m. At the backreef station, water depth was 1.2 m, and the ducted meter was 0.6 m above

Fig. 7.8. Coherence and phase angles between waves and currents at the forereef and backreef during Experiment 4. The horizontal line represents the 95% significance level.



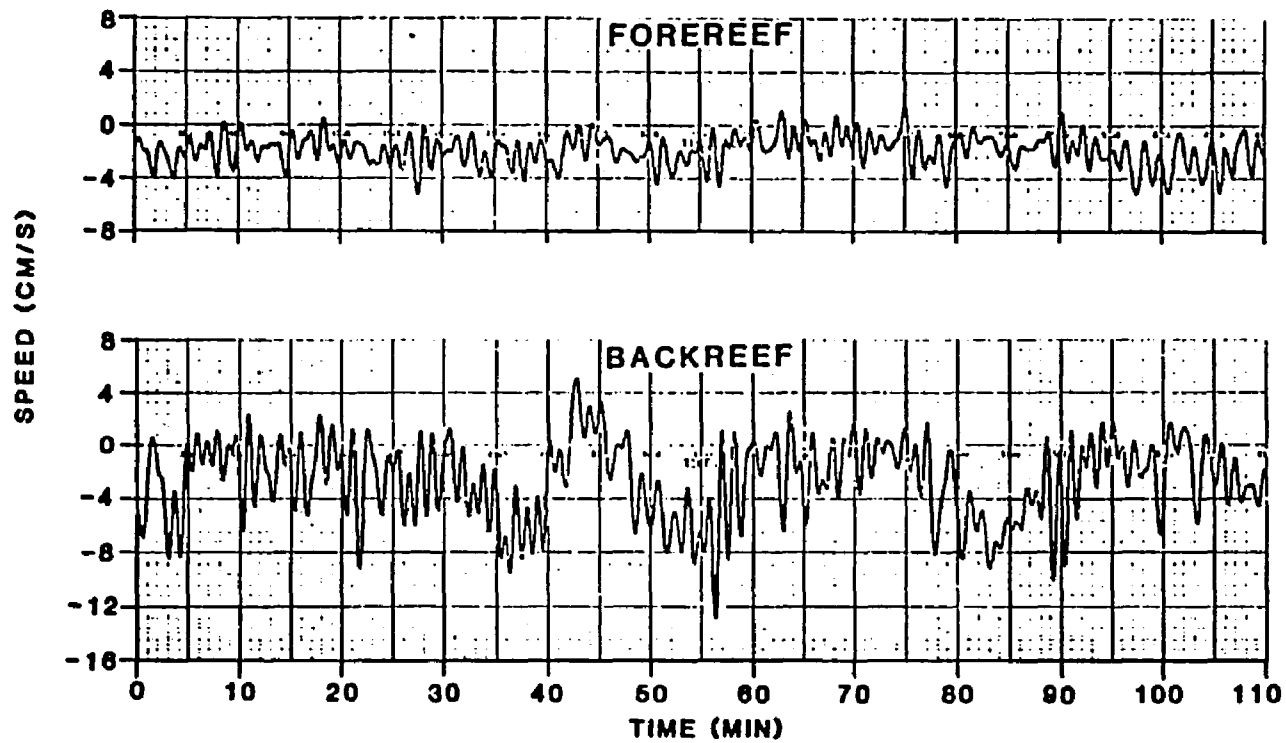


Fig. 7.9. Low pass (cut-off 1 min) of current records at the forereef and backreef during Experiment 4 showing 30 min oscillations.

the floor. The low-passed current was more interesting at the backreef site. Well-defined episodes of flow reversals were present at time scales of approximately 25 min, and the speed varied from near $10 \text{ cm}\cdot\text{s}^{-1}$ towards the lagoon to $4 \text{ cm}\cdot\text{s}^{-1}$ in the offshore direction. A time-averaged flow of $2.67 \text{ cm}\cdot\text{s}^{-1}$ was directed towards the lagoon. Oscillations with a period of 27 min were observed in both tide and wave records during this experiment (Fig. 6.12). These long period oscillations, unresolved by the spectrum analysis, were suggested by the low-pass filter technique. Roberts and Suhayda (1983) first reported the presence of infragravity waves in a reef environment and their probable importance to sediment transport. This study suggests a topographical origin for the infragravity waves measured at the Tague Bay reef site, their characteristics over the reef, and their importance for driving water motion across the reef.

Mass Transport

Results of wave and current measurements are used to estimate mass transport across the reef crest. This application requires the theory relating Eulerian measurements of speed and Lagrangian mass speed. Longuet-Higgins (1969) and Zimmerman (1979) have shown that if the current gradient is small, then the Lagrangian mass speed (V_L) is related to the record mean (V_E) and the mass transport (M) of the oscillatory flow by:

$$V_L = V_E + \frac{M}{\rho h}$$

where ρ is the fluid density, and h is the water depth. V_E is calculated by vertically averaging the time average of the records. Mass flux for pure progressive waves of constant profile is given exactly (Phillips, 1980) by:

$$M = \frac{E}{c}$$

where E is the wave energy density and c the phase speed. The transport is in the direction of wave propagation. To second order, the mass flux is given by:

$$M = \frac{1}{8} \rho k c H^2 \coth(kh)$$

where H is the wave height, k the wave number, and $\coth(x)$ the hyperbolic cotangent function. In shallow water this expression reduces to:

$$M = \frac{\rho g H^2}{8c}$$

where g is the acceleration due to gravity. Average mass transport across the reef is found by integrating the Lagrangian mass speed over time. Total volume transport across the reef is found by multiplying average transport by reef length (L). Justification for the use of the linear wave theory comes from the fact that the ratio of wave height to depth varies from 0 to 0.3 in this study.

The following speed statistics were computed from current records collected during Experiments 1 and 3: time average speed, largest offshore speed, and largest onshore speed for each record. These were then plotted against time (Fig. 7.10). Notice the striking asymmetry of the peak current bias towards the lagoon ($60 \text{ cm}\cdot\text{s}^{-1}$ onshore vs. $30 \text{ cm}\cdot\text{s}^{-1}$ offshore) and the small time average at each level. A possible malfunction of the upper meter is evident near hour 25. The plot of the statistics of the current records for data from Experiment 3 is presented in Fig. 7.11. Again, notice the asymmetry and the small time average during all records. This asymmetry should cause a net lagoonwards flow of water at the forereef and backreef stations. Similar results are also evident in the data collected during Experiment 2, which data are

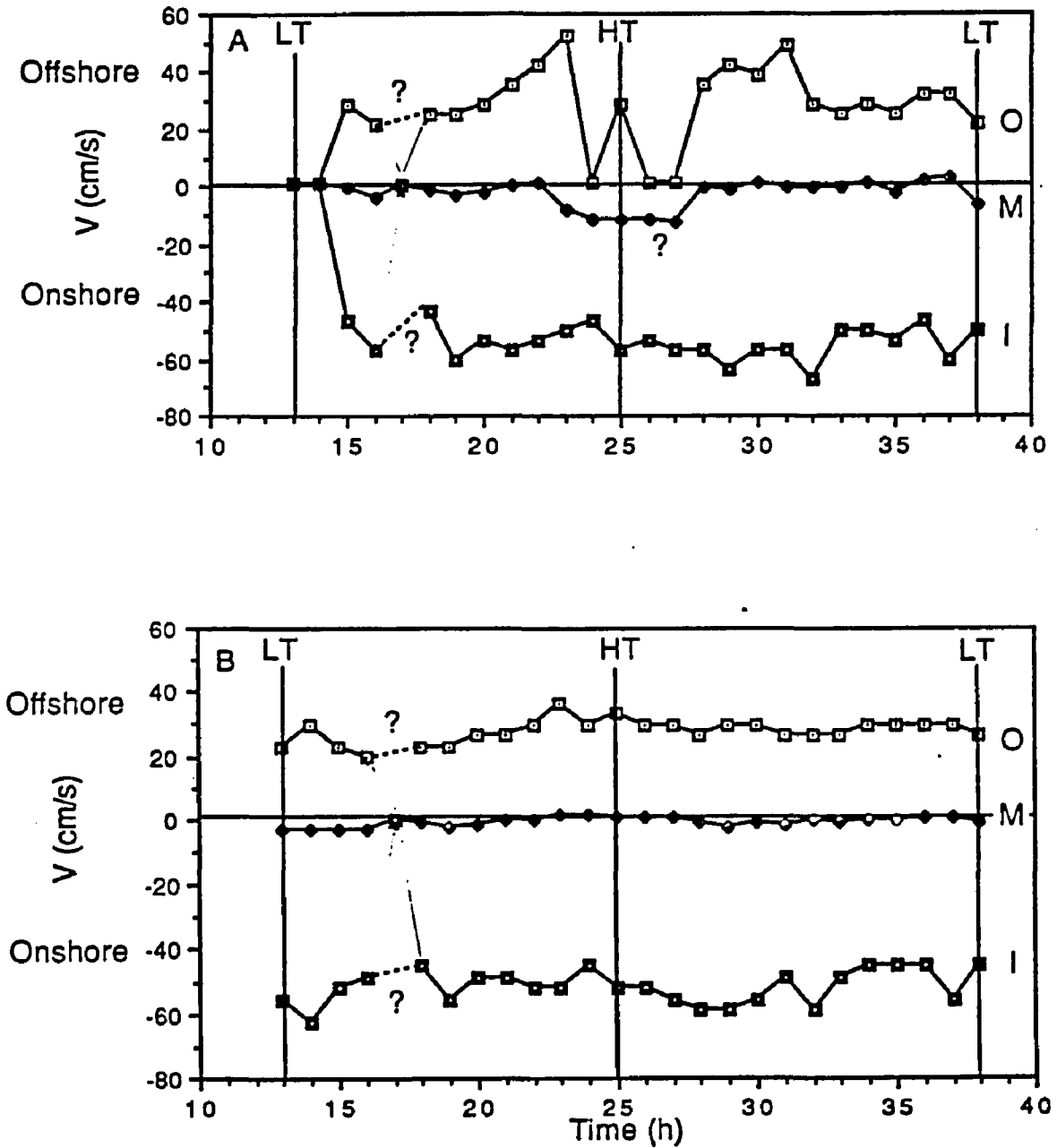


Fig. 7.10. Mean (M), largest onshore (I) and offshore (O) current speeds for each record collected at the reef crest during Experiment 1. Upper level (A) and lower level (B).

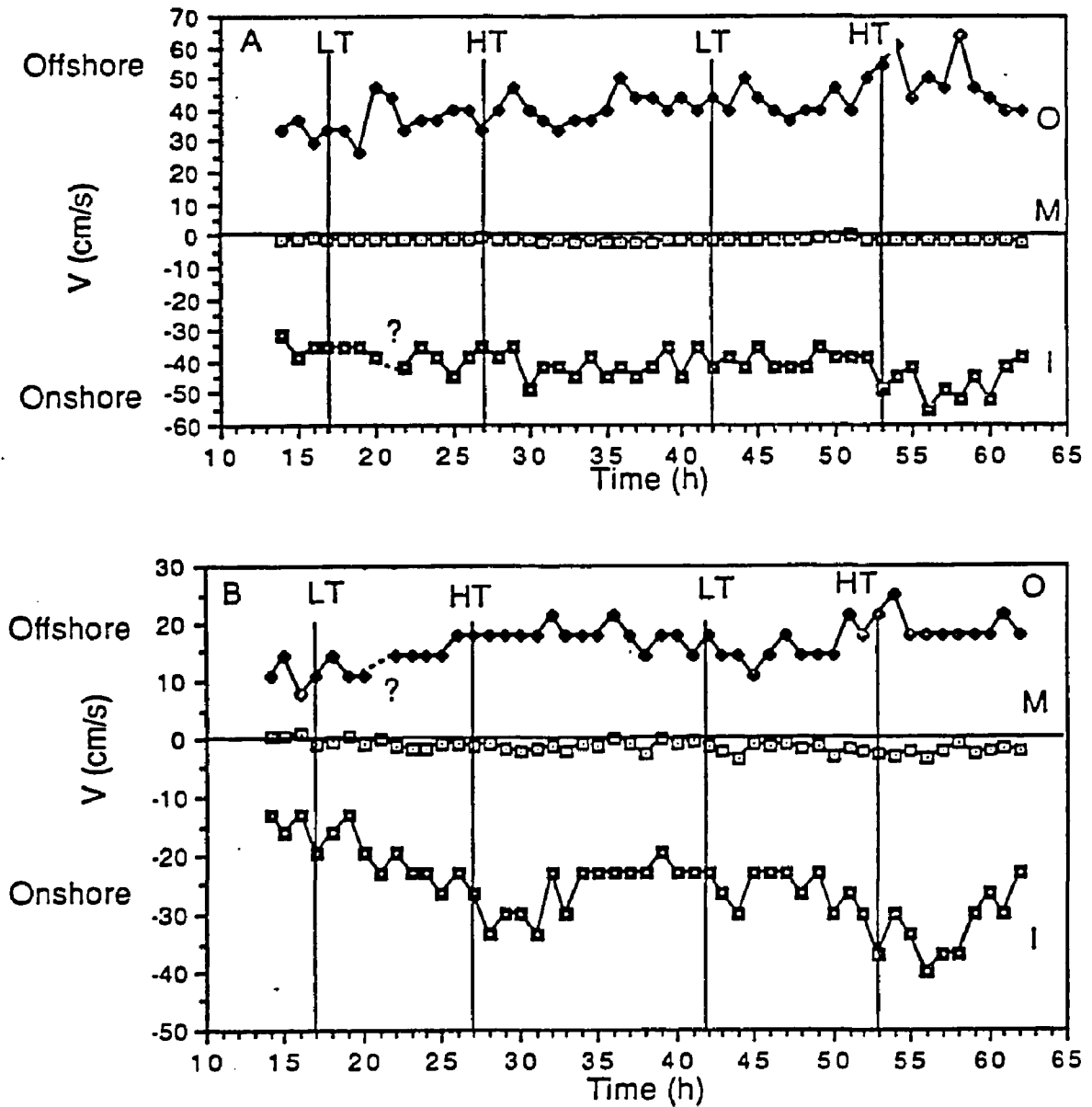


Fig. 7.11. Mean (M), largest onshore (I) and offshore (O) current speed for each record collected at the forereef (A) and backreef (B) during Experiment 3.

presented in Fig. B18 of Appendix B. No explanation can be offered for this asymmetry at this time.

Estimates of the total volume flux across a 1-m width of the reef crest and backreef, using all data available for each station, are presented in Table 7.1 using both linear wave and solitary wave theory.

Table 7.1. Average volume flux at the reef crest and backreef in m^3s^{-1} during the study using linear and solitary wave theories.

Reef Crest			Backreef		
	Linear	Solitary		Linear	Solitary
Exp. 2	0.0128	0.1017	Exp. 3	0.0236	0.0782
Exp. 3	0.0262	0.1095			

Notice that solitary wave estimates are, in general, an order of magnitude larger than the linear wave estimates. Total volume flux estimates across the whole reef, using the linear theory figures, are 77.0, 169.6, and 141.7 m^3s^{-1} with a mean value of 129.4 m^3s^{-1} . The average wave contribution to the total volume flux is 50% and varies from 77 to 36%. Calculating the volume of the lagoon, using its surface area and mean water depth, and dividing by the calculated flux provided three estimates of flushing time: 62 hrs, 28.1 hrs, and 33.7 hrs, with an average of 37 hrs. These estimates are larger than estimates for the comparatively small but similar system of Great Pond Bay (8 hrs) (Roberts et al., 1981a). Flushing times calculated using the solitary wave volume transports are less than 10 hrs in all instances.

Instantaneous Currents and Sediment Transport

Current spectra provide information on the distribution of speeds by time scale. However, spectra provide no information on the instantaneous speeds, which are responsible for the movement of particles on the reef floor. This information is obtained from the speed records directly. In Fig. 7.12 simultaneous 300-s portions of wave heights at the forereef and lower crest current meter at high tide are presented. During this period three wave groups, from 70 to 120 s; 150 to 210 s; and 220 to 270 s, with heights near 40 cm, are visible. Notice the modulation of the currents with these wave groups, a lag of about 6 seconds, and high speeds during large waves and low speeds during low waves. Also, speed asymmetry increases under high waves. During large wave groups, the onshore speed at the reef crest reaches $40 \text{ cm}\cdot\text{s}^{-1}$, and the offshore speed reaches $20 \text{ cm}\cdot\text{s}^{-1}$ only. During low wave groups, the speeds are symmetrical and vary between $20 \text{ cm}\cdot\text{s}^{-1}$ in both offshore and onshore directions. Low tide conditions are illustrated in Fig. 7.13. During this period the wave conditions are more homogeneous, and wave groups are not well-defined. The speed record from the lower meter at the crest generally illustrates currents directed onshore at $30 \text{ cm}\cdot\text{s}^{-1}$ and offshore speeds less than $16 \text{ cm}\cdot\text{s}^{-1}$. The upper current meter reflects similar speed variability, but the degree of onshore-offshore current asymmetry is greater than in the record from the lower meter. Under the onshore surges, particles of 0.2 mm in diameter can be moved forward, but only particles of 0.03 mm can be moved backwards. The asymmetry of the currents clearly contributes to the net movement of sediments into the lagoon since sands are transported only into the lagoon, not backwards.

Fig. 7.14 illustrates 300 seconds of sea surface and current variations at the forereef and backreef stations during high tide conditions. Two wave

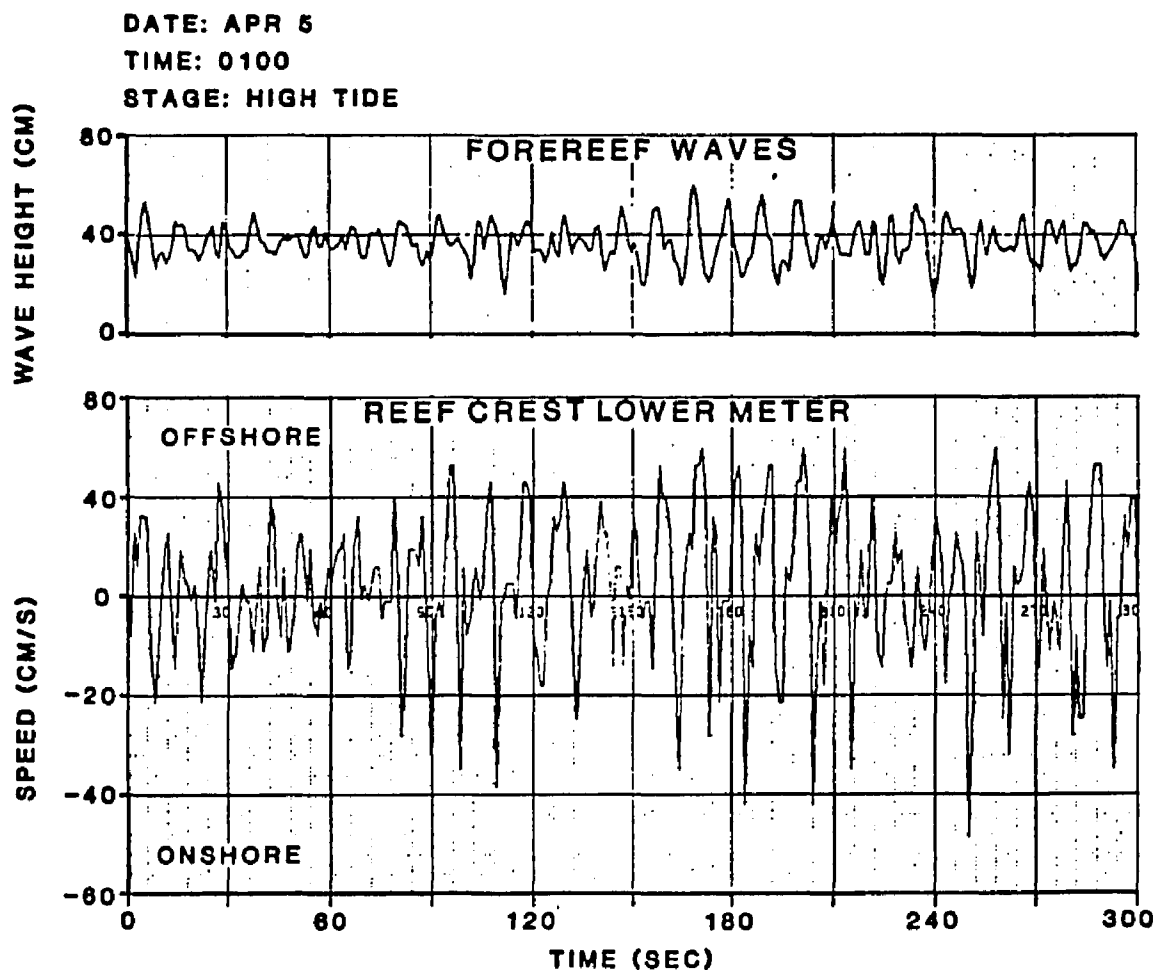


Fig. 7.12. A 300 s section of the forereef wave and lower current records collected at 0100 April 5, during Experiment 1.

DATE: APR 5
TIME: 1400
STAGE: LOW TIDE

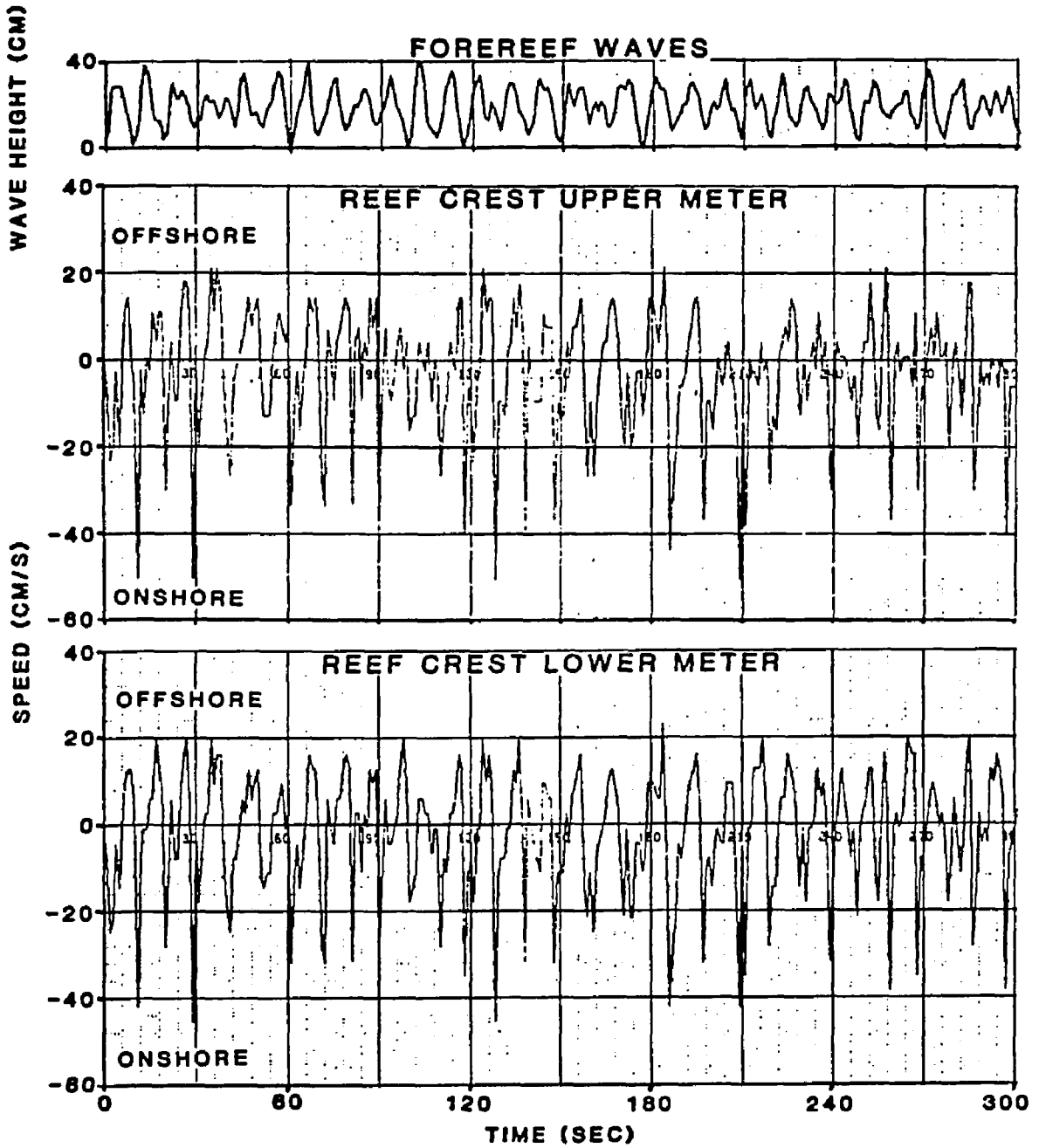


Fig. 7.13. A 300 s section of the forereef waves and lower and upper current records collected during April 5, 1400 during Experiment 1.

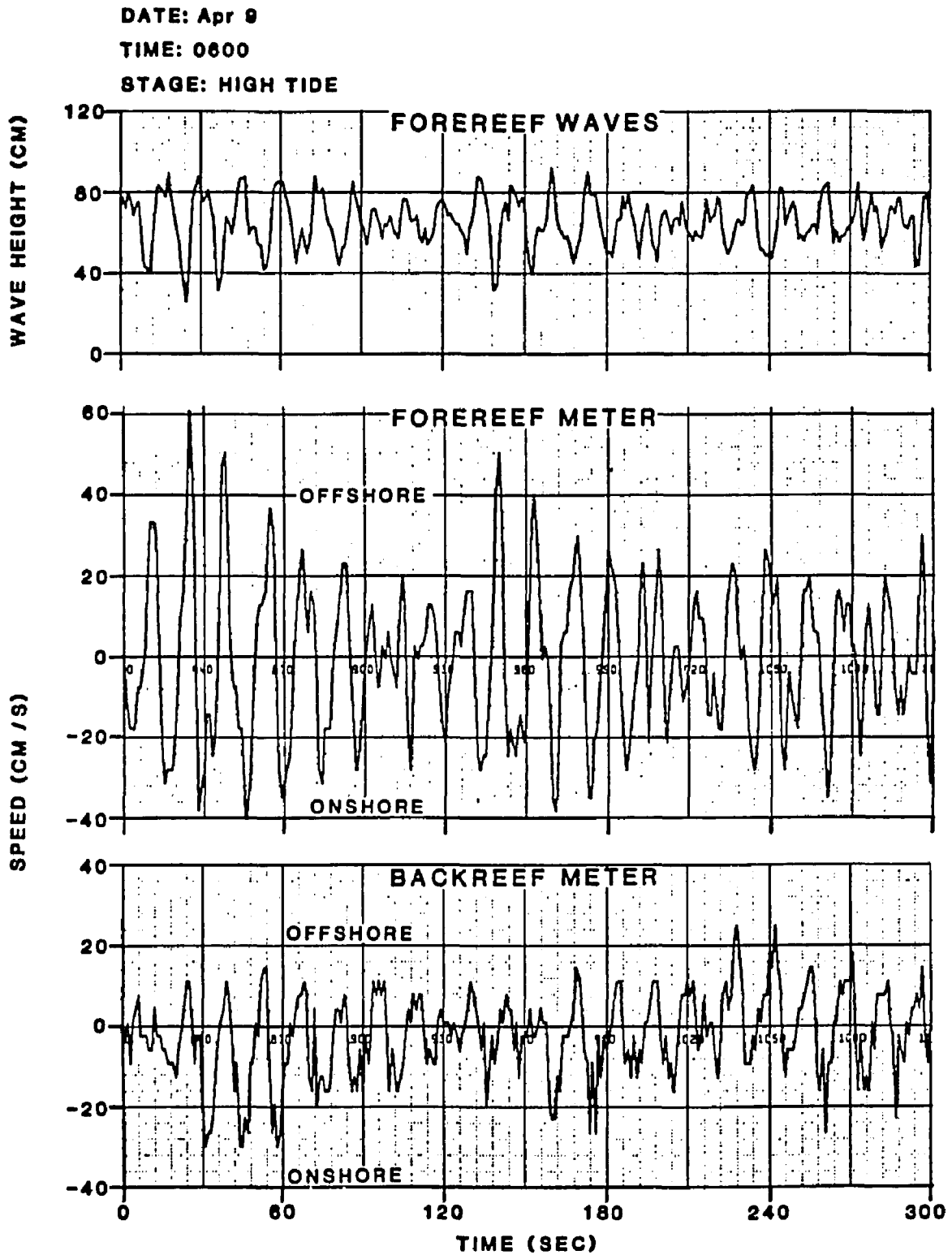


Fig. 7.14. A 300 s section of the forereef waves and currents, and backreef records collected during April 9, 0600 during Experiment 3.

groups are clearly visible with wave heights between 72 and 40 cm. Wave heights of 32 cm prevail between wave groups. Currents at the forereef are modulated by wave groups, and speeds are asymmetric. Maximum offshore speeds of $50\text{-}60\text{ cm}\cdot\text{s}^{-1}$ and onshore speeds of $36\text{-}40\text{ cm}\cdot\text{s}^{-1}$ are common during high wave conditions. The backreef station also indicates wave group modulation and current asymmetry. Offshore peak speeds are $12\text{ cm}\cdot\text{s}^{-1}$, and the onshore peaks are $30\text{ cm}\cdot\text{s}^{-1}$ under the wave groups, currents being stronger in the onshore direction. At these speeds, particles of 0.8 mm and 0.2 mm in diameter (Leeder, 1982) can be moved offshore and onshore by the waves at the forereef respectively. This size range corresponds to fine to coarse sands. Backreef speeds can move particles of 0.2 mm size, which represents fine sands (Leeder, 1982). An important point to stress is that current asymmetry at the forereef causes sand to move offshore aided by the pull of gravity over the inclined forereef floor. The suspended sediment moves onshore by the slower mean flow. At the backreef and reef crest, both sediment loads are moved onshore because both the net flow and the current asymmetry are directed shorewards. These estimates of particle size movement represent conservative estimates because effects of resuspension by waves and turbulence combined have not been considered. At the forereef the time average speed is $1.97\text{ cm}\cdot\text{s}^{-1}$ directed onshore. Thus, it appears that bottom particles may be driven offshore by the current asymmetry, while suspended material is transported onshore. This can give rise to a flux divergence of sediments at the forereef. However, because the divergence zone depends on the wave conditions, it is expected that this zone moves, blurring the effects of distributing the sediments away from the divergence zone.

8.0 Discussion of Results

Coral reef ecosystems are built by sessile organisms, which depend largely on the physical energy of the environment for their survival. In their evolution, corals and the structures they build have developed so as to modify and use the movement of surrounding waters as an energy subsidy to the ecosystem. It is these physical process modifications by corals reefs that this study was designed to investigate. In particular, the study focused on the role of tides, waves, and currents in modifying water motion over the reef. It is known, for example, that just a small fraction of water impinging atoll-reefs actually flows over it; most of it flows along the sides (Hamner and Wolanski, in preparation) or is deflected seawards. However, this limited cross-reef flow is of paramount importance because it links the reef-lagoon to the open sea. The linkage is established through currents produced by forcing agents such as tides, wind stress, wave-breaking transport, and related wave set-up. This section will discuss results of field measurements of temporal and spatial sea level variations, wave processes, and volume flux across a Caribbean reef crest. Wave processes include energy attenuation by turbulence and bottom friction, wave transmission, and induced currents. After these results are discussed, an integrated model of transport across the reef crest is presented.

Water Levels

Water level observations at the forereef and lagoon indicated a predominantly diurnal tide with a range of 30 cm. Spectrum analysis revealed that diurnal, semidiurnal, and infragravity signals were present in the water level records. The diurnal component had an amplitude of 6.9 cm, and the semidiurnal component 2.4 cm. Infragravity oscillations had a period near 27.7

min and an amplitude of 0.85 cm. The diurnal character of the tides at Tague Reef is well known (Kjerfve 1981; Ogden 1974; Roberts unpublished data); however, the observed tidal range was larger than previously reported by Kjerfve (1981). Infragravity waves at Tague Reef or around St. Croix have not been reported. However, similar oscillations have been observed on shelves (Geise et al., 1982; Geise and Hollander, 1987) and in coral reef environments off Nicaragua (Roberts and Suhayda, 1983). Roberts and Suhayda (1983) observed a period between 15 and 30 min and an amplitude of 4-8 cm. These values are in reasonable agreement with observations of infragravity waves at Tague Reef made during this study. The importance of these oscillations to reef dynamics lies in their fine-grain sediment transport potential (Roberts and Suhayda, 1983) and the associated volume flux over the crest.

Cross-spectrum analysis indicates a zero phase lag or time difference between the forereef and lagoon tides. The infragravity component has a phase lag of 1.7 min with the lagoon side lagging the forereef. The time difference between forereef and lagoon estimated from theory is 3.45 min. This agreement is reasonable considering the limitations of the model used to calculate phase lags (see Chapter 5). Current observations in Buck Island channel and inside the reef lagoon suggest that tides and infragravity waves are propagating alongshore and not cross-shore. This wave propagation and observed time lag produce sea level differences that can drive water across the reef crest. Similar conditions have been observed at Ningaloo Reef, Western Australia, a reef with a geometry similar to Tague Reef (Hearn and Parker, 1988).

Water Temperature

Temperature measurements derived from tide gages placed both in the forereef and lagoon indicate that lagoon water is warmer than forereef water. During daytime a gradient of 0.8°C exists across the reef, but the two water bodies reach thermal equilibrium at night. This temperature gradient is a function of water depth differences and available solar radiation. Temperature gradients reported from atolls are related to the restricted lagoon circulation (Pugh and Rayner, 1981; Kjerfve, 1978). Kjerfve (1978) states that the lagoon acts as a heat source during daytime and a heat sink during night as observed in this study. This temperature gradient is important because mixing of lagoon and forereef waters produces the reef crest water mass. This reef crest water has chemical properties differentiated from the forereef water, which has been changed by intense biological processes (Hamner and Wolanski, in preparation).

In-situ Winds

Wind measurements made during the reef experiment represent typical Caribbean trade wind conditions with speeds around $3\text{-}10\text{ m}\cdot\text{s}^{-1}$ from the NE-E. The alongshelf and cross-shelf wind components show that most of the energy is directed alongshore and westward. The mean speed in this direction is $3.9\text{ m}\cdot\text{s}^{-1}$. The spectrum of this component indicates that most of the energy is concentrated at periods between 12 and 24 hours. The cross-shelf component is weaker with a mean flow of $0.6\text{ m}\cdot\text{s}^{-1}$ directed into the lagoon. The wind spectrum shows that, again, most of the energy is between 20 and 37 hour periods.

Long-term Currents

Current measurements in Buck Island Channel (Fig. 5.11) were dominated by a bidirectional, semidiurnal flow with speeds around $10 \text{ cm}\cdot\text{s}^{-1}$ in agreement with shelf currents off the south coast (Roberts et al., 1981a,b). The alongshore component had a net westward flow of $3.1 \text{ cm}\cdot\text{s}^{-1}$ with considerable energy at diurnal and semidiurnal frequencies. The cross-shelf component had a net southward flow with considerable energy at diurnal frequencies.

Water Levels Differences

Sea level differences across the reef were primarily diurnal oscillations that modulated the infragravity waves. Even though cross-spectra showed zero phase lag at tidal frequencies, the surface slope spectra showed most of the signal's energy near diurnal frequencies. This discrepancy can be attributed to the short tidal record employed in the spectrum analysis. Other possible mechanisms that may have created water level differences were the reduction of tidal amplitude in the lagoon by friction or wind set-up. Cross-shelf winds displayed a positive correlation with the water level differences, and the correlation coefficient at zero lag was 0.40. A coherence squared of 0.89 between cross-shelf wind stress and water level differences existed between periods of 24-30 hours. The characteristic cross-shelf wind stress can produce a set-up of only 0.02 cm against the coastline, indicating that wind stresses were not creating the surface slope at diurnal frequencies. The water level differences at infragravity wave frequencies were measured at about 0.75 cm. Absolute level differences were not observed because of problems in the leveling of the tide gages. Superposition of infragravity and tidal oscillations makes this problem highly time dependent. Observations of sea level

differences on other coral reefs have concentrated on wave set-up, and these can be up to 10 cm in the Pacific and 1 cm in the Caribbean (Gerritsen, 1981; Munk and Sargent, 1948; Roberts unpublished data). Sea level differences were estimated analytically for the infragravity waves in Chapter 5. Assuming a balance between the surface slope, bottom friction, and net acceleration, the resulting speed can be calculated. As will be discussed later, 20-min current averages exhibited tidal variations, and a low-passed speed plot of data from Experiment 4 revealed reversals at time periods near 30 min.

Wave Results

As waves travel across the forereef into the lagoon, several transformations were found to be occurring on time scales of seconds and over distances of hundreds of meters. Based on these transformations, four wave zones were identified: (1) the shoaling zone characterized by increasing wave heights, (2) the breaking zone characterized by nonlinear processes, (3) the bore-like surf zone characterized by energy dissipation and wave height reduction, and (4) the lagoon where waves reform into oscillatory types. Spectral analysis of wave data from forereef, reef crest, and backreef sites indicated that total energy decreased as waves propagated lagoonward. However, not all energy at individual frequencies decreased; at some frequencies it increased. The increase can be accomplished by nonlinear energy transfer. Shapes of the spectra also changed. In particular, the spectrum peak at 9-10 s completely disappeared, while peaks at 14 s propagated with minor changes. These changes suggested that interfrequency exchange or convergence of energy and some selective processes occurred as waves traveled across the reef crest. Similar phenomena were observed by Gerritsen (1981) and Lee and Black (1978). A possible explanation of these phenomena

can be derived using nonlinear wave theory (Mei, 1984), but this topic will not be pursued here. Wave heights ranged from 30 to 40 cm at the forereef, 15 to 20 cm at the reef crest, 10 to 17 cm at the backreef, and near 5 to 15 cm at the lagoon. The study period was characterized by low wave conditions and represented the most common condition at Tague Reef. Average wave energy decreased 65% (range 80-44%) as waves traveled between forereef and reef crest. Average dissipation increased to 78% (range 90-58%) for waves traveling between forereef and backreef. These results agree with previous reports of energy dissipation by Munk and Sargent (1948)-95%; Roberts et al. (1975)-75%; and Lugo-Fernandez (1982)-80% between forereef and backreef. Energy dissipation increased 13% for waves crossing the reef crest to backreef. A similar increase in energy dissipation (18%) as waves go from the forereef to the backreef was found at Great Pond Bay, south coast of St. Croix (Roberts unpublished data).

Another significant finding of this study was the tidal modulation of wave energy dissipation. Low tide energy dissipation was found to be 15% more between forereef and reef crest and 20% more between forereef and backreef, as compared to high tide conditions. Tidal modulation of wave height has been observed by Roberts (1980), Roberts and Suhayda (1983), and Young (1987). Kono and Tsukuyama (1980) observed that depth reduction at the reef crest increased the dissipation of energy and significantly changed the spectrum shape. Studies of submerged breakwaters have shown that water depth at the crest controls wave height changes and attenuation across the structure (Ahrens, 1987; Nakamura et al., 1966). The Tague Reef study illustrated that wave heights at the reef crest were water depth limited, and that 68% and 75% of the wave energy were dissipated as waves traveled from the forereef to the

crest and backreef, respectively. Even small variations in the depth over the crest of modern reefs (30 cm in this study) can cause significant changes to wave dynamics and related processes.

Wave transmission creates wavy surfaces that are important to fisheries and for the design of man-made structures in coral reefs (Nakamura et al., 1966; Nelson and Lesleighder, 1985). Average wave height transmission during this study was 46% (65-32%) and was modulated by the tide. Low transmission correlates with low tide, and high transmission correlates with high tide. The explanation for this tidal modulation is the water depth variation at the reef crest which in turn controls the wave height. Studies of submerged breakwaters have found a similar dependence of wave transmission on water depth at the crest of the structure (Ahrens, 1987; Young, 1987). Wave transmission in the St. Croix study occurs by waves propagating over the reef crest and overtopping during wave breaking but not by run-up or through the reef structure. The principle of energy conservation applied to submerged breakwaters yields the following equation, which can be employed in this study (Nakamura et al., 1966):

$$1 = K_R^2 + K_T^2 + D^2$$

where K_R and K_T are the reflection and transmission coefficients, and D^2 is the energy dissipation. This equation assumes no wave overtopping of the structure. Substituting the energy dissipation (0.78) and wave transmission (0.46) results in a reflection coefficient of 40%. A wave energy dissipation of 0.88 by waves traveling into the lagoon with the same wave transmission (0.46) yields a reflection coefficient of 0.12. A reflection coefficient of 0.28 is obtained using depth changes between forereef and crest and the methods of Chapter 6.

This variability of the reflection coefficient (10-40%) indicates that more field measurements are needed in this research area. Another consequence is that energy studies cannot disregard reflection without a proper evaluation of the specific reef and its geomorphic and bottom roughness variabilities.

Wave period computed in this study was the period associated with the spectral peak. There was no tendency for wave periods to decrease as waves crossed the reef. The only noticeable changes were associated with periods of 9-10 s, which in some instances increased. Another interesting aspect of this problem was that backreef periods showed less variability than forereef or reef crest periods. In cases where the wave spectra contained peaks at 10 and 14 s, the 10-s peak was completely attenuated as waves traveled across the reef, and the 14-s waves passed into the backreef lagoon. In this case the reef acted as a low-pass filter. These results are in general agreement with those of Ahrens (1987) who found that peak periods were conserved as wave fields crossed the reef breakwater. However, other studies have found different results regarding wave periods. Nakamura et al. (1966) indicated that peak wave periods decreased for wave fields crossing the reef. Similarly, Suhayda and Roberts (1977) observed that mean wave periods decreased 50-75 % in the lagoon. Lee and Black (1978) and Gerritsen (1981) reported that significant wave periods decreased for waves crossing the reef. It appears that wave periods based on spectral moments tend to decrease because of energy redistribution and dissipation as waves travel across the reef. Also, the reef acted as a low-pass filter that let longer period waves pass and suppressed the shorter period waves effectively.

Wave height reduction across the reef profile indicated that energy is being dissipated; however, no information as to the responsible mechanisms

was obtained. To study the energy dissipating mechanisms, a steady state wave energy equation was employed with bottom friction and turbulence used as dissipating functions. This equation was solved following procedures of Thornton and Guza (1983). The model requires prior knowledge of the wave-to-water depth ratio during wave breaking and a bottom friction coefficient. The wave-to-water depth ratio, estimated from measurements at the reef crest, accurately reproduces the wave breaking position observed.

The model indicates that wave-breaking position does not change significantly through the tidal cycle. Energy dissipation by turbulence during wave breaking is smaller than that due to bottom friction, a result totally unexpected. A possible explanation is that wave breaking as a function of the low wave state was not intense and widespread. Visual observations at the study site support this hypothesis since many waves passed unbroken across the reef crest. It must be emphasized that these results apply only to low wave conditions. Prediction of bottom friction dissipation depends strongly on the friction coefficient. Estimates of bottom friction coefficients in this study are close to 0.8, which is about 10 times greater than sandy bottom coefficients. These high values of bottom friction coefficients in coral reefs have been documented by Roberts et al. (1975) and Young (1989). Another noteworthy aspect is that an increase of wave period causes the friction coefficients to decrease by almost half. This trend may indicate that a possible change of scales of bottom roughness took place. Energy dissipation by bottom friction is greater than turbulence dissipation at all times. Only during low tide did both estimates approach equality. Wave height predictions of this model have a 20% error. Inclusion of wave refraction reduces the error by about half. Reflection of wave energy from the reef between depth changes never exceeds

a value of 0.1 except at the lagoon, where a large depth change occurs. Thus, given estimates of bottom roughness and the ratio of wave height to depth at the breaking point, the model of Thornton and Guza (1983) does a reasonable job in predicting wave heights across the reef. Better estimates of bottom roughness, the ratio of wave height to depth at the breaking point, and inclusion of wave refraction and reflection should increase the accuracy of wave height predictions.

Another analysis used to study wave energy reduction was a time-delay linear model. Results of the model illustrated that low frequencies suffered the least while frequencies around the spectral peak suffered the most energy loss. This model was effective for wave height predictions when information regarding the physics of energy dissipation was not important or desired.

Currents, Mass and Sediment Transport

High frequency current and wave spectra at all stations contain similar frequency information at each measurement site, indicating that waves are driving these currents. Coherence analysis shows that currents at frequencies higher than 0.046 cps (periods less than 22 s) are driven by waves. Currents at frequencies lower than 0.046 cps (periods longer than 22 s) are not wave related. Instantaneous speeds at the forereef varied from $65 \text{ cm}\cdot\text{s}^{-1}$ directed offshore to $52 \text{ cm}\cdot\text{s}^{-1}$ directed onshore over two tidal cycles. Time averages over 20-min measurement periods ranged from $0.4 \text{ cm}\cdot\text{s}^{-1}$ offshore to $1.9 \text{ cm}\cdot\text{s}^{-1}$ onshore and resulted in net onshore motion. Current measurements over the reef crest throughout one tidal cycle revealed no vertical shear of the currents between 60 and 95 cm above the reef floor. Instantaneous speeds (sampled every 1 s) varied from $36.7 \text{ cm}\cdot\text{s}^{-1}$ directed offshore to $62.4 \text{ cm}\cdot\text{s}^{-1}$ directed onshore. The time average over 20 min varied from $3.2 \text{ cm}\cdot\text{s}^{-1}$

offshore to $6.9 \text{ cm}\cdot\text{s}^{-1}$ directed onshore. Backreef instantaneous speeds ranged from $24.7 \text{ cm}\cdot\text{s}^{-1}$ offshore to $40.2 \text{ cm}\cdot\text{s}^{-1}$ onshore. The 20-min means varied between $0.8 \text{ cm}\cdot\text{s}^{-1}$ offshore to $3.4 \text{ cm}\cdot\text{s}^{-1}$ onshore over the same time interval. Speed observations at the reef crest were in agreement with values reported at other reefs in the Caribbean: $10\text{-}60 \text{ cm}\cdot\text{s}^{-1}$ at Belize (Kjerfve, 1982) and $10\text{-}180 \text{ cm}\cdot\text{s}^{-1}$ at Nicaragua (Roberts and Suhayda, 1983), and $10\text{-}120 \text{ cm}\cdot\text{s}^{-1}$ in the Pacific (Maragos, 1978). Mean speeds at the reef crest were tidally modulated but lower than values reported by Roberts and Suhayda (1983) and varied from 8 to $16 \text{ cm}\cdot\text{s}^{-1}$ over one tidal cycle. These values reflected low wave heights and wind conditions, but during high waves higher values would be expected at all stations. Using estimates of sand resuspension (Leeder, 1982), sand of 0.8 mm in diameter can be transported offshore by the forereef instantaneous currents and sand of $0.3\text{-}0.2 \text{ mm}$ in diameter can be transported into the lagoon by the instantaneous currents at the crest and backreef, Fig. 8.1. These results agree with Roberts and Suhayda (1983), who suggested that sand-sized particles can be moved within the reef during ambient conditions as well as storms. Offshore movement of forereef sediments was hypothesized by Harmelin-Vivien and Laboute (1986) to explain damage to corals on the forereef slope that were beyond the depth of destructive wave action.

Currents across the reef are also modulated by the 27.7-min infragravity oscillation, creating alternations of flow in the offshore-onshore directions. The speed fluctuations varied from $2 \text{ cm}\cdot\text{s}^{-1}$ in the forereef to $6 \text{ cm}\cdot\text{s}^{-1}$ at the backreef. Volume flux at the reef crest, using linear wave theory, indicated that $0.02 \text{ m}^3\text{s}^{-1}$ crossed it and that 50% of this flux was contributed by waves. This volume flux is small when compared with $0.9 \text{ m}^3\text{s}^{-1}$ at high tide to $0.06 \text{ m}^3\text{s}^{-1}$

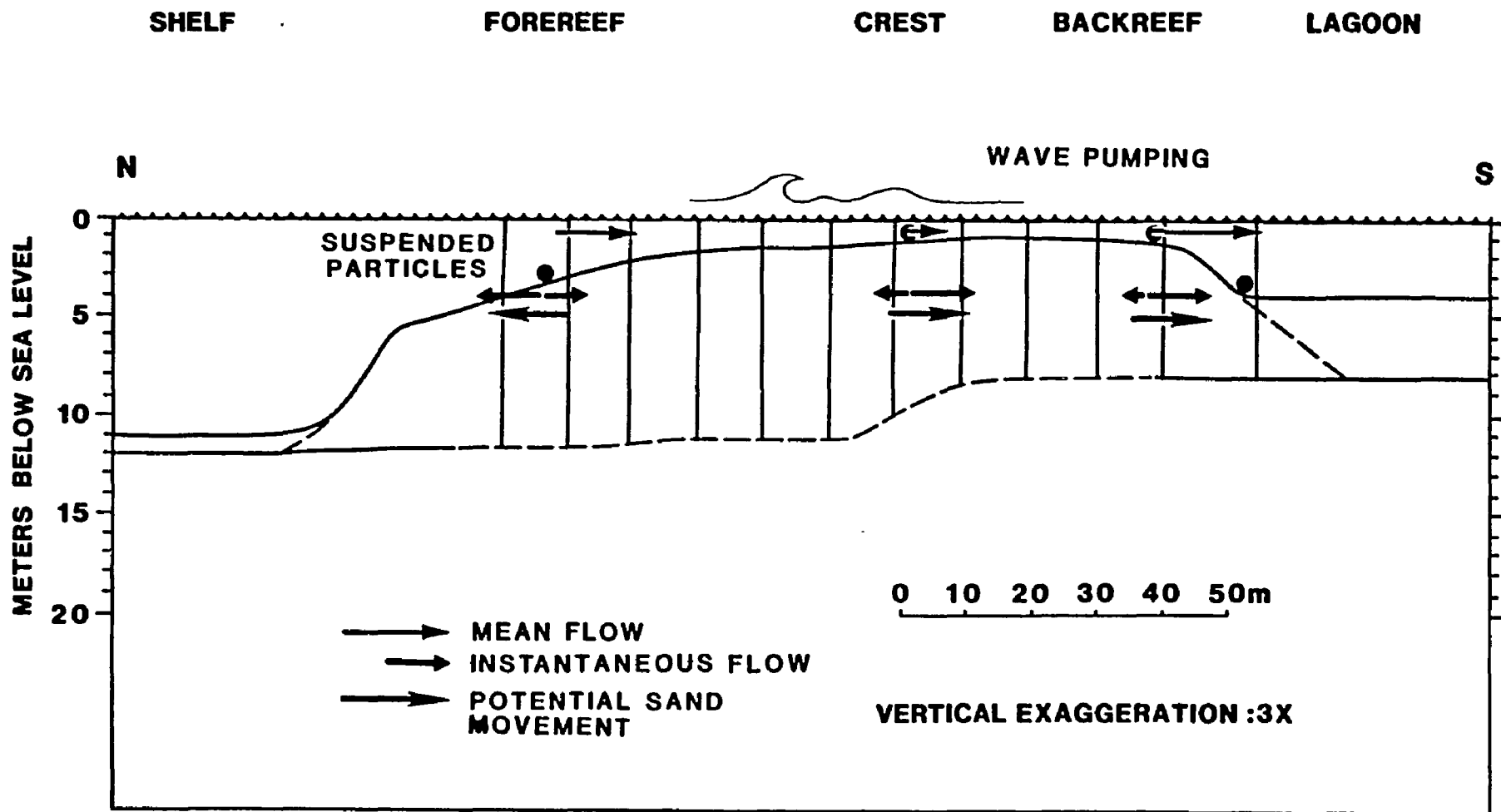


Fig. 8.1. Summary diagram showing the time scales of the currents across the reef and potential particle movement.

at low tide at Eniwetok Atoll (Maragos, 1978), and $0.13 \text{ m}^3\text{s}^{-1}$ in Davies Reef, Great Barrier Reef (Pickard, 1986). Pickard (1986) estimated that at least 40% of the flux he measured was due to waves, a percentage that compares favorably with estimates from this study. Wave contribution to the lagoon volume flux cannot be estimated because suitable current measurements were not made inside the lagoon. Flushing time of the lagoon with the observed volume flux at the reef crest was 37 hours, which is smaller than flushing times for large systems like Bikini, 39 days (von Arx, 1948); and Britomar reef, 4 days (Wolanski and Pickard, 1983); and larger than for Great Pond Bay along St. Croix's south coast, 8 hrs (Roberts et al., 1981a).

Integrated Circulation Model

Circulation models for atoll lagoons have been formulated by von Arx (1948), Frith (1981), and Ludington (1979). They showed that wind stress, tides, and wave set-up were the main forces important to lagoon circulation. Wolanski and Pickard (1983) demonstrated that, over the reef flat, the force balance was between the bottom friction and the surface slope because the cross-shelf winds were insignificant. In the Caribbean, trade winds blow from the NE-E, and for Tague Reef the cross-shelf winds are very weak. Therefore, a mathematical expression of the balance of forces postulated by Wolanski and Pickard (1983), but including the time dependence, can be given using the vertically and time integrated momentum equation. The alongshore component is not included because data collected contain no information about surface slopes in this direction. The mathematical expression for the momentum balance across the reef is:

$$\frac{dV}{dt} = -g \frac{d\eta}{dy} - \frac{\tau_B}{\rho h}$$

where τ_B is the bottom friction, $d\eta/dy$ is the surface slope, and dV/dt is the net acceleration of the water. Expressing the bottom friction as a linear function of the speed, a linear differential equation is obtained:

$$\frac{dV}{dt} = -g \frac{d\eta}{dy} - \frac{\kappa V}{h}$$

where κ is the bottom friction coefficient. Another simplification can be made if the surface slope is expressed as a sinusoidal function of the form:

$$\frac{d\eta}{dy} = \frac{a\theta_{xy} \cos(\omega t)}{d}$$

where the expression in the numerator was derived in Chapter 5. The analytical solution of the resulting differential equation is:

$$V(t) = \frac{ga\theta_{xy}}{d(\alpha^2 + \omega^2)} \left[(\alpha \cos(\omega t) + \omega \sin(\omega t)) \right]$$

where $\alpha = \kappa/h$, ω is the frequency of the motion, θ_{xy} is the phase difference of the forereef and lagoon waves. Substitution of the following values: $g = 9.8 \text{ m}\cdot\text{s}^{-2}$, $a = .0085 \text{ m}$, $\theta_{xy} = 0.39$, $\kappa = 0.01$, $h = 1.2 \text{ m}$, $\omega = 0.004$, and $d = 80 \text{ m}$ gives:

$$V(t) = 3.96\cos(\omega t) + 1.9\sin(\omega t)$$

for speeds expressed in $\text{cm}\cdot\text{s}^{-1}$. This expression gives values that vary from 4.4 to $1.96 \text{ cm}\cdot\text{s}^{-1}$ over the wave period and are nearly out of phase with regard to the water level oscillations. These conclusions agree with features that can be observed by comparing Figs. 6.12 and 7.9. At tidal frequencies a similar force balance is expected to occur; however, sea level differences are inconclusive for tidal periods because of problems during the leveling of the instruments. Another important difference for tidal frequencies is that if $\alpha > \omega$, then the ω squared term can be neglected in the solution. Friction is the dominant term in the model. The friction coefficient is probably higher for tides because the infragravity speed fluctuations contribute to the turbulence at

longer frequencies. A similar force balance between bottom friction and surface slopes at the reef flat has been postulated by Wolanski and Pickard (1983). They suggest that friction is the dominant factor in the dynamics of the reef flat. With these approximations the cross-reef speeds driven by tidal sea level differences are smaller than the infragravity speeds. Other predictions based on this model are as follows: at high tide the sea level is higher in the forereef, and speeds are directed onshore or towards the lagoon. At low tide, the sea level is higher in the lagoon, and flow is directed offshore or towards the forereef. This behavior can be observed in the mean speed obtained from records collected at forereef and lagoon sites during Experiment 3 (Fig. 8.2). In summary, (a) flow across Tague Reef is driven by wave pumping at the reef crest, which flow is always directed onshore, and (b) sea level differences are induced by a phase lag due to shallow water and frictional effects at 27.7-min and tidal periods.

The model developed above describes currents that oscillated back and forward across the reef crest. The unidirectional nature of the flow is explained by the wave pumping and set-up in the breaker zone. Frequency and strength of currents resulting from wave pumping depend on incident wave height (Bruun and Viggosson, 1977). Since heights are tidally modulated, the currents induced by the waves also show tidal modulation. At low tide, wave heights are lower, so the wave pumping is minimal. Currents at the crest are small. At high tide, wave heights are bigger, and the wave pumping is maximized. Currents at the crest are larger. This behavior of the reef crest current field is precisely what is observed in both the currents and volume flux over the reef. In conclusion, currents at the reef crest show three time scales, waves induced by pumping and set-up, infragravity fluctuations induced by

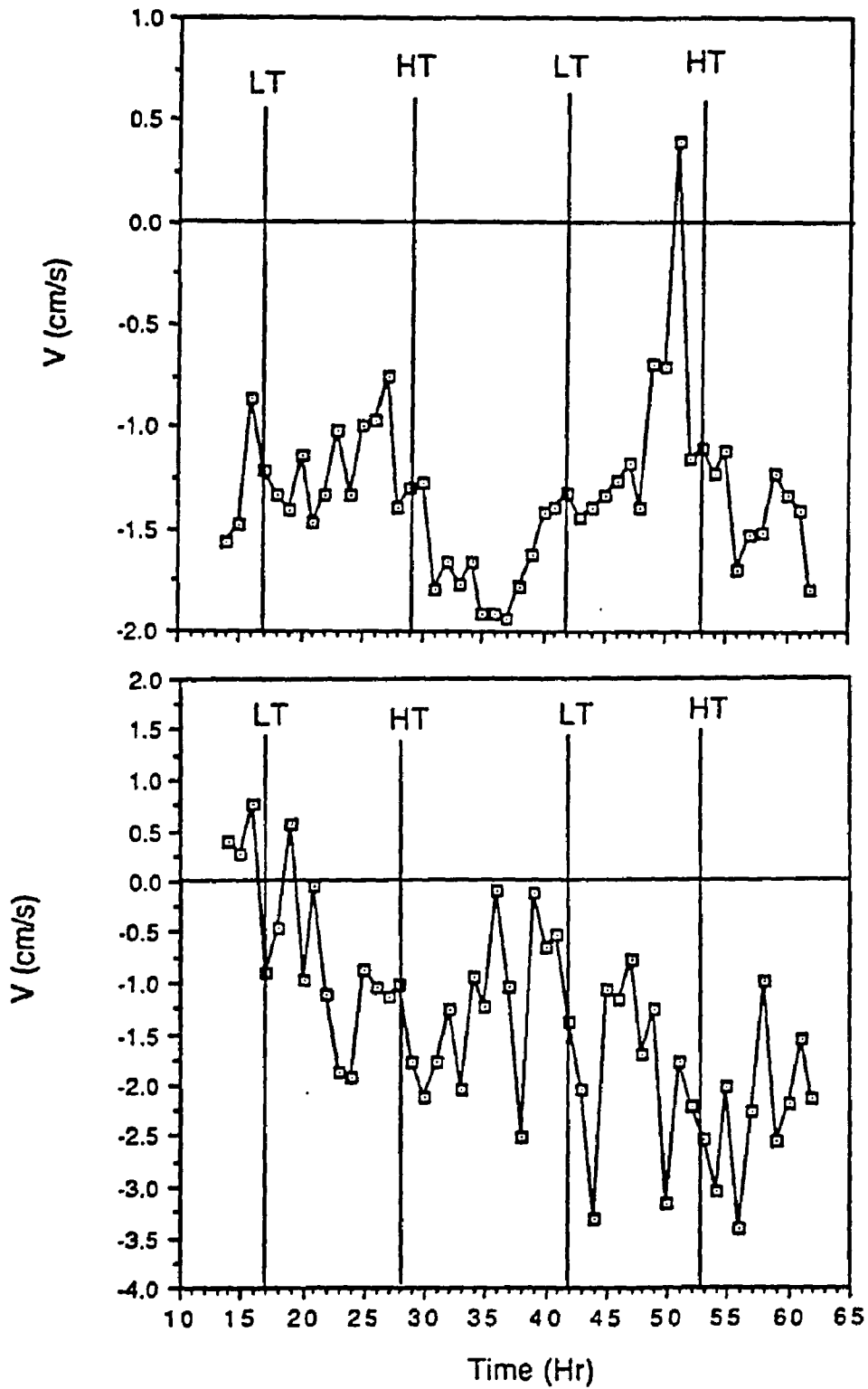


Fig. 8.2 Mean currents at the forereef and backreef showing the tidal modulation.

water slopes of 27.7-min periods, and diurnal variations induced by surface slopes whose origin is uncertain at this time. Suspended sediments, water, and nutrients at the reef are continuously being transported lagoonwards; at the forereef sediments are transported offshore.

9.0 Conclusions

In previous chapters, research results pertinent to physical processes on coral reefs were discussed. The discussion also examined the effects and importance of these physical processes to the reef ecosystem. The following paragraphs present a synopsis of the main results of this study.

- A. Long-period water level variations at Tague Reef were energetic at diurnal and semidiurnal frequencies, with amplitudes of 7.1-6.9 and 2.4-2.5 cm respectively. An wave oscillation of 27.7 min period that contributed to for the movement of waters around the reef was detected. The measurements suggested that these waves were propagating parallel to the coastline. As they propagated through the lagoon, shallow water effects and friction produced minor phase lags and changes in the amplitudes that were manifested as water level differences across the reef.
- B. Long-period currents were semidiurnal and bidirectional (east-west) with speeds of 10-20 $\text{cm}\cdot\text{s}^{-1}$. The flow was predominantly alongshore and westward with a mean speed of 3.1 $\text{cm}\cdot\text{s}^{-1}$; the cross-shore mean flow was onshore at a low speed. Such weak cross-shelf flow precluded any reef crest wave-tidal current interaction that may have influenced wave characteristics and their effects.
- C. Water level differences displayed up to a 1-cm relative slope across the reef. The slope oscillated diurnally and was related to the tidal phase lags or winds. Another energetic component of the water level differences was an infragravity oscillation of 27.7-min period and 0.5 cm amplitude caused by phase lags between the forereef

and lagoon wave fronts. Cross-shore winds and water level differences were positively correlated (correlation coefficient of 0.40); however, a surface slope of only 0.02 cm was potentially set-up by the mean cross-shelf wind stress.

D. Spectral analysis of wave data showed that spectrum shape was conserved between forereef and reef crest and changed for waves between the forereef and backreef or lagoon. A broadening of the spectrum caused by energy dissipation and energy redistribution occurred across the reef. Significant wave heights based on these spectra were 30-40 cm at the forereef, 15-20 cm at the crest, 10-17 cm at the backreef, and 5-15 cm in the lagoon. Wave height changes implied energy reduction of 65% from forereef to crest and 78% between forereef and backreef. Energy dissipation occurred mostly at the peak frequencies. Interfrequency comparison of spectrum estimates revealed that at some frequencies energy increased, while at other frequencies it decreased, indicating that exchange of energy occurred as waves traveled across the reef. Dissipation of energy at low tide was higher than at high tide for waves between forereef and crest (15% more) and between forereef and backreef (20% more). Tidal modulation of energy dissipation and water depth at the reef crest affected wave heights and transmission. Wave heights increased at high tide and decreased at low tide; wave transmission was 62% at high tide, 32% at low tide, and averaged 46%. Wave period based on the spectral peak varied between 9 and 17 s throughout the study and was conserved as waves crossed the reef. Wave height prediction across the reef using

Thornton and Guza's (1983) model produced acceptable estimates of wave heights using parameters estimated from the data collected or the values suggested by them. Bottom friction coefficients varied between 0.4 and 0.8 at the reef crest and were 10 times larger than for sandy bottoms. The model revealed that bottom friction and turbulence dissipation are of equal importance in the reef environment. A linear time-delay spectral model can be used to predict wave heights and intrafrequency energy changes.

E. Currents and sea level variations across the reef have similar spectra, and coherence calculations between both signals showed that currents with time scales shorter than 22 s were linearly related to the waves at the same site. Results from current data derived from vertically stacked meters at the reef crest indicated no current shear 60 cm above the reef floor at this site. The mean flow was generally directed onshore at all stations, and speed ranged from 6.9 to 1.0 $\text{cm}\cdot\text{s}^{-1}$. A diurnal modulation of the mean speeds was detected; this modulation is interpreted as the result of diurnal changes of the water level differences. Wave-induced speeds were asymmetrical at all stations, but onshore speeds were greater at the reef crest and backreef, while offshore speeds dominated at the forereef. Instantaneous speeds were 50-60 $\text{cm}\cdot\text{s}^{-1}$ offshore and 36-40 $\text{cm}\cdot\text{s}^{-1}$ onshore at the forereef, 20 $\text{cm}\cdot\text{s}^{-1}$ offshore and 40 $\text{cm}\cdot\text{s}^{-1}$ onshore at the reef crest, and 12 $\text{cm}\cdot\text{s}^{-1}$ offshore and 20 $\text{cm}\cdot\text{s}^{-1}$ onshore during high tide at the backreef. A low-pass filtered version of the current records indicated speed fluctuations of 2 $\text{cm}\cdot\text{s}^{-1}$ at the forereef

and $6 \text{ cm}\cdot\text{s}^{-1}$ at the backreef at periods of 25-30 min. These currents were interpreted as being driven by water level differences at infragravity periods. Infragravity currents were explained in terms of surface slope and bottom friction forces acting across the reef crest. In summary, currents at the reef varied at three time scales, gravity wave, infragravity periods and diurnally. Volume flux based on measurements was estimated as $0.020 \text{ m}^3\text{s}^{-1}$ at the reef crest and $0.024 \text{ m}^3\text{s}^{-1}$ at the backreef. This flux flushed the lagoon in 37 hrs. Instantaneous speeds were capable of moving sand-size sediment particles offshore at the forereef and onshore at the crest and backreef stations. Suspended particles over the reef would be transported lagoonwards at all times.

10.0 References

- Adams JB (1974) Environmental geology of St. Croix: The impact of man on the natural resources of an island. In: Multer HG, Gerhard LC (eds) Guidebook to the geology and ecology of some marine and terrestrial environments, Sp Pub No 5. Fairleigh Dickinson Univ, St. Croix: 145-153
- Ahrens JP (1987) Characteristics of reef breakwaters. Coastal Eng. Res. Center US Army Corps of Engineers Techn. Report CERC-87-17: 62
- Andrews JC, Dunlap WC, Bellamy NF (1984) Stratification in a small lagoon in the Great Barrier Reef. Aust. J. Mar. Freshw. Res. 35: 273-284
- Atkinson M, Smith SV, Stroup ED (1981) Circulation in Enewetak Atoll lagoon. Limnol Oceanogr 26: 1074-1083
- Baines GBK, Beveridge PJ, Maragos JE (1974) Storms and island building at Funututi Atoll, Ellice Islands. Proc 2nd Int Coral Reef Symp 2: 485-496
- Basco DR, Svendsen IA (1984) Modeling turbulent bore propagation in the surf zone. Proc. 19th Conf. Coastal Eng., Huston, Texas, 1: 99-114
- Bendat JS, Piersol AG (1986) Random data analysis and measurement procedures 2nd ed. John Wiley & Sons, New York
- Blumenstock DI (1958) Typhoon effects at Juliat Atoll in the Marshall Islands. Nature 182: 1267-1269
- Bradbury RH, Young PC (1981) The effects of a mayor forcing function, wave energy, on a coral reef ecosystem. Mar Ecol 5:229-241
- Brestchneider CL, Reid RO (1954) Modification of wave height due to bottom friction, percolation, and refraction. Corps of Eng., Beach and Erosion Board, Tech. Mem. No. 45

- Bruun P, Viggosson G (1977) The wave pump: Conversion of wave energy to current energy. *J Waterway, Port, Coastal and Ocean ASCE* 103: 449-469
- Climatological Data (1987) Tropical Surface Charts. U.S. Department of Commerce
- Dally WR, Dean RG, Dalrymple RA (1984) Modeling wave transformation in the surf zone. US Army Corps of Engineers Misc. Paper CERC-84-8
- Dana JD (1853) On coral reefs and islands. G.P. Putnam and Co, New York
- Darwin C (1842) The structure and distribution of coral reef. The Univ of Arizona Press, Arizona
- Davies PJ (1977) Modern reef growth Great Barrier Reef. *Proc 3rd Int Coral Reef Symp* 2: 326-330
- Davies PJ, Hughes H (1983) High-energy reef and terrigenous sedimentation, Boulder Reef, Great Barrier Reef. *BMR J Aust Geol Geophys* 8: 201-209
- Davis WM (1928) The coral reef problem. *Am Geographical Soc SP* No 9
- Dollar SJ (1982) Wave stress and coral community structure in Hawaii. *Coral Reefs* 1: 71-81
- Farrow GE, Brander KM (1971) Tidal studies on Aldabra. *Philo. Trans. Royal Soc. of London* 260, series B: 93-122
- Fredsøe J (1984) Turbulent boundary layer in wave-current motion. *J Hydraulic Eng. ASCE* 110: 1103-1119
- Frith CA (1981) Circulation in a platform reef lagoon, One Tree Reef, Southern Great Barrier Reef. *Proc 4th Int Coral Reef Symp* 1: 347-353
- Gerritsen F (1981) Wave attenuation and wave set-up on a coastal reef. Look Lab Tech Report No 48, Sea Grant Program, Univ. of Hawaii

- Giese GS, Hollander RB (1987) The relationship between coastal seiches at Palawan Island and tide-generated internal waves in the Sulu Sea. *J Geophys Res* 92: 5151-5156
- Giese GS, Hollander RB, Fancher JE and Giese BS (1982) Evidence of coastal seiche excitation by tide-generated internal solitary waves. *Geophys Res Lett* 9: 1305-1308
- Gill IP, Hubbard DK (1987) Subsurface geology of the St. Croix carbonate rocks system, Phase III. Univ Virgin Islands, St. Thomas, Tech Rep 28: 79
- Glynn PW (1977) Aspects of the ecology of coral reefs in the Western Atlantic Region. In: Jones OA, Endean R (eds) *Biology and Geology of Coral Reefs 2, Biology 1*. Academic Press, New York: 1-54
- Glynn PW, Almodóvar LR, González JG (1964) Effects of Hurricane Edith on marine life in La Parguera, Puerto Rico. *Caribb J Sci* 74: 335-345
- Goode's World Atlas 17th Edition (1982). Espenshade EBJr (ed) Rand McNally, New York, pp 367
- Grant WD, OL Madsen (1979) Combined wave and current interaction with a rough bottom. *J Geophys Res* 84: 1797-1808
- Greer JE, Kjerfve B (1982) Water currents adjacent to Carrie Bow Cay, Belize. In: Rützler K, MacIntyre IG (eds) *The Atlantic Barrier Reef ecosystem at Carrie Bow Cay, Belize, 1 Structure and Communities*. Smithsonian Contr Mar Sci 12. Smithsonian Inst Press, City of Washington: 53-58
- Hamner WM, Hauri IR (1981) Effects of island mass: water flow and plankton pattern around a reef in the Great Barrier Reef Lagoon, Australia. *Limnol Oceanogr* 26: 1084-1102
- Handbook of Physics and Chemistry (1976) 56th ed. Weast RC editor. CRC Press Cleveland Ohio

- Harmelin-Vivien ML, Laboute P (1986) Catastrophic impact of hurricanes on atoll outer reef slopes in the Tuamotu (French Polynesia). *Coral Reefs* 5:55-62
- Hasselmann K, Barnett TP, Bouws E, Carlson H, Cartwright DE, Enke K, Ewing JA, Gienapp H, Hasselmann DE, Kruseman P, Meerburg A, Müller P, Olbers DJ, Richter K, Sell W, Walden H (1973) Measurements of wind-wave growth and swell decay during the Joint North Sea Wave Project(JONSWAP). Deutsches Hydrographisches Institut, Hamburg, Reihe A(8^o), Nr. 12: 1-95
- Hearn CJ, Parker IN (1988) Hydrodynamics processes on the Ningaloo Coral Reef, Western Australia. 6th International Coral Reef Symposium, Australia, 1988.
- Hernandez-Avila ML, Roberts HH, Rouse LJ (1977) Hurricane-generated boulder rampart formation. *Proc 3rd Int Coral Reef Symp* 2:71-78
- Horikawa K, Kuo CT (1966) A study on wave transformation inside surf zone. *Proc. on the 10th Conf. Coastal Eng. Tokyo, Japan* 1: 217-234
- Huthnance JM (1985) Flow across reefs or between islands, and effects on shelf-sea motions. *Continental Shelf Res.* 4: 709-731
- Johns B (1983) Turbulence modelling beneath waves over beaches. In: Johns B (ed) *Physical oceanography of coastal and shelf seas*, Elsevier, New York: 11-134
- Jonsson IG (1966) Wave boundary layers and friction factors. *Proc. 10th Conf. Coastal Eng. Tokyo, Japan* 1: 127-148
- Jonsson IG (1980) A new approach to oscillatory rough turbulent boundary layers. *Ocean Eng.* 7: 109-152
- Kamphuis WJ (1975) Friction factors under oscillatory waves. *J Waterways, Harbors and Coastal Eng. Div. ASCE* 101: 135-144

- Kennett JP (1982) *Marine Geology*. Prentice-Hall, New Jersey
- Kim YY, LH Simons (1974) Sea state measurements from pressure records. Proc. Symp. on Ocean Wave Measurements, Am. Soc. Civil Eng., Louisiana, 40-53.
- Kjerfve B (1978) Diurnal energy balance of a Caribbean barrier reef environment. *Bull. Mar. Sci.* 28: 137-145
- Kjerfve B (1981) Tides of the Caribbean. *J Geophys Res* 86: 4243-4247
- Kjerfve B (1982) Water exchange across the reef crest at Carrie Bow Cay, Belize. In: Rützler K, MacIntyre IG (eds) *The Atlantic Barrier Reef ecosystem at Carrie Bow Cay, Belize, 1 Structure and Communities*. Smithsonian Contr Mar Sci 12. Smithsonian Inst Press, City of Washington: 59-62
- Kono T, Tsukayama S (1980) Wave transformation on reef and some consideration on its application to field. *Costal Engineering in Japan* 23: 45-57
- Lee TT, Black KP (1978) The energy spectra of surf waves on a coral reef. Proc. 16th Coastal Eng. Conf., Hamburg, Germany: 588-608
- Leeder MR (1982) *Sedimentology process and product*. George Allen & Unwin, London
- Lin SC, Hwang JS (1986) Wave transformation and mean sea level variation. *Proc. Coastal Eng.* 1: 481-496
- Longuet-Higgins MS (1969) On the transport of mass by time-varying ocean currents. *Deep-Sea Research* 16: 431-447
- Longuet-Higgins MS (1980) On the distribution of heights of sea waves: Some effects of nonlinearity and finite bandwidth. *J Geophys Res* 85: 1519-1523

- Longuet-Higgins MS, Stewart RW (1962) Radiation stress and mass transport in gravity waves, with application to "surf beats". *J Fl Mech* 13: 481-504
- Loya Y (1978) Plotless and transect methods. In: Stoddart DR, Johannes RE (eds) *Coral reefs: research methods*, UNESCO : 197-217
- Ludington CA (1979) Tidal Modifications and associated circulation in a platform reef lagoon. *Aust J Mar Freshwater Res* 30: 425-430
- Lugo-Fernandez A (1982) Wave energy distribution on Margarita Reef, Southwestern Puerto Rico. Unpublished Master Thesis Univ of Puerto Rico
- MacIntyre IG (1977) Distribution of submarine cements in a modern fringing reef, Galeta Point, Panama. *J Sed Pet* 47: 503-516
- MacIntyre IG, SV Smoth, JC Zieman (1974) Carbon Flux through a coral reef ecosystem: a conceptual model. *J Geo* 82: 161-171
- Maragos JE (1978) Measurement of water volume transport for flow studies. In: Stoddart DR, Johannes RE (eds) *Coral reefs: research methods*, UNESCO, pp 353-360
- Marsh JAJr, Ross RM, Zolan WJ (1981) Water circulation on two Guam Reef flats. *Proc 4th Int Coral Reef Symp* 1: 355-360
- Mei CC (1984) *The applied dynamics of ocean surface waves*. John Wiley & Sons, New York
- Milliman JD (1977) Caribbean coral reefs. In: Jones OA, Endeian R (eds) *Biology and Geology of Coral Reefs, Geology 1*. Academic Press, New York: 1-44
- Munk WH, Sargent MC (1948) Adjustment of Bikini Atoll to ocean waves. *Trans Am Geophys Union* 29: 855-860
- Murray SP (1969) Current meters in use at the Coastal Studies Institute. *Louisiana State Univ Press Bulletin* 3: 1-15

- Nakamura M, Shiraishi H, Sasaki Y (1966) Wave damping effect of submerged dike. Proc. 10th Conf. Coastal Eng. Tokyo, Japan 1: 254-267
- Nelson RC, Leslie (1985) Breaker height attenuation over platform coral reefs. Australian Conf. on Coastal and Ocean Eng., Christchurch, N.Z., 2: 9-16
- Oceanographic Monthly Summary (1987) National Oceanic Administration. U.S. Department of Commerce
- Ogden JC (1974) The major marine environments of St. Croix. In: Multer HG, Gerhard LC (eds) Guidebook to the geology and ecology of some marine and terrestrial environments, Sp Pub No 5. Fairleigh Dickinson Uni, St. Croix, pp 5-19
- Oliver JK, Willis BL (1987) Coral-spawn slicks in the Great Barrier Reef: preliminary observations. Mar Biol 94: 512-529
- Phillips OM (1982) The dynamics of the upper ocean, 2nd ed. Cambridge Univ Press, Cambridge
- Pickard GL (1986) Effects of wind and tide on upper-layer currents at Davies Reef, Great Barrier reef, during MECOR (July-AUGUST 1984). Aust J Mar Freshw Res 37: 545-565
- Pickard GL, Emery WJ (1982) Descriptive physical oceanography 4th ed. Pergamon Press, New York
- Pugh DT (1987) Tides, surges and mean sea-level. John Wiley & Sons, New York
- Pugh DT, Rayner RF (1981) The tidal regimes of three Indian Ocean atolls and some ecological implications. Estuarine, Coastal and Shelf Science 13: 389-407
- Roberts HH (1974) Variability of reefs with regard to changes in wave power around an island. Proc 2nd Int Coral Reef Symp 2: 497-512

- Roberts HH (1980) Physical processes and sediment flux through reef-lagoon systems. Proc 17th Coastal Eng Conf, Sydney, Australia: 946-962
- Roberts HH, Coleman JM, Murray SP, Hubbard DK (1981b) Offshelf sediment transport on the downdrift flank of a trade wind island. Proc 4th Int Coral Reef Symp 1: 389-397
- Roberts HH, Murray SP (1984) Developing Carbonate platform: Southern Gulf of Suez, Northern Red Sea. Mar Geol 59: 165-185
- Roberts HH, Murray SP, Suhayda JN (1975) Physical processes in a fringing reef system. J Mar Res 33: 233-260
- Roberts HH, Murray SP, Suhayda JN (1977) Physical processes in a fore-reef shelf environment. Proc 3rd Int Coral Reef Symp 2: 507-515
- Roberts HH, Suhayda JN (1983) Wave-current interactions on a shallow reef (Nicaragua, Central America). Coral Reefs 1: 209-214
- Roberts HH, Wiseman WJ Jr, Suchanek TH (1981a) Lagoon Sediment transport: The significant effect of *Callianasa* bioturbation. Proc 4th Int Coral Reef Symp 1: 459-465
- Rogers SC, Suchanek TH, Pecora FA (1982) Effects of hurricanes David and Frederic (1979) on shallow *Acropora palmata* reef communities: St. Croix, U.S. Virgin Islands. Bull Mar Sci 32: 532-548
- Ruffner JA, Bair FE (1978) Climates of the States. Gale Research Comp, Detroit
- Sabir RA (1962) Effects of two dimensional roughness elements on Froude's number and resistance coefficients in rapid regime in steep, rough, rectangular flume. MS Thesis, Virginia Polytechnic Institute, Blacksburg, Virginia
- Seelig WN (1983) Laboratory study of reef-lagoon system hydraulics. J Waterways, Port, Coastal and Ocean Eng. 109: 380-391

- Shiau JC, Wang H (1977) Wave energy transformation over irregular bottom. *J Waterway, Port, Coastal and Ocean ASCE* 103: 57-68
- Snodgrass FE, Munk WH, Miller GR (1962) Long-period waves over California's continental borderland. Part 1. Background spectra. *J Mar Res* 20: 3-30
- Steel RGD, Torrie JH (1980) *Principles and Procedures of Statistics: a Biometrical Approach*, 2nd ed. McGraw-Hill, Inc, New York.
- Stoddart DR (1962) Catastrophic storm effects on the British Honduras reefs and cays. *Nature* 196: 512-515
- Stoddart DR (1969) Ecology and morphology of recent coral reefs. *Biol Rev* 44: 433-498
- Stoddart DR (1969b) Post-hurricane changes on the British Honduras reefs and cays: re-survey of 1965. *Atoll Res Bull* 131: 1-25
- Suhayda JN, Roberts HH (1977) Wave action and sediment transport on fringing reef. *Proc 3rd Int Coral Reef Symp* 2: 65-70
- Summerfield WC (1969) On the trapping of wave energy by bottom topography. *Horace Lamb Centre Res. Paper 30, The Flinders Univ. South Australia, Australia*
- Tait RJ (1972) Wave set-up on coral reefs. *J Geophys Res* 77: 2207-2217
- Thornton EB, Guza RT (1983) Transformation of wave height distribution. *J Geophys. Res.* 88: 5925-5938
- U. S. Navy (1955) *Marine Climatic Atlas of the World , North Atlantic Ocean Vol 1. Navaer 50-1C-528*
- U.S. Corps of Eng. (1984) *Shore Protection Manual, 2nd Ed.*
- U.S. Department of Transportation (1975) *Hydraulic design of energy dissipators for culverts and channels. Hydraulic Engineering Circular No. 14*

- U.S. Department of Transportation (1984) Guide for selecting Manning's roughness coefficients for natural channels and flood plains. Rept. No. FHWA-TS-84-204
- Umbgrove JHF (1929) The influence of the monsoons on the geomorphology of coral islands. 4th Pac Sci Congress 2A: 49-54
- von Arx WS (1948) Circulation systems of Bikini and Rongelap lagoons. Trans Am Geophys Union 29: 861-870
- von Arx WS (1962) An Introduction to Physical Oceanography, 7th ed. Addison-Wesley Publishing Company, Massachusetts
- Whetten JT (1974) Field guide to the geology of St. Croix. In: Multer HG, Gerhard LC (eds) Guidebook to the geology and ecology of some marine and terrestrial environments, Sp Pub No 5. Fairleigh Dickinson Uni, St. Croix: 129-143
- Wolanski E, Pickard GL (1983) Currents and flushing of Britomart Reef lagoon, Great Barrier Reef. Coral Reefs 2: 1-8
- Wüst G (1964) Stratification and circulation in the Antillean-Caribbean basins, Part 1. Columbia Univ Press, New York
- Young IR (1987) Wave attenuation on reef structures. Proc. 8th Australian Conf. on Coastal and Ocean Eng., Launceston: 5-9
- Young IR (1989) Wave transformation over coral reefs. Abst. EOS, Trans Am Geophys Union, 70(4): 49-64
- Zimmerman JTF (1979) On the Euler-Lagrange transformation and the Stokes' drift in the presence of oscillatory and residual currents. Deep-Sea Res 26: 504-520

Appendix A

A1 Conversion of tide gage pressure output into water depths

As mentioned in the text, the total pressure (P_t) measured by the tide gage is the sum of atmospheric pressure (P_a) and the water pressure (P_w); in symbols:

$$P_t = P_a + P_w$$

The water pressure can be approximated using the following expression:

$$P_w = -\rho_s * g * (z + \eta)$$

where ρ_s = sea water density, g = gravity acceleration (9.8 ms^{-2}), z = depth below surface taken as negative, and η = instantaneous sea surface. Inserting the last equation into the first equation gives:

$$P_t = P_a - \rho_s * g * (z + \eta) .$$

The term $-(z + \eta)$ represents the water depth (h) measured from the sea surface to the instrument's sensor. The water depth at any given time can be determined only if the prevailing atmospheric pressure is known. In this study the atmospheric pressure was not observed, therefore it is impossible to estimate the water depth. Instead an equivalent water depth (h_e) that equals the water depth plus a water layer whose pressure equals the atmospheric pressure was calculated. This equivalent depth is plotted in the tidal curves of the lagoon and fore reef after suitable conversion of units. In symbols:

$$P_t = \rho_s * g * (h_e) .$$

To express the equivalent depth (centimeters) the following equation which includes conversion factors to account for changes in units was employed:

$$h_e \text{ (cm)} = P_t * 0.0689476 * 985.9 .$$

A2 Justification for using tide gage temperature as water temperature

This section presents evidence that justifies the use of tide gage temperature as in-situ water temperature. The first piece of evidence is a comparison between temperature measurements made in the lagoon with a mercury thermometer and the tide measurements (Table A1).

Table A1. Temperature measurements made with thermometer and tide gage

Date	Thermometer	Tide gage
4/4	27.0°±0.5°	27.5°
4/4	27.0°±0.5°	27.1°
4/9	28.0°±0.5°	28.1°

Differences observed in the table are within the error of the instruments so they are not significant. Even though there are only three points in the comparison, the results are in agreement with the assumption of thermal equilibrium. The other piece of evidence, is indirect, it shows the tide gage response time to be smaller than the time required to reach thermal equilibrium after a temperature changes. To show this relationship, Newton's law of cooling is the starting point. It states that the rate of temperature change of a body is proportional to the temperature difference between the medium and the body. Application of this law results in the following equation:

$$T(t) = c \cdot \exp(-kt) + T_0,$$

where c and k are constants to be determined, and T_0 is the medium temperature taken as 26.34 °C in these waters. The value of c was determined from the observed instrument temperature before entering the water, around

from the observed instrument temperature before entering the water, around 32.8 °C for both gages. The value of k was determined by plotting $[(T(t) - T_0)/c]$ during the cooling stage on semi-log paper for each instrument and calculating the slope of the resultant line. The estimated values were 1.70 hr⁻¹ and 1.86 hr⁻¹. These values represent response times of about 35 min for both instruments. Since we are interested in temperature changes over one hour or more, it is safe to equate that observed temperatures by the tide gages with water temperature.

A3 Calibration and statistical analysis of the pressure sensors

In order to verify the accuracy of the tide gage pressure sensors a calibration test was performed on each instrument after the study was completed. The tests were conducted at the CSI shop using a pneumatic apparatus acquired recently. Each test consisted of applying a known pressure and recording the output, then subtracting the ambient pressure as measured by each instrument. This procedure was repeated three times for each tide gage and the averaged value computed. These results are presented in Fig. A1 plotted against the known applied pressure. The response is highly linear and very accurate as indicated by the value of the slope. An ideal system should have a slope value of unity, the calculated values for the instruments were 0.9985 and 0.9984. The errors or deviations from the applied pressure showed that SN27 had a zero offset and SN20 a 3.7 cm offset. Another interesting aspect of these plots is the fact that the slopes, which represent the errors of the instruments in water depth determinations are 0.15%, a value 10 times larger than the precision. These facts have been corroborated by means of tests in the laboratory. Effects of temperature on the pressure have not been

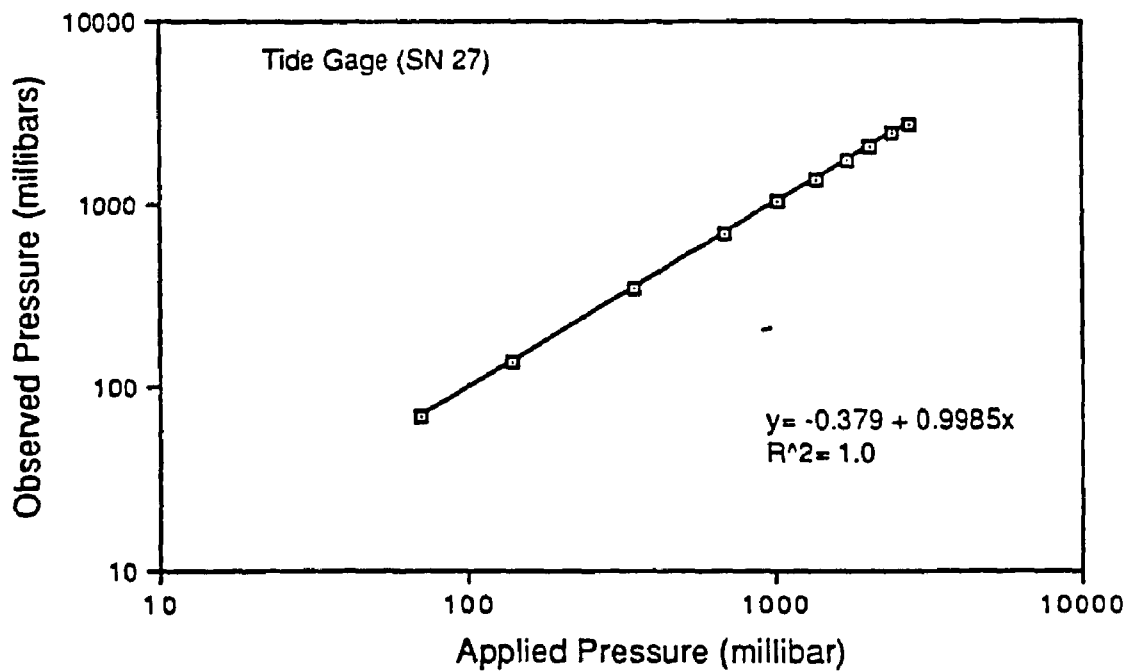
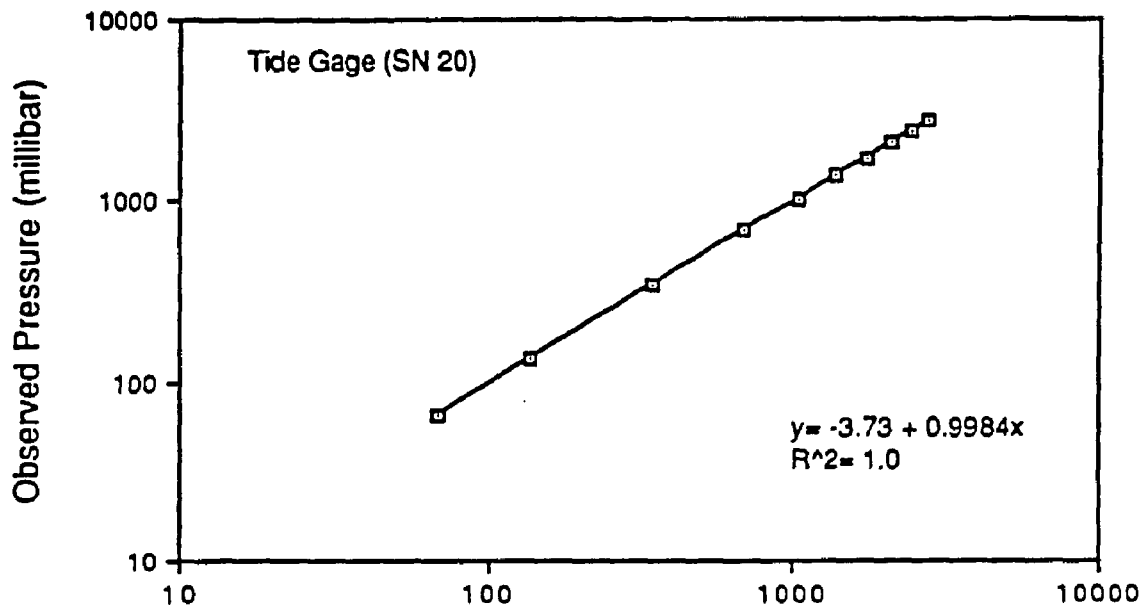


Fig. A1 Tide gage calibration curves.

considered directly, however, laboratory conditions during tests showed that temperature changes of almost 1 degree have little effect on the pressure.

The three wave sensors had to be calibrated before the study started. These test were also conducted in the CSI shop by Mr. Rodney Fredericks. Each test consisted of applying a known pressure using a piston system and recording the output voltage. The calibration data for each sensor is presented in Fig. A2. Response of the sensors is highly linear as indicated by the values of 1.0 the r-squared. Error curves characteristics of the regression lines are so small the their net effect is to increase the width of the lines in the plots. Examination of the regression equations for each meter shows similar values for the slopes and intercepts close to zero. The question as to whether there is a significant difference between the slopes or if the intercepts are statistically equal to zero arises naturally. To answer these questions a statistical techniques described in Steel and Torrie (1980) was used. Application of these tests at the 95% confidence interval shows that the slopes are statistically different from each other, and that the intercepts are statistically different from zero.

Once the regression equations were established, and the gain factors from electronics circuits established, the equations to convert from electrical units to engineering units were established. The equations were of the form:

$$\eta \text{ (cm)} = C \cdot 5 \cdot \beta - \alpha$$

where C are the counts from the digitizer, β and α are constants calculated from the electronics, water densities used, and parameters of the regression equations. Values of the constants for each sensor are presented in Table A2.

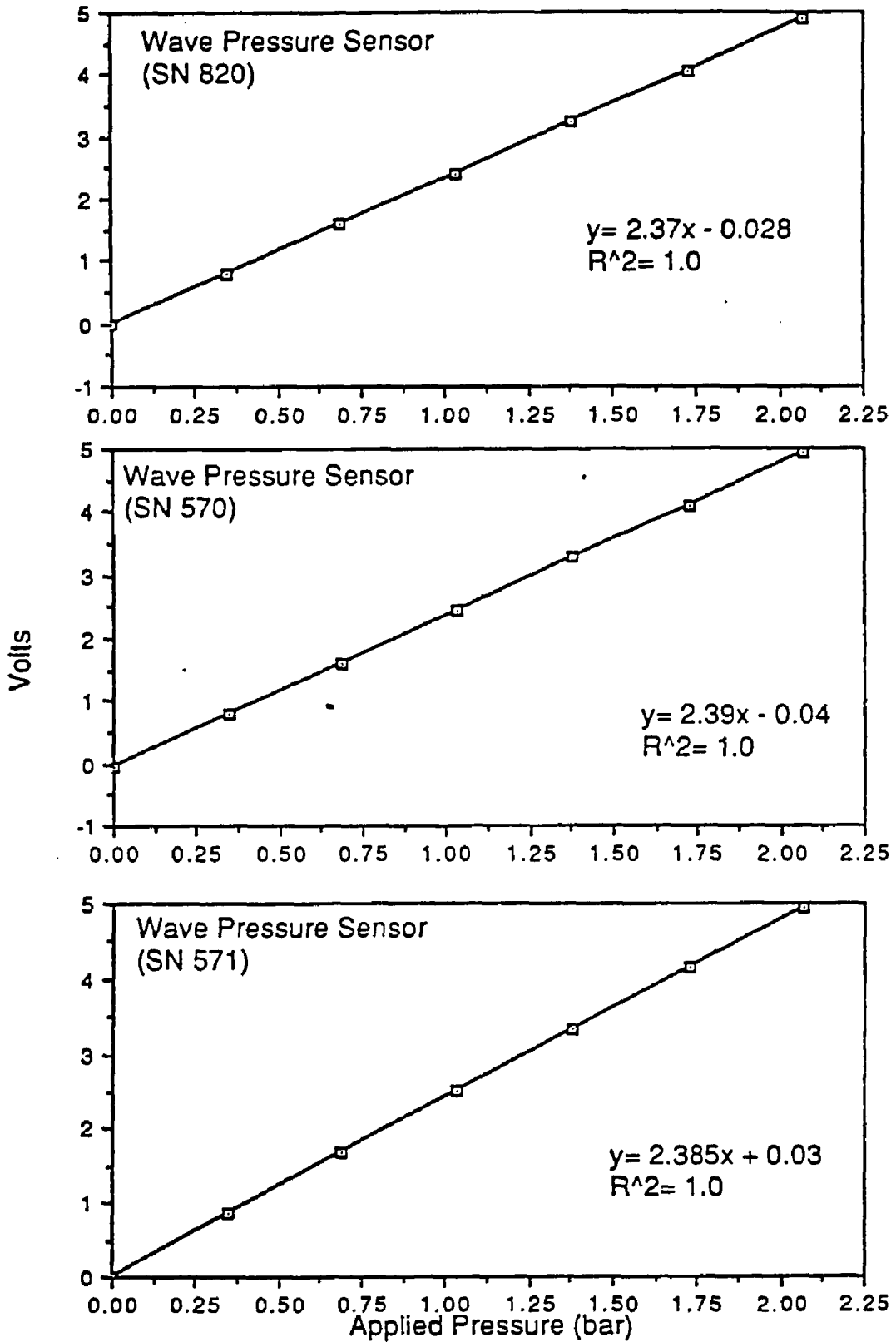


Fig. A2. Wave pressure sensor calibration curves.

Table A2. Calibration constant for each wave sensor

Sensor	β	α
570	0.219	-16.690
571	0.244	12.724
820	0.224	-11.875

A4 Calibration of the ducted current meters

Calibration data for the ducted current meters was collected in 1979 on the US Geological Survey Laboratory at NSTL, Mississippi. The data are display graphically in Fig. A3. Each meter has a highly linear response as shown in the figure and the r-squared value of 1. Statistical tests similar to the ones used for the wave sensors were performed regarding slopes and intercepts of the ducted current meters. Results at the 95% confidence level, reveal that the slopes were not statistically different . The average value of the slopes, 3.417, was used in the equations. The intercepts were statistically different from zero. Inspection of the converted data revealed that wiring of one of the sensors had a reverse polarity, and the meter used at the upper level of the crest station malfunction after Experiment 1 concluded.

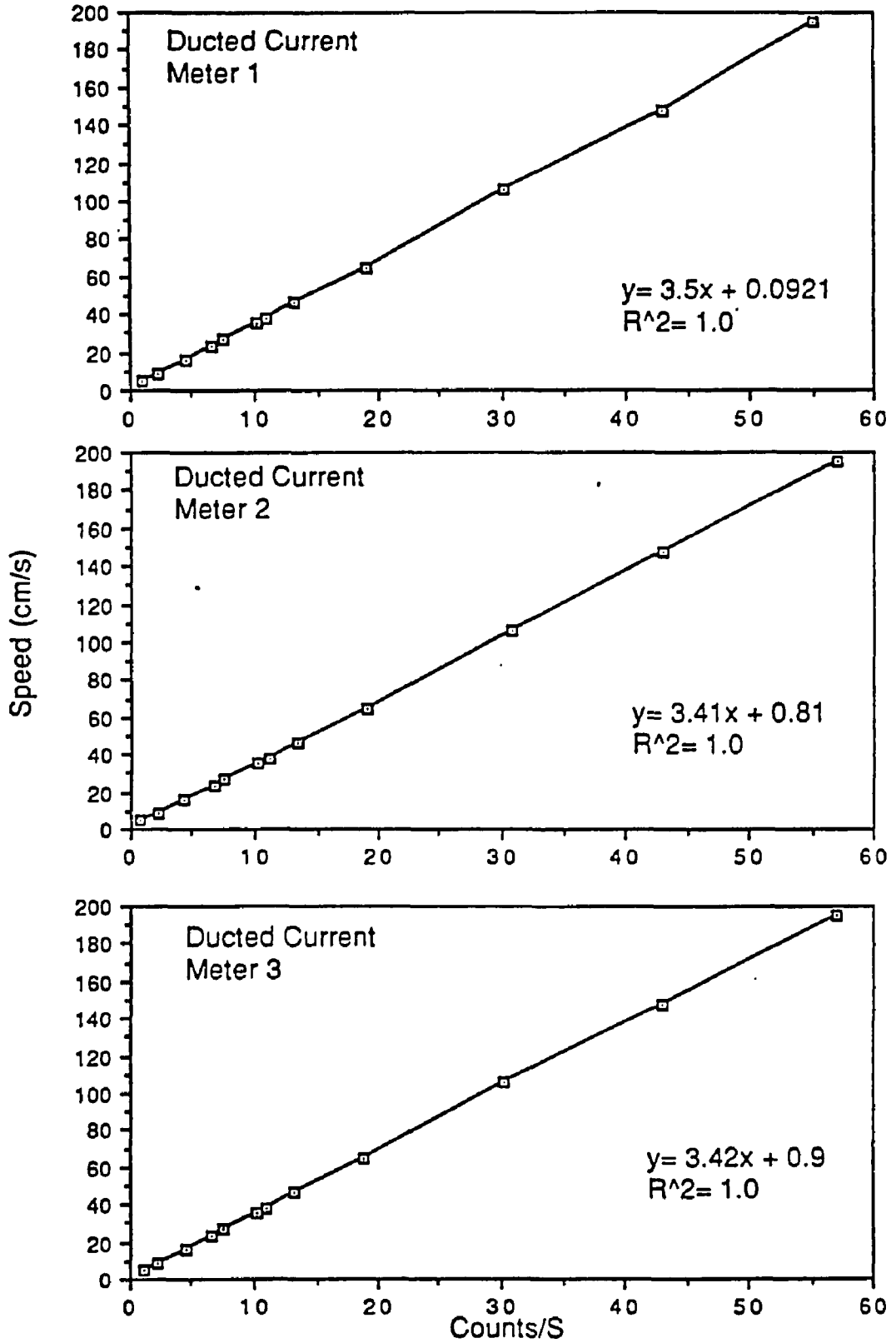


Fig. A3 Calibration curves for ducted current meters.

Appendix B

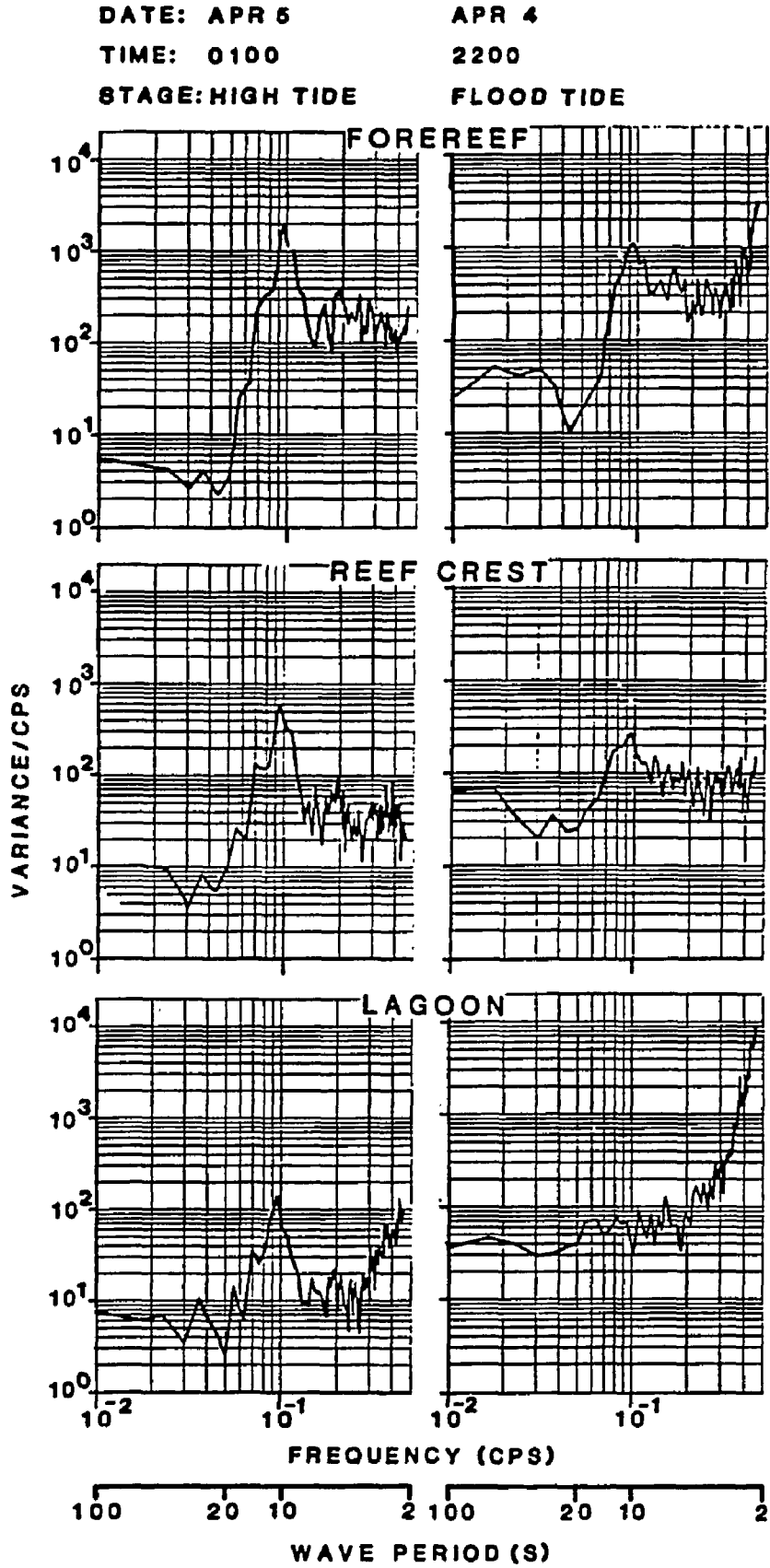


Fig. B1. Wave autospectra across the reef profile during Experiment 1 for high and flood tide conditions.

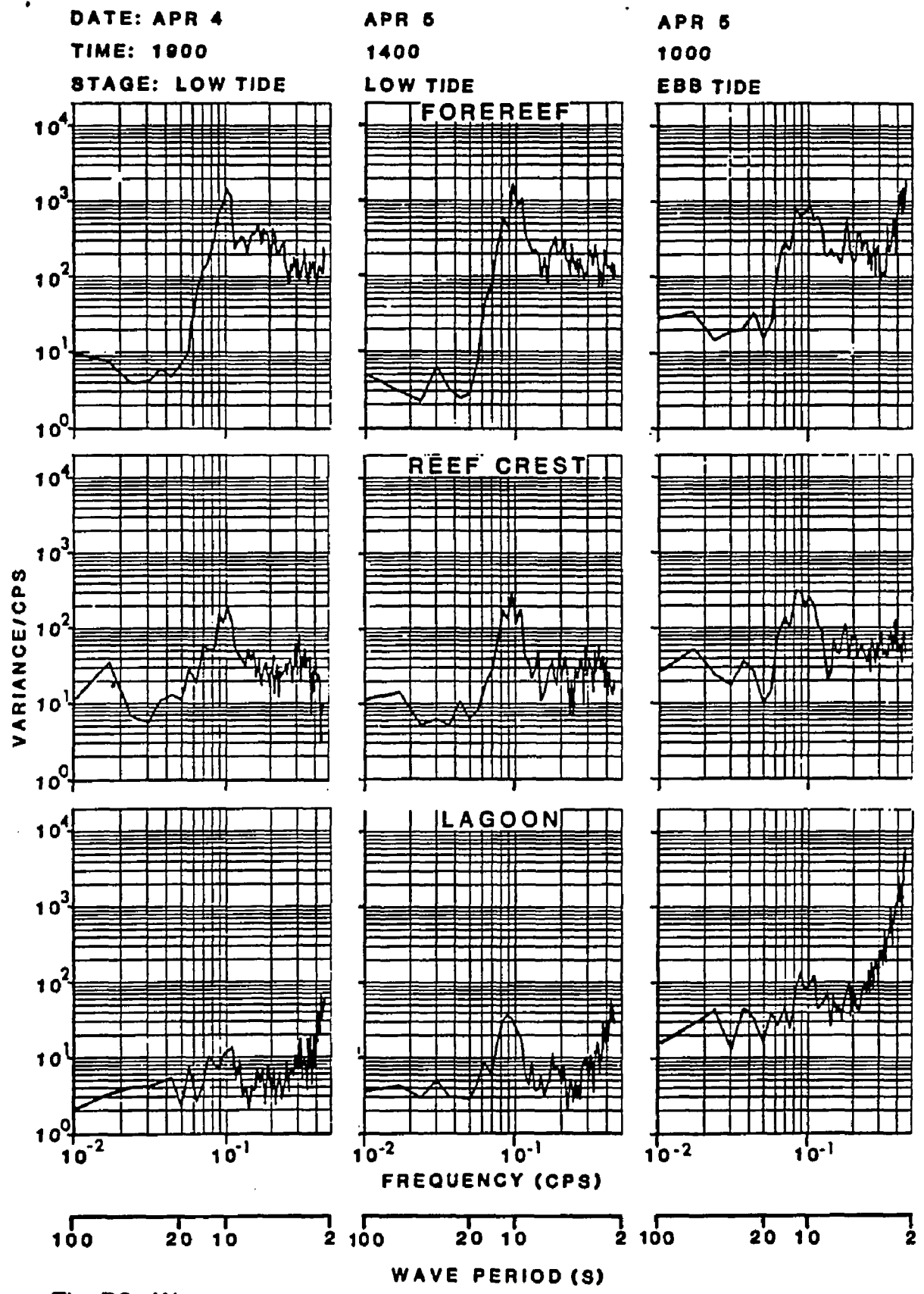


Fig. B2. Wave autospectra across the reef profile during Experiment 1 for low and ebb tide conditions.

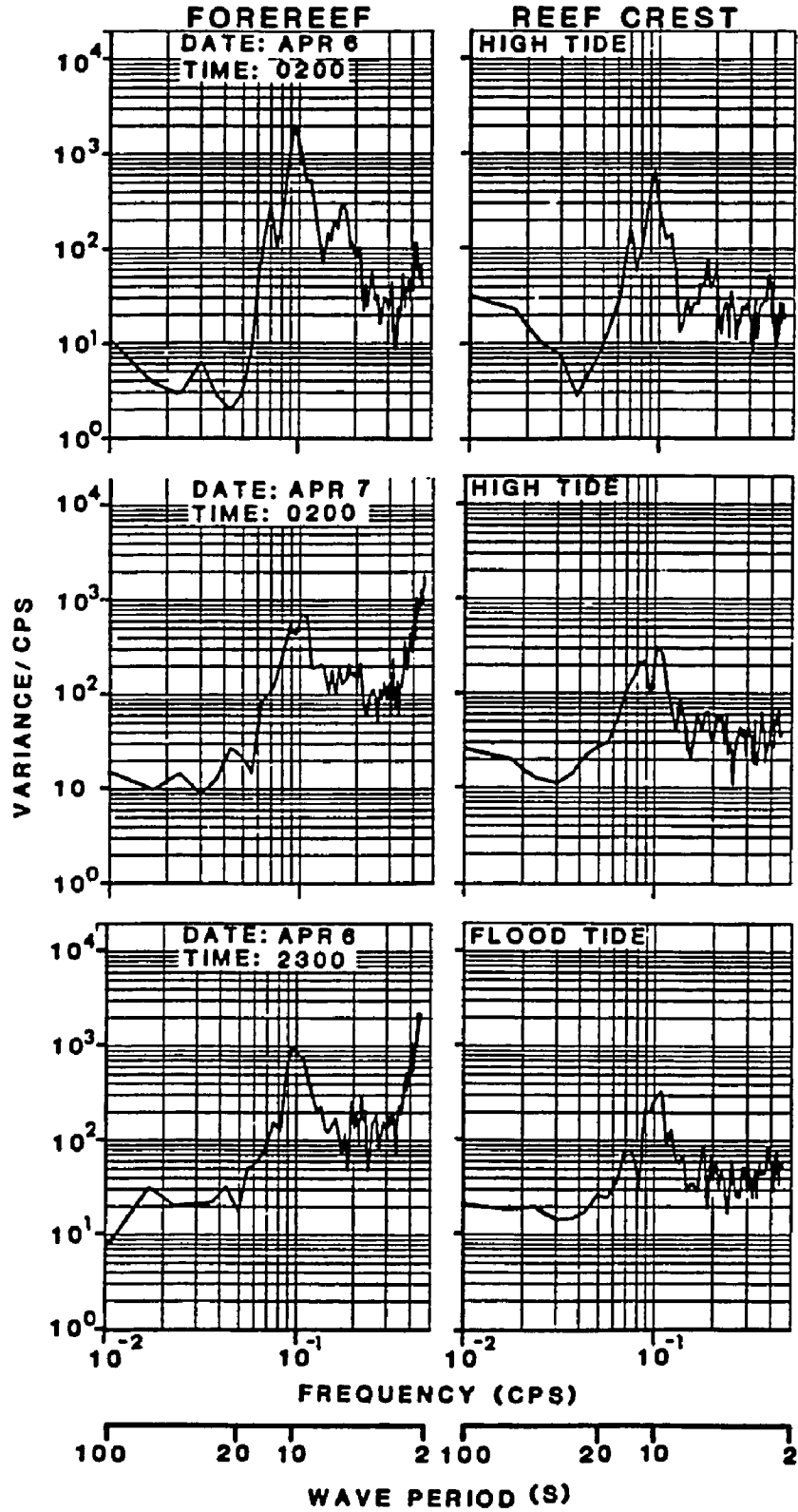


Fig. B3. Wave autospectra at the forereef and reef crest during Experiment 2 for high and flood tide conditions.

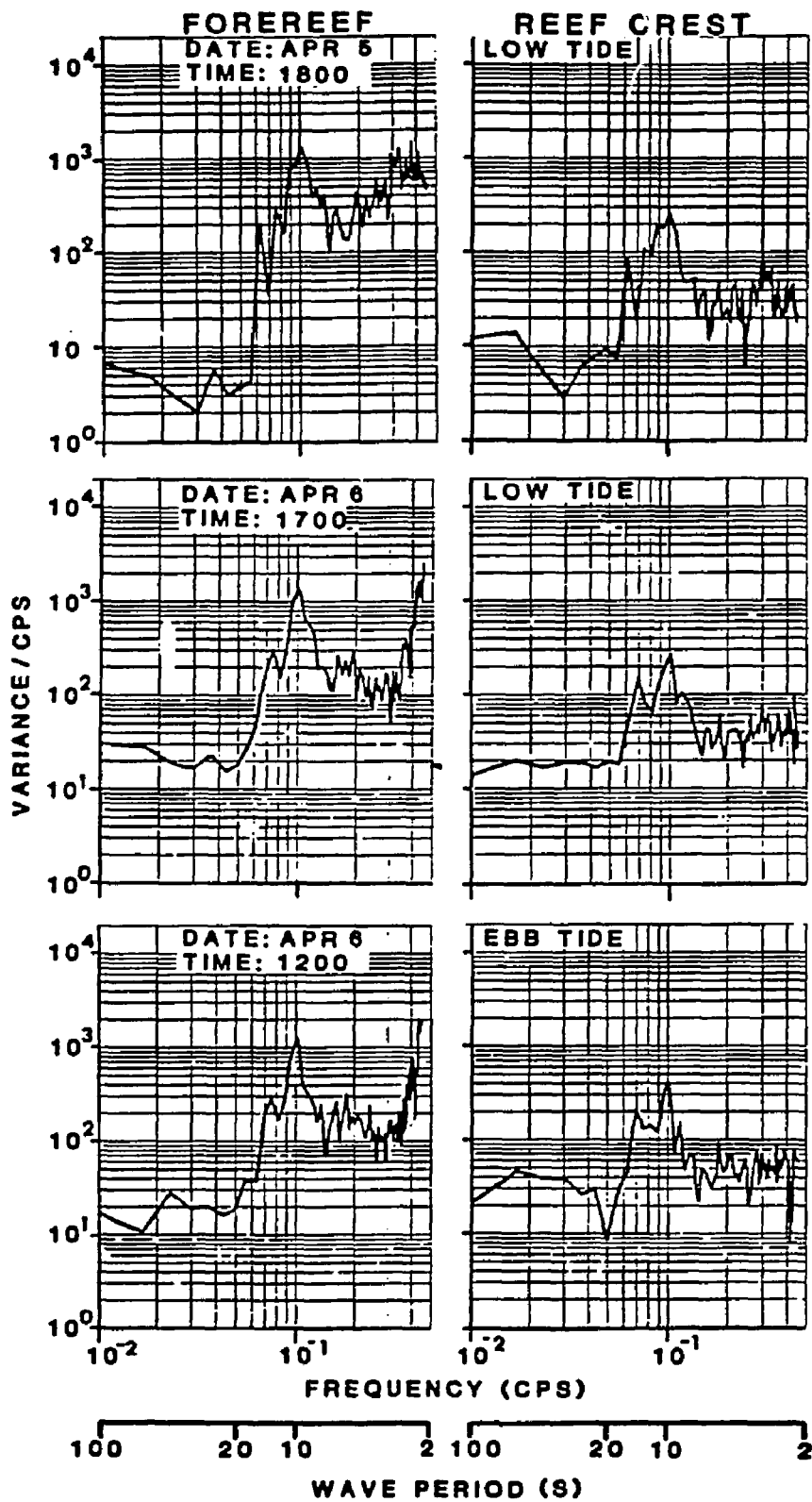


Fig. B4. Wave autospectra at the forereef and reef crest during Experiment 2 for low and ebb tide conditions.

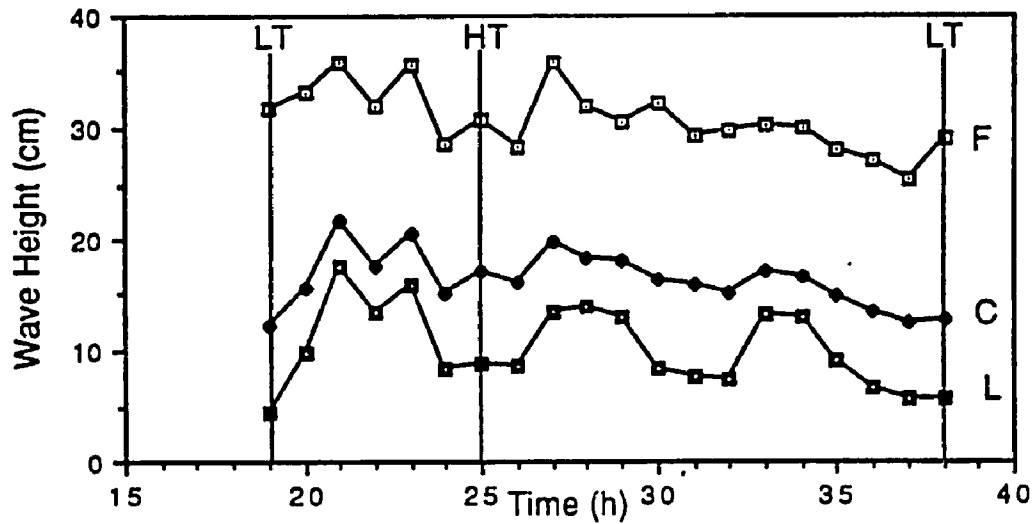


Fig. B5. Wave height time series at forereef (F), crest (C), and lagoon (L) during Experiment 1. (HT= high tide, LT= low tide).

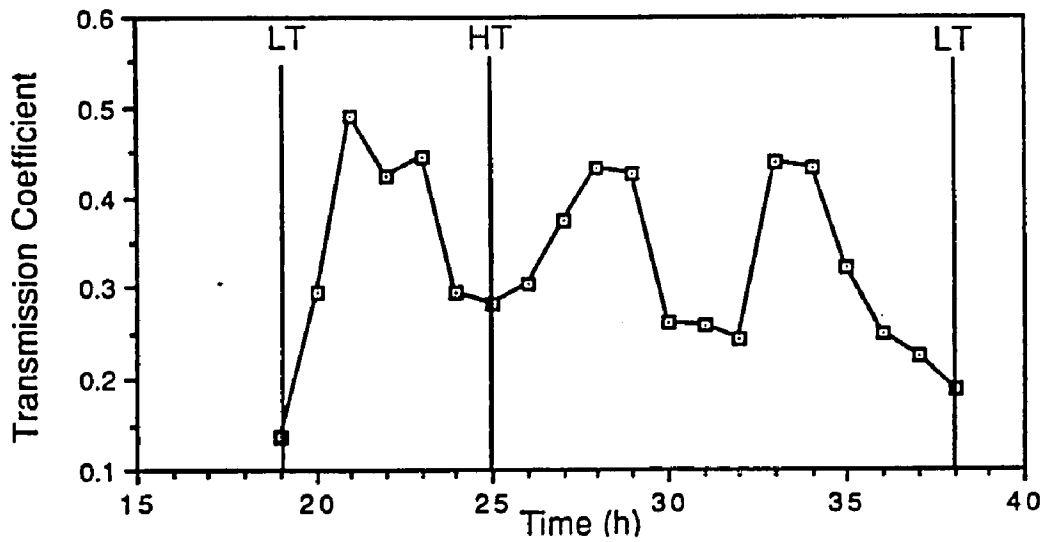


Fig. B6. Wave transmission from forereef to lagoon during Experiment 1. (HT= high tide, LT= low tide).

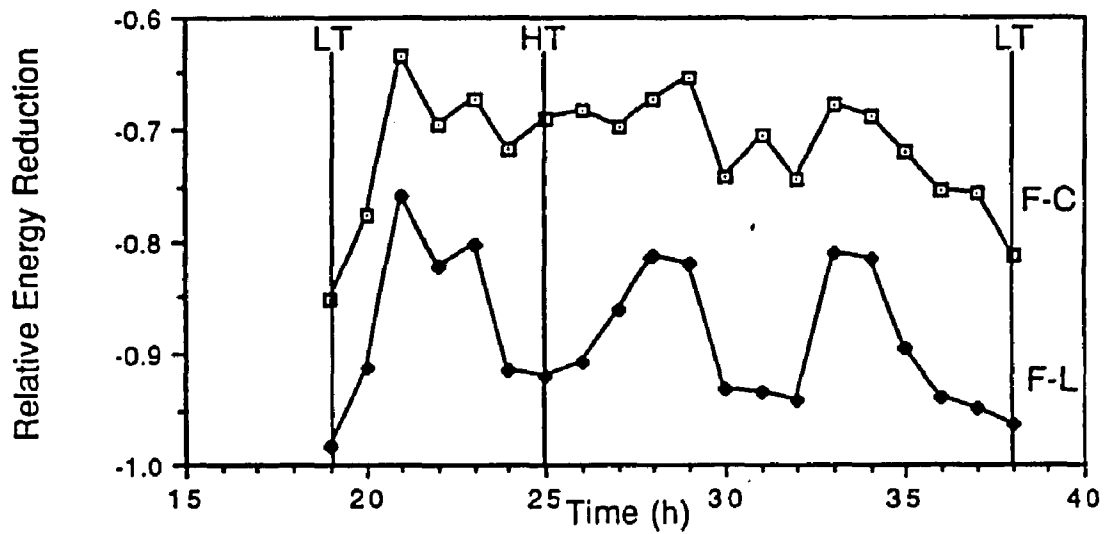


Fig. B7: Relative energy change from forereef to crest (F-C), and forereef to lagoon (F-L) during Experiment 1. (HT= high tide, LT= low tide).

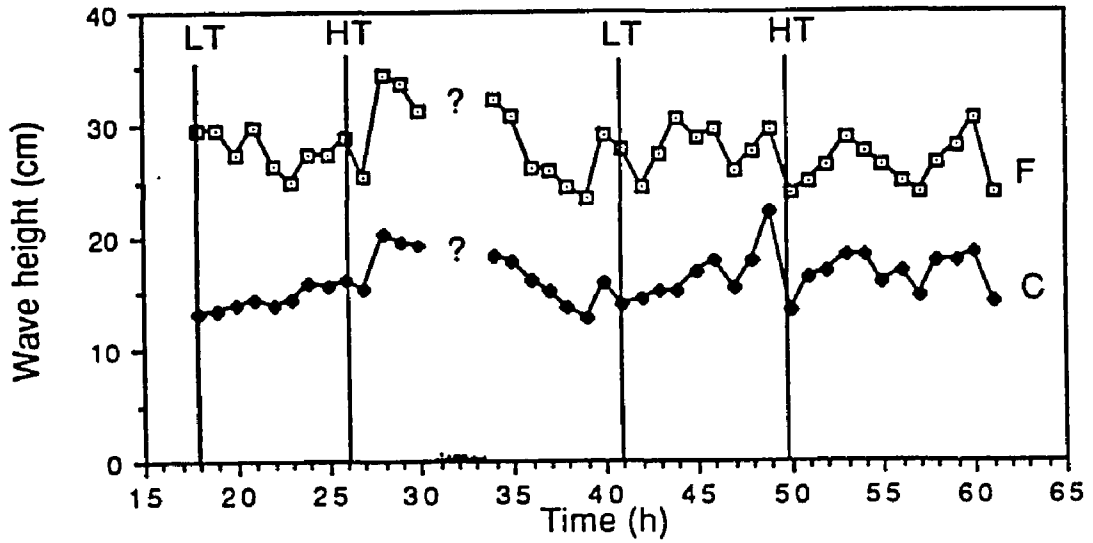


Fig. B8. Wave height time series at forereef (F), and crest (C) during Experiment 2. (HT= high tide, LT= low tide).

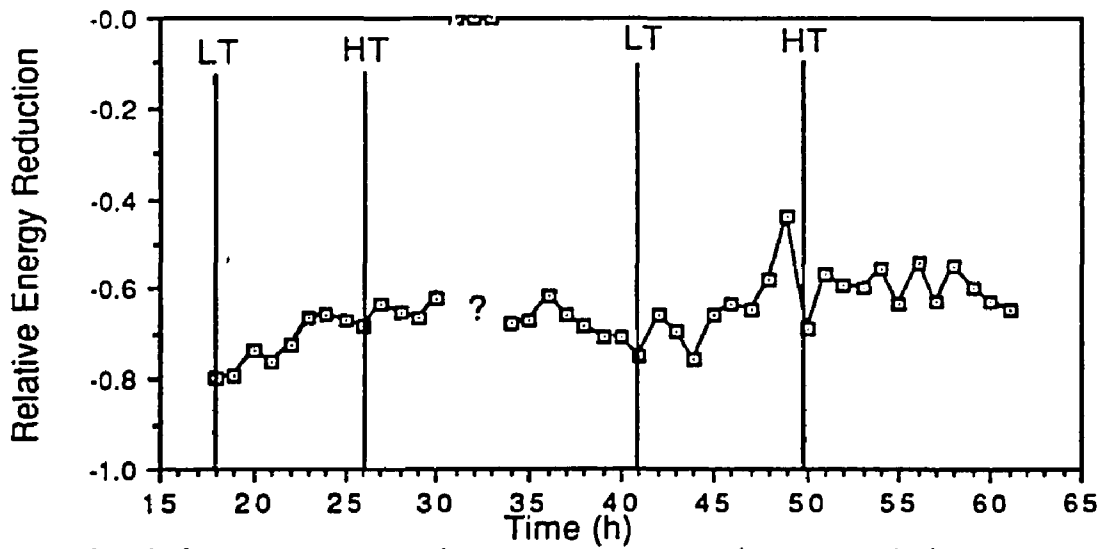


Fig. B9. Relative energy change from forereef to crest during Experiment 2. (HT= high tide, LT= low tide).

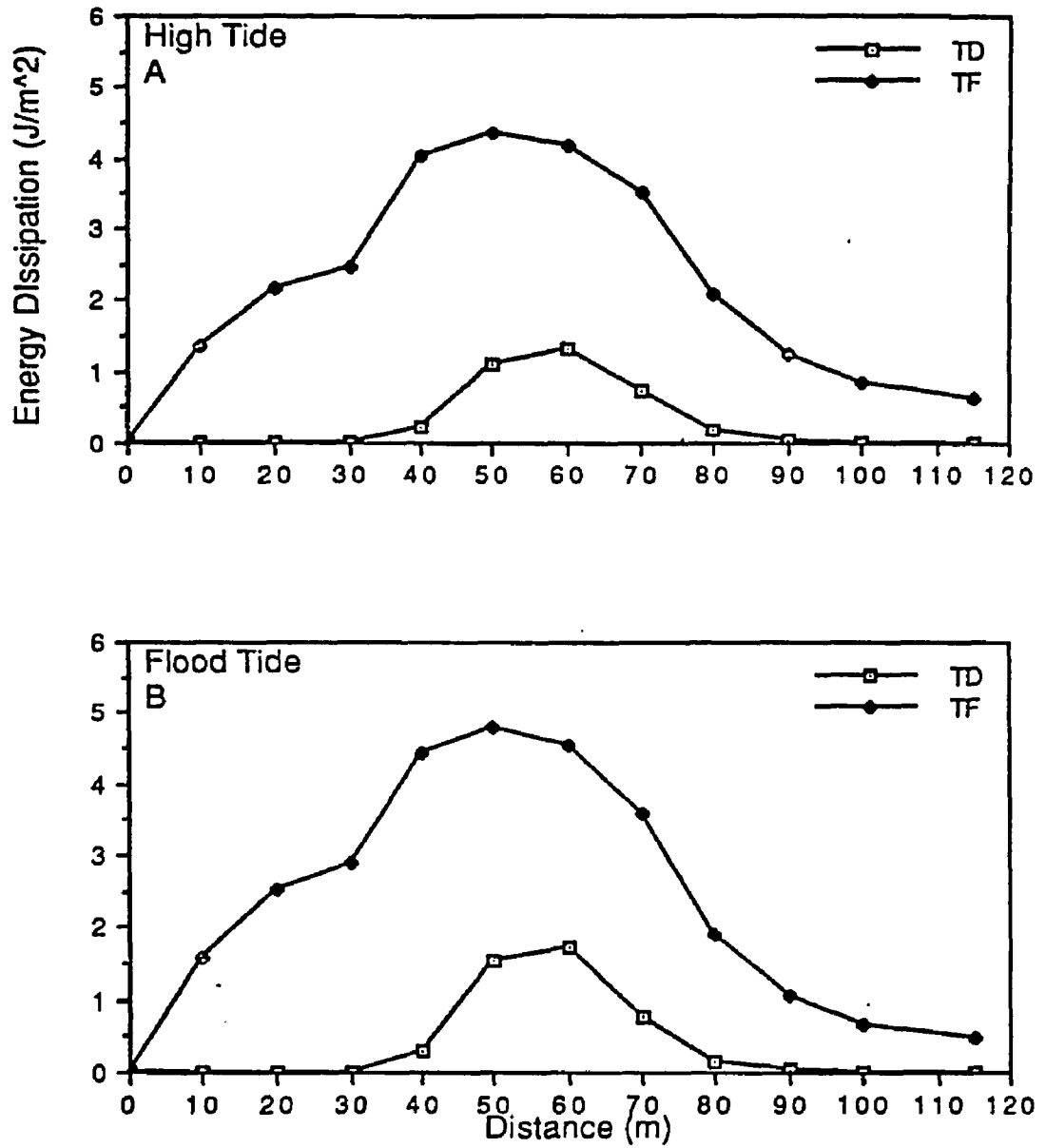


Fig. B10. Energy dissipation across the reef. High tide A; flood B during Experiment 1. (TF= bottom friction dissipation, TD= turbulence dissipation).

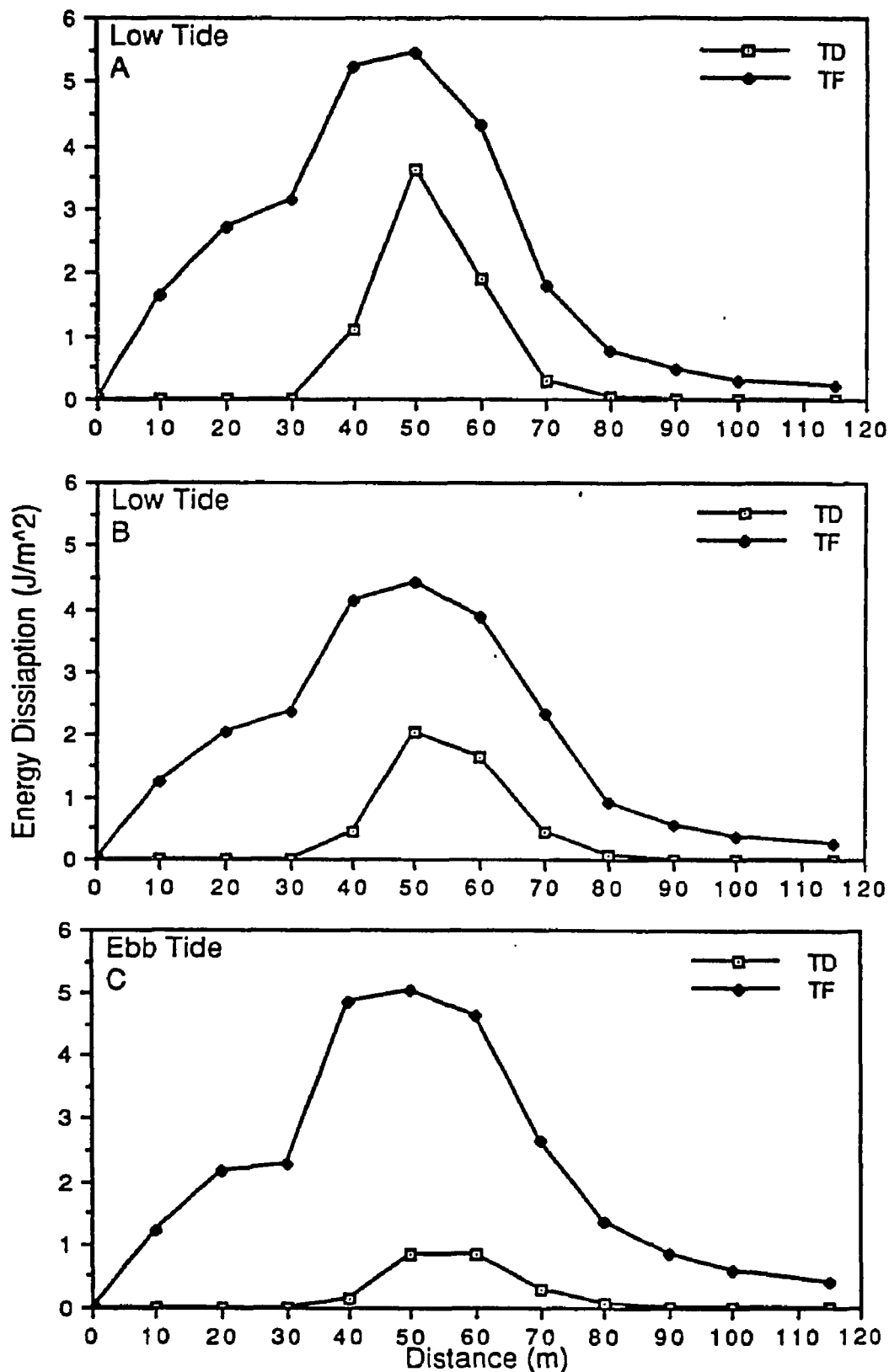


Fig. B11. Energy dissipation across the reef. Low tide A,B; ebb C during Experiment 1. (TF= bottom friction dissipation, TD= turbulence dissipation).

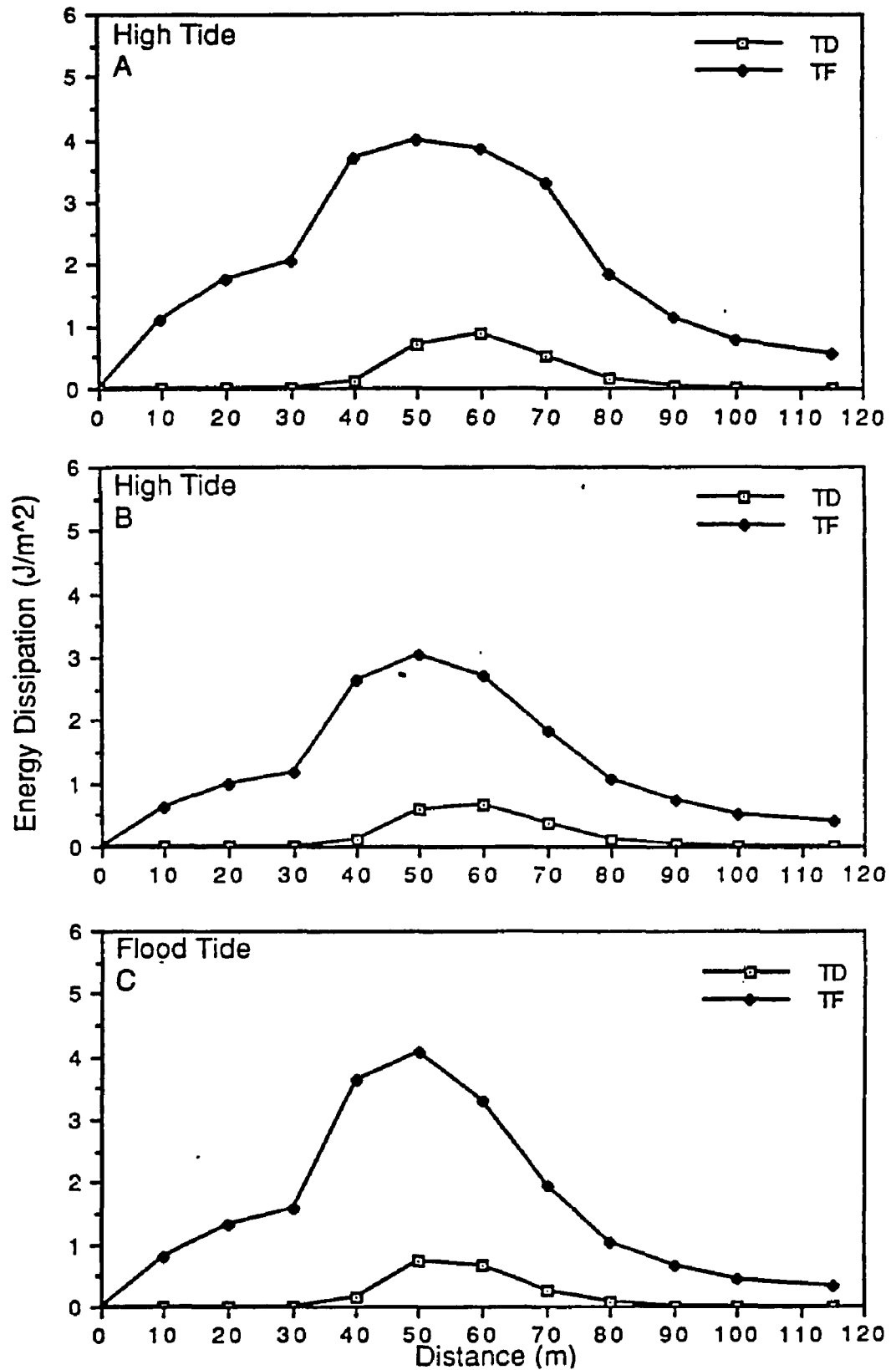


Fig. B12. Energy dissipation across the reef. High tide A,B; flood C during Experiment 2. (TF= bottom friction dissipation, TD= turbulence dissipation).

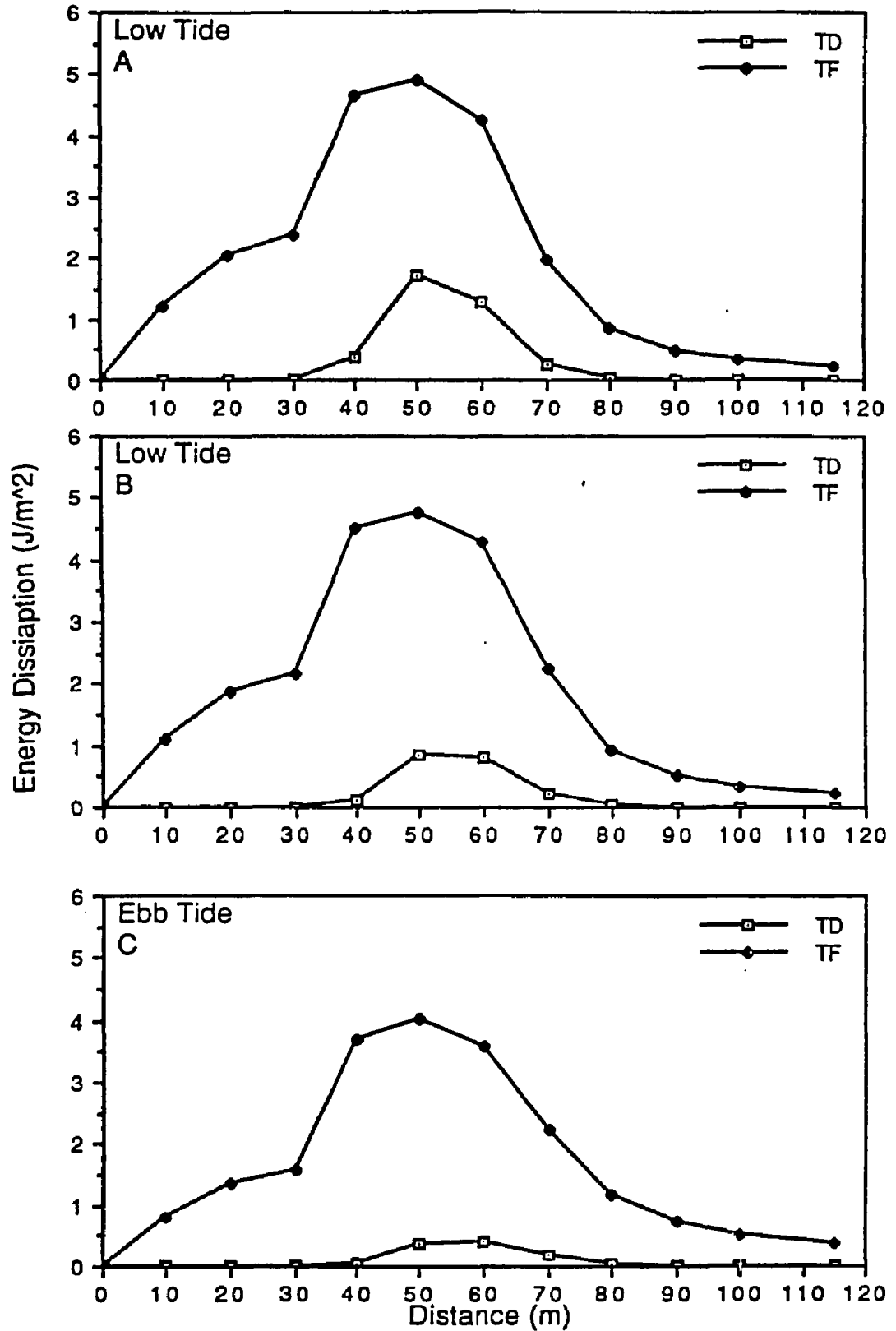


Fig. B13. Energy dissipation across the reef. Low tide A,B; ebb C during Experiment 2. (TF= bottom friction dissipation, TD= turbulence dissipation).

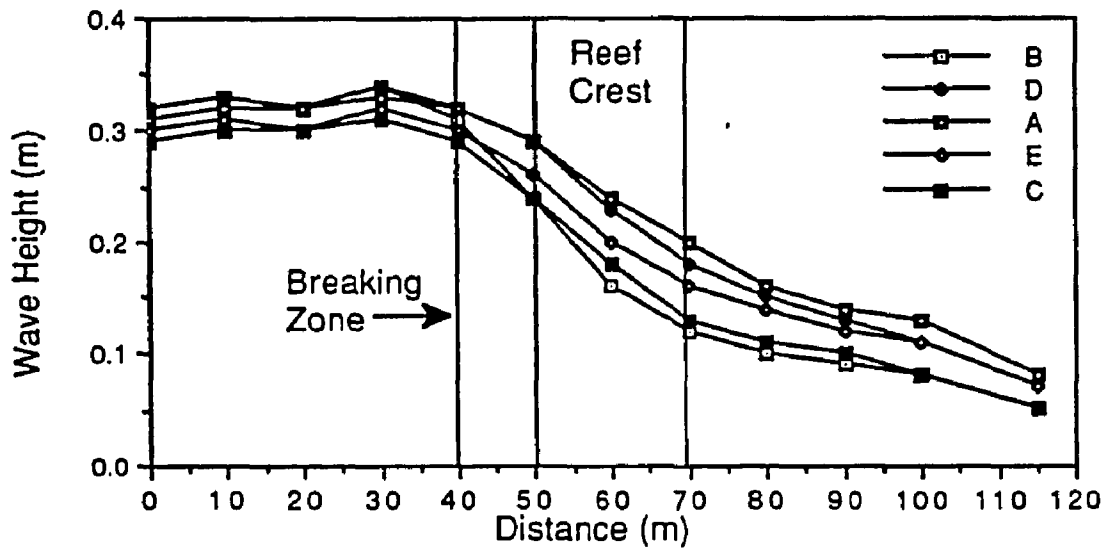


Fig. B14. Predicted wave height across the reef during Experiment 1. High tide A; low tide B,C; flood D; ebb E.

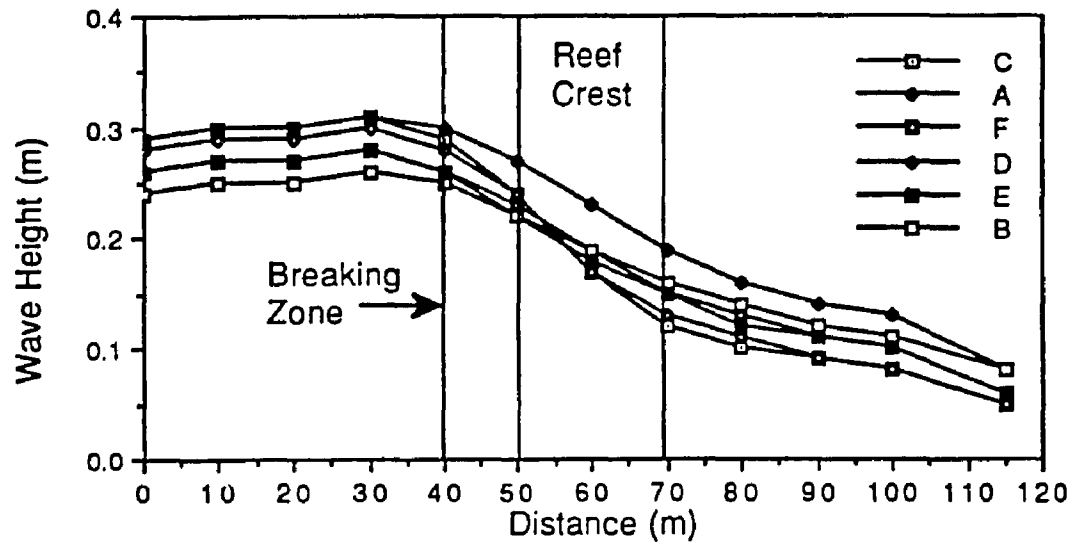


Fig. B15. Predicted wave height across the reef during Experiment 2. High tide A,B; low tide C,D; flood E; ebb F.

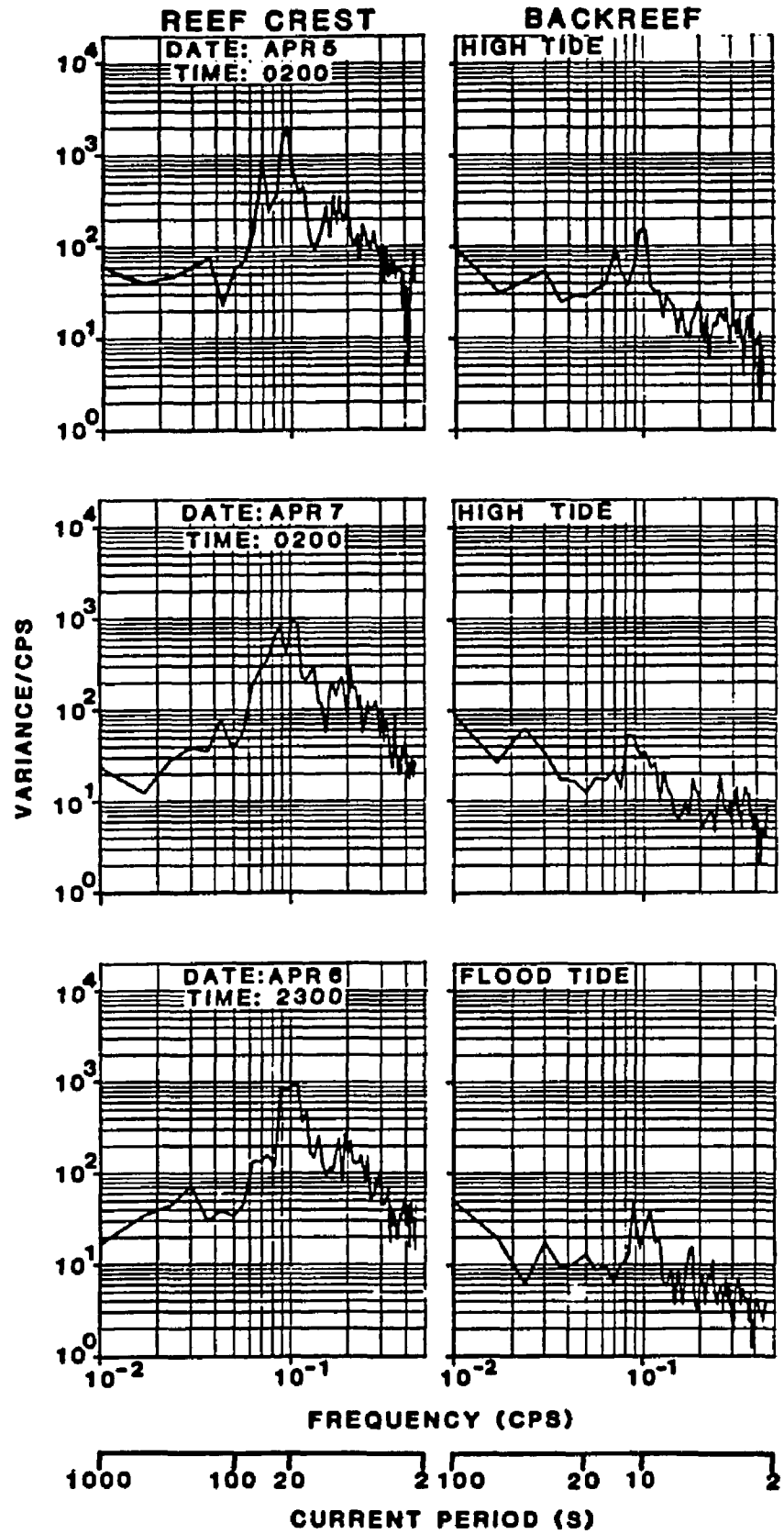


Fig. B16. Current autospectra at the reef crest and backreef during Experiment 2 for high and flood tide conditions.

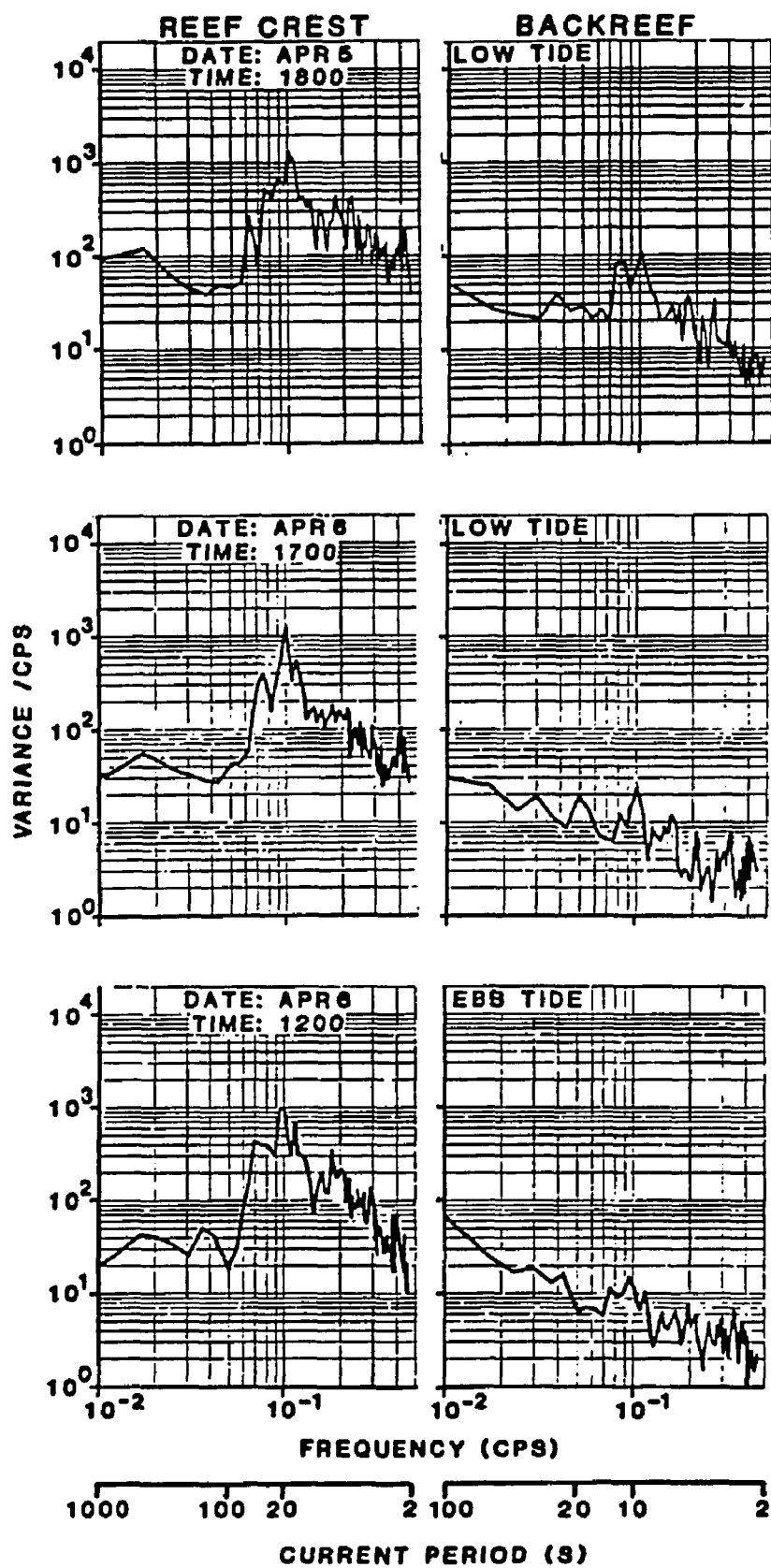


Fig. B17. Current autospectra at the reef crest and backreef during Experiment 2 for low and ebb tide conditions.

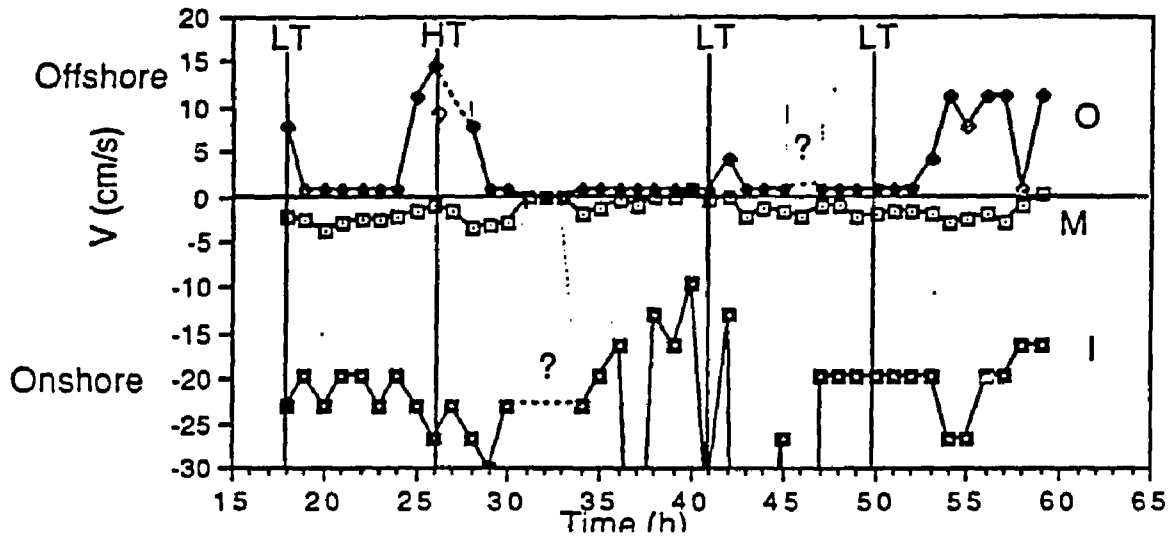


Fig. B18. Mean (M), largest onshore (I) and offshore (O) currents for each record during Experiment 2 at the backreef meter.

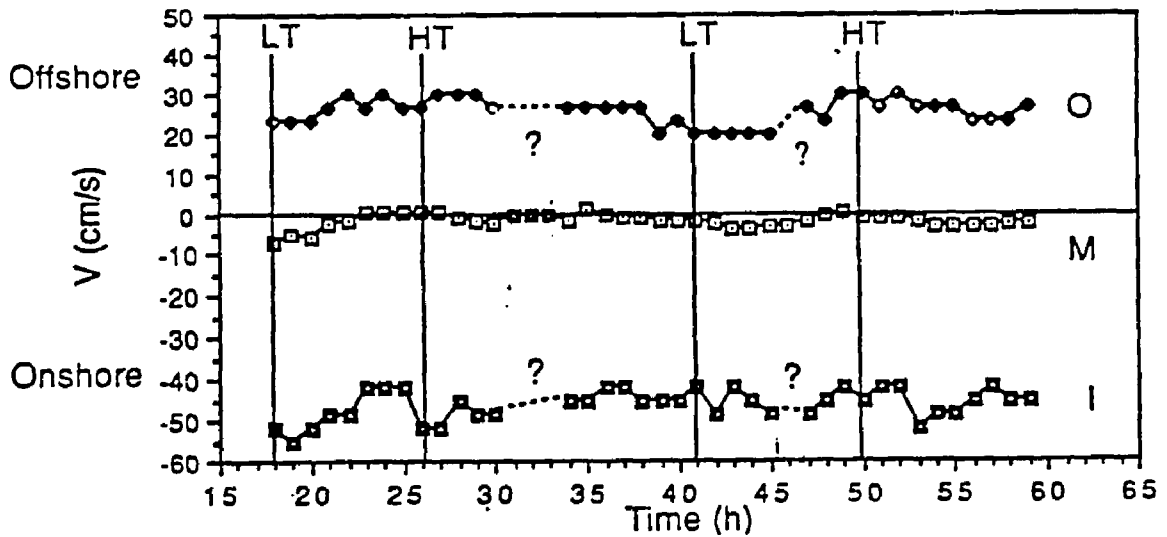


Fig. B19. Mean (M), largest onshore (I) and offshore (O) currents for each record during Experiment 2 at the reef crest lower level meter.

Appendix C

Recommendations to improve experimental design:

- 1- Add wave measurements in front of the reef and just prior to the wave breaking point.
- 2- Install current meters in the reef lagoon for mass balance calculations.
- 3- Increase record duration to 30 min and sample at 0.5 s interval with a burst of data every two hours.
- 4- Collect bottom roughness data throughout the reef profile using several methods to determine the most adequate.
- 5- Secure more reliable and sensitive current meters to measure wave induced currents.

Suggested future research:

- 1- Conduct a similar experiment with at least two experimental sites over the reef.
- 2- Conduct a lagoon circulation study using field and numerical methods.
- 3- Study seasonal and/or high wave energy events.
- 4- Study the infragravity wave phenomena in detail.
- 5- Study energy exchanges between frequencies and harmonic generation over the reef crest.

Vita

Name: Alexis Lugo-Fernandez

Date and Place of Birth: February 17, 1955

Quebradillas, Puerto Rico

Degrees: 1977 B.S., Physics, Universidad de Puerto Rico

1983 M.S., Marine Sciences, Universidad de Puerto Rico

Major Field: Marine Sciences

Minor Field: Civil Engineering

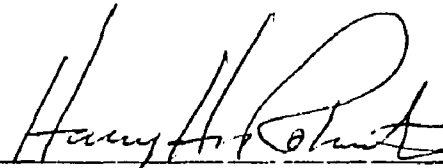
DOCTORAL EXAMINATION AND DISSERTATION REPORT

Candidate: Alexis Lugo-Fernandez

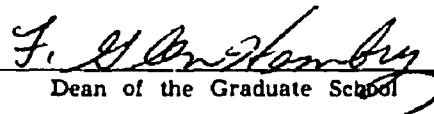
Major Field: Marine Sciences

Title of Dissertation: Wave Height Changes and Mass Transport on Tague Reef, a Caribbean Reef, North Coast of St. Croix, U.S. Virgin Islands.

Approved:

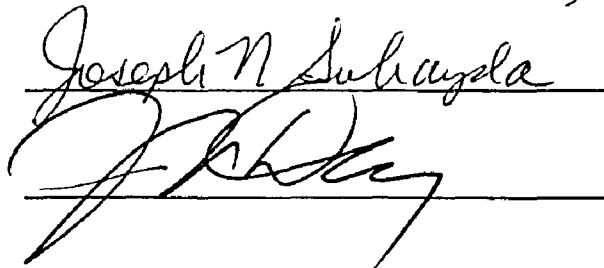
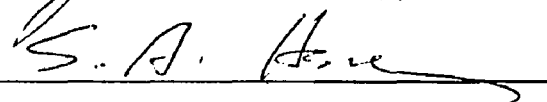
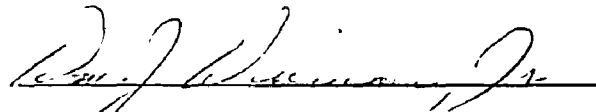


Major Professor and Chairman



Dean of the Graduate School

EXAMINING COMMITTEE:



Date of Examination:

November 20, 1989